LBL-2999
c.2

α-TRANSFER STUDIES VIA THE (α,^{8}Be) REACTION AT HIGH ENERGIES

Gordon John Wozniak
(Ph.D. thesis)

August, 1974

Prepared for the U. S. Atomic Energy Commission
under Contract W-7405-ENG-48

TWO-WEEK LOAN COPY

This is a Library Circulating Copy which may be borrowed for two weeks. For a personal retention copy, call Tech. Info. Division, Ext. 5545

LAWRENCE BERKELEY LABORATORY
UNIVERSITY OF CALIFORNIA
BERKELEY

LBL-2999
c.2

DISCLAIMER

This document was prepared as an account of work sponsored by the United States Government. While this document is believed to contain correct information, neither the United States Government nor any agency thereof, nor the Regents of the University of California, nor any of their employees, makes any warranty, express or implied, or assumes any legal responsibility for the accuracy, completeness, or usefulness of any information, apparatus, product, or process disclosed, or represents that its use would not infringe privately owned rights. Reference herein to any specific commercial product, process, or service by its trade name, trademark, manufacturer, or otherwise, does not necessarily constitute or imply its endorsement, recommendation, or favoring by the United States Government or any agency thereof, or the Regents of the University of California. The views and opinions of authors expressed herein do not necessarily state or reflect those of the United States Government or any agency thereof or the Regents of the University of California.

α-TRANSFER STUDIES VIA THE (α, ^{8}Be) REACTION AT HIGH ENERGIES

Contents

Abstract v

I. Introduction 1

II. ^{8}Be Identifier Design Considerations 7

A. ^{8}Be decay 8

B. Simple identifier 12

C. Modified identifier 22

III. Experimental Technique 28

A. Cyclotron, external beam facilities and experimental area 28

B. Targets 30

C. Simple identifier 33

D. Modified identifier 43

E. Data acquisition and analysis 55

IV. Theoretical Considerations 57

A. α-cluster transfer 57

B. Selection rules 58

C. Direct reaction theory 59

V. Experimental Results and Discussion 74

A. ^{8}Be breakup distribution 74

B. The ^{12}C(α, ^{8}Be)^{8}Be reaction 78

C. The ^{16}O(α, ^{8}Be)^{12}C reaction 87

D. The $^{10}B(\alpha, {}^{8}Be)^{6}Li$ reaction 96

E. The $^{11}B(\alpha, {}^{8}Be)^{7}Li$ reaction 102

F. The $^{14}N(\alpha, {}^{8}Be)^{10}B$ reaction 106

G. The $^{15}N(\alpha, {}^{8}Be)^{11}B$ reaction 108

H. Relative ground state spectroscopic factors 114

I. Comparison of diffraction model to full finite-range DWBA with recoil 118

J. Comparison of $(\alpha, {}^{8}Be)$ with $(\alpha, 2\alpha)$ results 123

VI. Summary and Conclusion 126

Acknowledgments 129

Footnotes 131

References 132

α-TRANSFER STUDIES VIA THE (α, ^{8}Be) REACTION AT HIGH ENERGIES

Gordon John Wozniak

Department of Chemistry and Lawrence Berkeley Laboratory
University of California, Berkeley, California 94720

August 1974

ABSTRACT

The (α, ^{8}Be) reaction was investigated on ^{16}O, ^{15}N, ^{14}N, ^{12}C, ^{11}B, and ^{10}B targets at bombarding energies between 63.2 and 72.5 MeV with a ^{8}Be identifier of high detection efficiency. Differential cross sections were measured from $\theta_{c.m.}$ = 20°-70° for solid targets and over a more restricted range for the nitrogen gas targets. An excitation function of the ^{12}C(α, ^{8}Be)^{8}Be reaction at five bombarding energies between 63.2 and 67.3 MeV was obtained which conclusively demonstrated the direct nature of the (α, ^{8}Be) reaction at high bombarding energies. This reaction was found to proceed predominantly via a direct α-cluster pickup mechanism and to strongly populate only levels consistent with this mechanism. The angular distributions on spin 0 targets exhibited a strong dependence on the value(s) of L, the angular momentum transfer. Experimental distributions for L = 0 and L = 2 transfers were both oscillatory, but with the latter showing a much larger strength at back angles. The distributions for transitions where more than one L-transfer was allowed were approximately constant in magnitude with little structure.

A plane wave diffraction model was used to analyze the cross section data. This model which included finite-range and recoil effects adequately reproduced the L = 0 and L = 2 data from spin 0 targets. However, it failed to describe the shape of the angular distributions for transitions involving more than one L-transfer. The neglect of distortion in these calculations was investigated and found to be unimportant at forward angles ($\theta_{c.m.} < 70°$). Using the above model, relative α-spectroscopic factors were extracted which are in qualitative agreement with those of Kurath.

I. Introduction

There has been much interest in whether significant clustering of nucleons exists in light nuclei, especially in the form of α-like clusters. This idea of α-clustering was suggested in 1937 by Wigner (Wi 37) to explain the mass systematics of light nuclei. More recently Wilkinson (Wi 61) concluded from an analysis of knockout and K^- meson capture experiments that in the nuclear surface there is a higher probability of finding nucleons grouped together forming α-particles than one would expect from isolated nucleons. The existence of α-clusters in the low-density surface region is possible because the Pauli principle plays a smaller role there and in fact the formation of α-clusters is favored because of the large internal binding energy of the α-particle.

Moreover, in light nuclei, due to the small number of nucleons, α-clusters may occur throughout the nucleus. In fact for some light $N = Z$ nuclei, Hartree-Fock calculations, which did not include any explicit assumption about an α-clustering effect, showed that the nucleons tend to group together in small clusters which may be identified as α-clusters (Ri 68). Also, for light nuclei the α-particle model has been shown to be a successful method for describing the deformed ground states and rotational bands excited in α-transfer reactions (Br 66). Furthermore, it is well known that shell-model wave functions can be rewritten in cluster form (Wi 58, Ph 60). Evidence for α-like four-body correlations (two protons and two neutrons with relative quantum numbers $S = 0$, $T = 0$) is discussed in detail in Fr 63,

Bro 66, Ge 67, Ei 69, Wi 66, Ar 71, and Ar 71a.

A very good experimental probe which has been used recently to obtain information on the α-cluster wave functions of target nuclei is the α-particle pickup reaction. If the four nucleons are transferred in a single step process as a cluster having the internal quantum numbers of a free α-particle, then such a reaction should selectively populate final states which closely resemble the ground state of the target nucleus minus an α-particle. The parity of the final state is $\pi_f = (-1)^L \pi_i$, where π_i is the parity of the target and L is the orbital angular momentum of the transferred cluster. Thus unnatural-parity states can not be populated by direct α-cluster transfer on even-even targets. Among the lighter projectiles two possible α-cluster transfer reactions, (d, ^{6}Li) and (^{3}He, ^{7}Be), have been extensively investigated to determine if they proceed via a direct α-cluster transfer (e.g., Be 70, Ga 72). A brief summary of these results is given below.

The (d, ^{6}Li) reaction has been studied over a bombarding energy range of 15-55 MeV (De 66, Ei 70, Ce 71, Gu 71, Mc 71, Co 72, Ma 73, Be 72). Transitions to the ground state of the final nucleus seem to proceed mainly via a direct process at an incident energy of 15 MeV (De 66). Also, at higher bombarding energies where many more final states can be observed, the experimental evidence generally supports the assumption that the (d, ^{6}Li) reaction proceeds mainly through a direct α-cluster pickup (Be 70, Ga 72). It should be noted, however, that at 28 MeV (Co 72) this reaction on even-even 1p and 2s-1d shell targets systematically populated unnatural parity states

with large relative cross sections. This result suggests the presence of multistep processes, making questionable the extraction of α-clustering information with distorted-wave Born approximation (DWBA) calculations. Nevertheless, experimental spectroscopic factors for some transitions have been determined by fitting the experimental angular distributions with ones calculated in both the zero-range and the exact finite-range DWBA theory. Exact finite-range calculations performed by Gutbrod et al. (Gu 71) using a zero-node wave function for ^{6}Li lead to experimental spectroscopic factors in good agreement with the predictions of the shell model. However, poor agreement was obtained if a one-node wave function was used for ^{6}Li. Martin et al. (Ma 73) found that the magnitude of the angular distributions calculated in the zero-range approximation was strongly dependent on the number of nodes of the bound-state wave-function, and that both the magnitude and shape were very sensitive to the ^{6}Li optical parameters. Thus the reliability of experimental spectroscopic factors seems to be unclear at the moment.

Over the energy range of 30-70 MeV, the experimental data from the (^{3}He, ^{7}Be) reaction (De 70, Fo 70, Cr 71, De 71, Za 71, Br 72, De 72) indicate that the dominant mechanism is also a direct α-transfer process. An excitation function has been measured (Aro 71) between 37.5 and 41.5 MeV incident energies for the ^{19}F(^{3}He, ^{7}Be) ^{15}N(g. s.) transition and was observed to be quite smooth. At a bombarding energy of 41 MeV the transfer of a 2p + 2n fragment in a T = 1 state was ~ 20% of the α-cluster transfer strength (De 72). This 20%

only measures the contribution of a particular non-α-cluster transfer mechanism, and therefore, represents a lower limit for non-α-cluster transfer processes.

A zero-range approximation can not be expected to provide a reliable description of the (^{3}He, ^{7}Be) reaction since the α-particle inside ^{7}Be is in a P-state. Therefore, the data have been fit with finite-range DWBA calculations and qualitative spectroscopic factors extracted which for s-d shell nuclei are in considerable disagreement with shell-model predictions. Also, the ratio of extracted experimental spectroscopic factors for transitions to the first 0^+ and 2^+ states of ^{12}C was determined to be ~35 whereas theoretical estimates give a ratio of ~6. It is not clear whether the above quantitative disagreement with theory and also with the (d, ^{6}Li) results is due to the reaction mechanism, the lack of ^{7}Be optical potentials or approximations involved in treating ^{7}Be as ^{4}He and ^{3}He in a relative P-state. However, on a qualitative basis an α-transfer description does account for most of the observed properties of the (^{3}He, ^{7}Be) transitions, including some observed selection rules. An experimental complication associated with this reaction is the bound first excited state in ^{7}Be(.43 MeV) which causes "shadow" peaks and imposes constraints on the energy resolution.

Since both the (d, ^{6}Li) and (^{3}He, ^{7}Be) reactions seem to have sizeable non-direct contributions and because of theoretical difficulties associated with each of these reactions, the (α, ^{8}Be) reaction was investigated as a possible alternative. There are several reasons for

believing that this reaction will proceed via a direct process and that it will be particularly suited for studying α-clustering phenomena. It has been pointed out by Holmgren (Ho 69) that the α-cluster used to describe the ground state of the target may not have the same structure as the α-cluster in ^{6}Li or ^{7}Be, and furthermore that all of these structures may differ from that of the free α-particle. As the ^{8}Be ground state is unbound by 92 keV, the two α-clusters should be virtually identical with free α-particles. This conjecture is supported by the fact that ^{8}Be has no excited states other than those of almost pure α+α parentage below an excitation energy of 16 MeV and by its large calculated ^{8}Be→ 2α spectroscopic factor (Ku 73). Since the ground states of both the α-particle and ^{8}Be have zero spin, the transferred angular momentum is unique for targets having spin 0 or 1/2 in contrast with the more complicated selection rules for the (d, ^{6}Li) and (^{3}He, ^{7}Be) reactions.

A further attractive feature of this reaction is the identical entrance channel which it shares with the (α, 2α) reaction. The exit channels are also very similar as (α, ^{8}Be) is the same as (α, 2α) if the 2α-particles are in a relative S state. Typically, the two α-particles from the (α, 2α) reaction are detected on either side of the beam axis at or near the quasielastic angle where the product nucleus is left with approximately zero recoil momentum. Thus these two reactions will probe different momentum regions of the target α-cluster wave function. Since the (α, 2α) reaction at an incident energy of 90 MeV (Sh 73) selectively populates the ground state of the final nucleus and only weakly populated excited states, it will be especially interesting to compare these results to those of the (α, ^{8}Be) reaction.

Although the original (α, ^{8}Be) experiments by Brown et al. (Br 65) employing α-α coincidence techniques showed that at 35.5-41.9 MeV bombarding energies nondirect processes appeared predominant, it was hoped that direct processes would dominate at higher energies. Because theoretical α-structure amplitudes are known for 1 p-shell nuclei, this investigation was confined to this shell on ^{10,11}B, ^{12}C, ^{14,15}N and ^{16}O targets.

Since the ^{8}Be ground state is particle-unstable ($t_{1/2} \sim 10^{-16}$ sec), it must be detected indirectly by means of its decay products. (A detection technique developed for this investigation is described in Section II.) Fortunately, compared to typical nuclear transit times, ^{8}Be is sufficiently long-lived to be treated as a stable particle in nuclear reactions. Thus the (α, ^{8}Be) reaction can be described by two-body kinematics and each ^{8}Be nucleus will have a unique energy at a given laboratory angle. Moreover shadow peaks due to reactions forming ^{8}Be* (2.9 MeV) can be experimentally eliminated from the data (see Section II).

Experimental equipment and procedures are outlined in Section III. A simple model of the (α, ^{8}Be) reaction mechanism is developed in Section IV and experimental and theoretical results are presented in Section V.

II. ^{8}Be Identifier Design Considerations

The study of reactions with ^{8}Be nuclei as the detected particles is complicated by the fact that the ^{8}Be ground state decays promptly ($t_{1/2} \sim 10^{-16}$ sec), and therefore must be observed indirectly by means of its breakup α-particles. The essential difficulty lies in detecting these two α-particles with high efficiency, while at the same time accurately determining the energy and direction of the original ^{8}Be event.

Previous methods of detecting ^{8}Be nuclei fall into two general categories: those observing the two α-particles in coincidence in two separate detectors (Br 65, Ch 67, Cr 73, Ja 68, Ho 72, Ma 72, Ja 73, Ro 73, Br 73), and those using a single counter telescope (Wo 72, Me 74). The latter technique utilizes the fact that two approximately equal-energy α-particles simultaneously traversing a ΔE-E telescope identify as a ^{7}Li event; however, the range of excitation that can typically be observed with this technique is limited (Ha 72) to ~10 MeV. Both of these methods rely on collimation to reduce kinematic broadening, so that one must strike a balance between detection efficiency and energy resolution, particularly on light targets. High efficiency requires a ^{8}Be identifier subtending a large solid angle, while a restricted solid angle is necessary for small kinematic broadening.

In the detection technique discussed below a position-sensitive detector is used to measure both the direction and the energy of a ^{8}Be event, thereby permitting both good detection efficiency and reasonable energy resolution. Although ^{8}Be events can then be selectively observed by employing a divided collimator before this detector (as shown

below), substantial background reduction of chance coincident events can be achieved by also employing a transmission (ΔE) detector.

The ^{8}Be identifier--consisting of a divided collimator, a transmission detector and a position-sensitive E detector--was developed to study the (α, ^{8}Be) reaction on p-shell targets (Wo 73). Because of the large α-structure amplitude of ^{8}Be, it was hoped that this reaction would be a useful spectroscopic probe with which to investigate theoretical α-structure amplitudes, such as those given by Kurath (Ku 73) for p-shell nuclei. Both a simple ^{8}Be identifier, employing a single ΔE detector or twin ΔE detectors, and a modified one, with subnanosecond pileup rejection to achieve low backgrounds at high counting rates (50 kHz), are discussed (Wo 74).

A. ^{8}Be Decay

The decay of ^{8}Be (^{8}Be = ^{8}Be$_{gs}$, hereafter) is characterized by a single decay channel, a small breakup energy (Q = 0.092 MeV), two identical charged products (α-particles) and, since all the spins involved are zero, an isotropic distribution of the decay products in the center of mass. By designing a detection system optimized for high-energy ^{8}Be events ($E_8 > 35$ MeV, $E_8 \equiv E_{^8Be}$) to which discussion below is restricted, advantage can be taken of the strong kinematic focussing of the α-particle into a narrow cone whose axis is in the direction of the original ^{8}Be nucleus, and whose half angle (β_{max}) is given by

$$\beta_{max} = \arcsin[(Q/E_8)^{1/2}]. \qquad (2\text{-}1)$$

This kinematic focussing of the α-particles from the decay of a high energy ^{8}Be nucleus is shown in Fig. 2-1. Depicted are the ^{8}Be velocity vector ($\vec{V}_8$), center of mass ($\vec{C}$) and laboratory velocity vectors ($\vec{V}_1$, $\vec{V}_2$) of the breakup α-particles, and the angle in the center of mass (γ) and the laboratory (β_1) at which α_1 is emitted relative to $\vec{V}_8$. In part b is illustrated the breakup cone within which the α-particles are confined. Also, shown are the target to detector distance(D), the maximum angle in the laboratory (β_{max}) at which a breakup α-particle is emitted relative to $\vec{V}_8$ and the radius of the breakup cone (r_m).

For high energy ^{8}Be events, β_{max} is small (2.9°) and the angles β_1 and β_2 are approximately equal [$|\beta_1 - \beta_2|/\beta_{max} < 5\%$]. In this approximation, the radial distribution, R(r), of α-particles across a detector is given by:

$$R(r)\,dr = (r/r_m^2)\,(1 - r^2/r_m^2)^{-1/2}\,dr, \qquad (2\text{-}2)$$

where $r_m = D\tan\beta_{max}$ (see Fig. 2-1). This function is plotted in Fig. 2-2 and illustrates that the probability of finding an α-particle near the edge of the breakup cone is much larger than that of finding one near the center.

By integrating this expression, the fraction, F(r), of breakup α-particles which fall between r and r_m is obtained:

$$F(r) = (1 - r^2/r_m^2)^{1/2}. \qquad (2\text{-}3)$$

From this it follows that 71% of the α-particles lie between $r = 0.7\,r_m$ and $r = r_m$ (see Fig. 2-2). This result can be visualized by realizing that 71% of the breakup α-particles have a direction in the center of

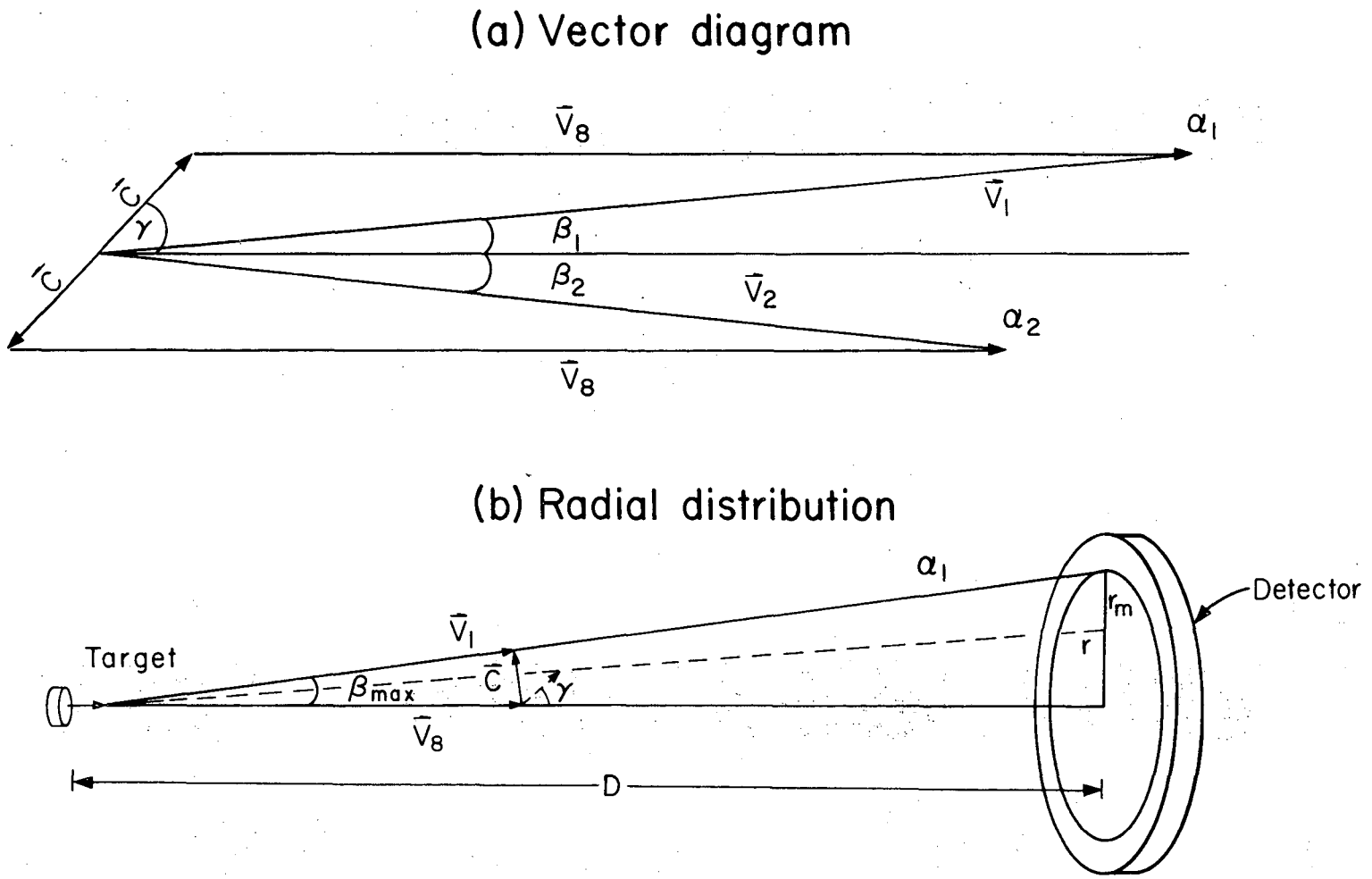

XBL 7311-4447

Fig. 2-1. a) Kinematic focussing of the α-particles from the decay of a high energy ^{8}Be nucleus. b) An illustration of the cone, within which the breakup α-particles are confined. See text for definition of symbols.

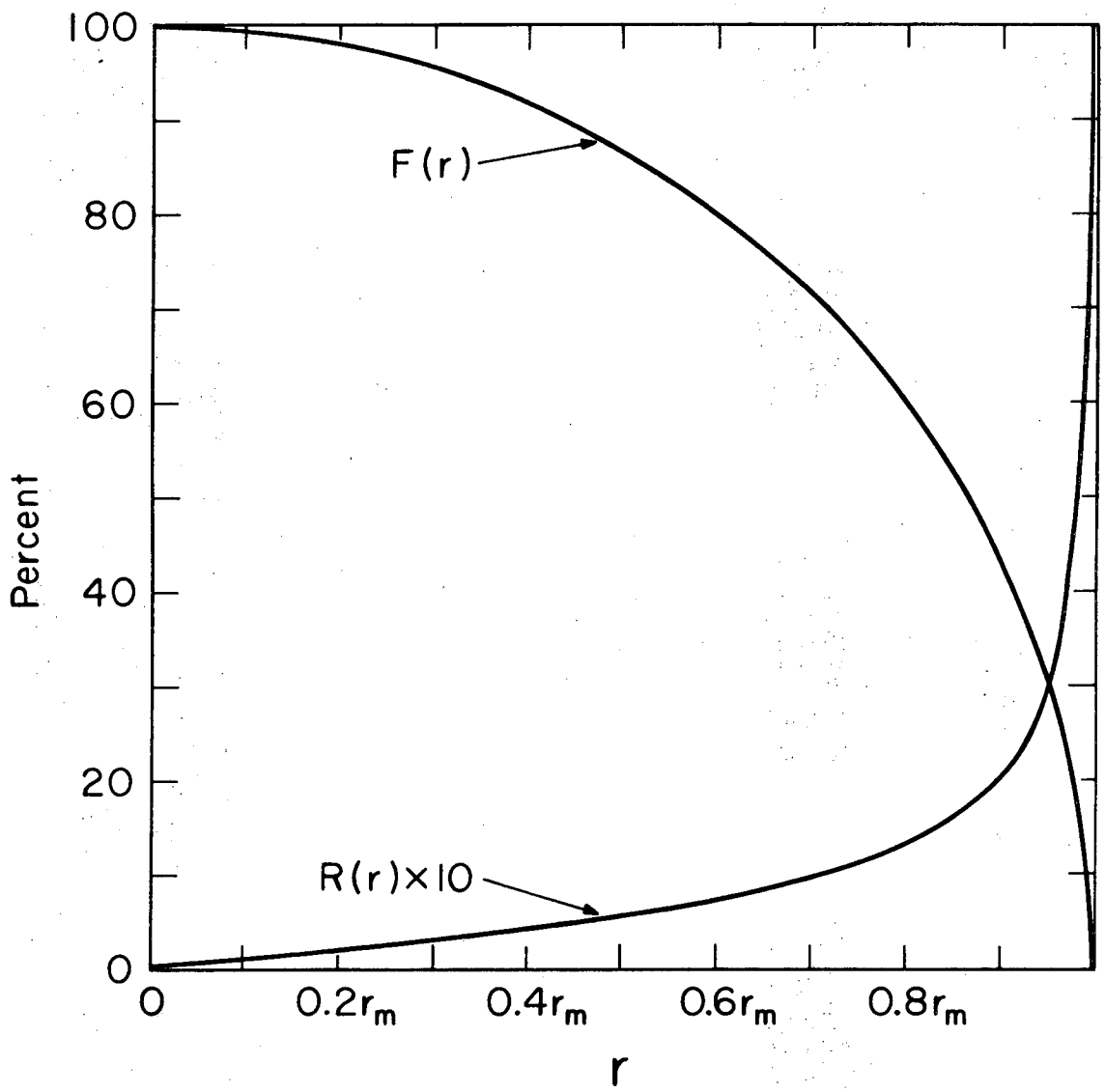

XBL 745-3045

Fig. 2-2. A plot of the radial distribution R(r) of the two α-particles across the base of the breakup cone and the fraction F(r) which fall between r and r_m. See discussion in text.

mass corresponding to $\gamma \geqslant 45°$, which in the laboratory is equivalent to $r \geqslant 0.7\, r_m$ since $r = r_m \sin\gamma$ (see Fig. 2-1).

B. Simple Identifier

1. Position-sensitive detector

The distribution of the breakup α-particles suggests that, in order to detect a substantial fraction of the ^{8}Be events, a detector must subtend an angle at least as large as that of the breakup cone (~5°). However, such a large angular acceptance allows considerable variation in the detection angle (θ_{lab}) of the ^{8}Be events. On light targets ($A \leqslant 16$), a typical value of $dE/d\theta$ is around 500 keV/deg for the (α, ^{8}Be) reaction at $E_\alpha \sim 65$ MeV. The substantial kinematic broadening that would arise from this large value of $dE/d\theta$ is avoided by using a position-sensitive detector (PSD). A particle striking such a detector generates both an energy signal (E), and a signal (XE) proportional to the product of the energy (E) and the distance of impact from one side of the detector (X) (see Fib. 2-3a). For high energy ^{8}Be events, the breakup Q-value is small compared to the ^{8}Be energy, and so the two breakup α-particles have, to a first approximation, equal energies [$|E_1 - E_2|/(E_1 + E_2) < 10\%$]. On striking a position-sensitive detector, one α-particle therefore produces a signal $X_1E/2$, the other $X_2E/2$. Since both alphas arrive within a fraction of a nanosecond, the individual E and XE signals are automatically summed and the resultant E signal gives the energy of the ^{8}Be event. The position signal (X) obtained by dividing out the energy dependence is given by:

$$X = (X_1E/2 + X_2E/2)/(E/2 + E/2) = (X_1 + X_2)/2. \qquad (2\text{-}4)$$

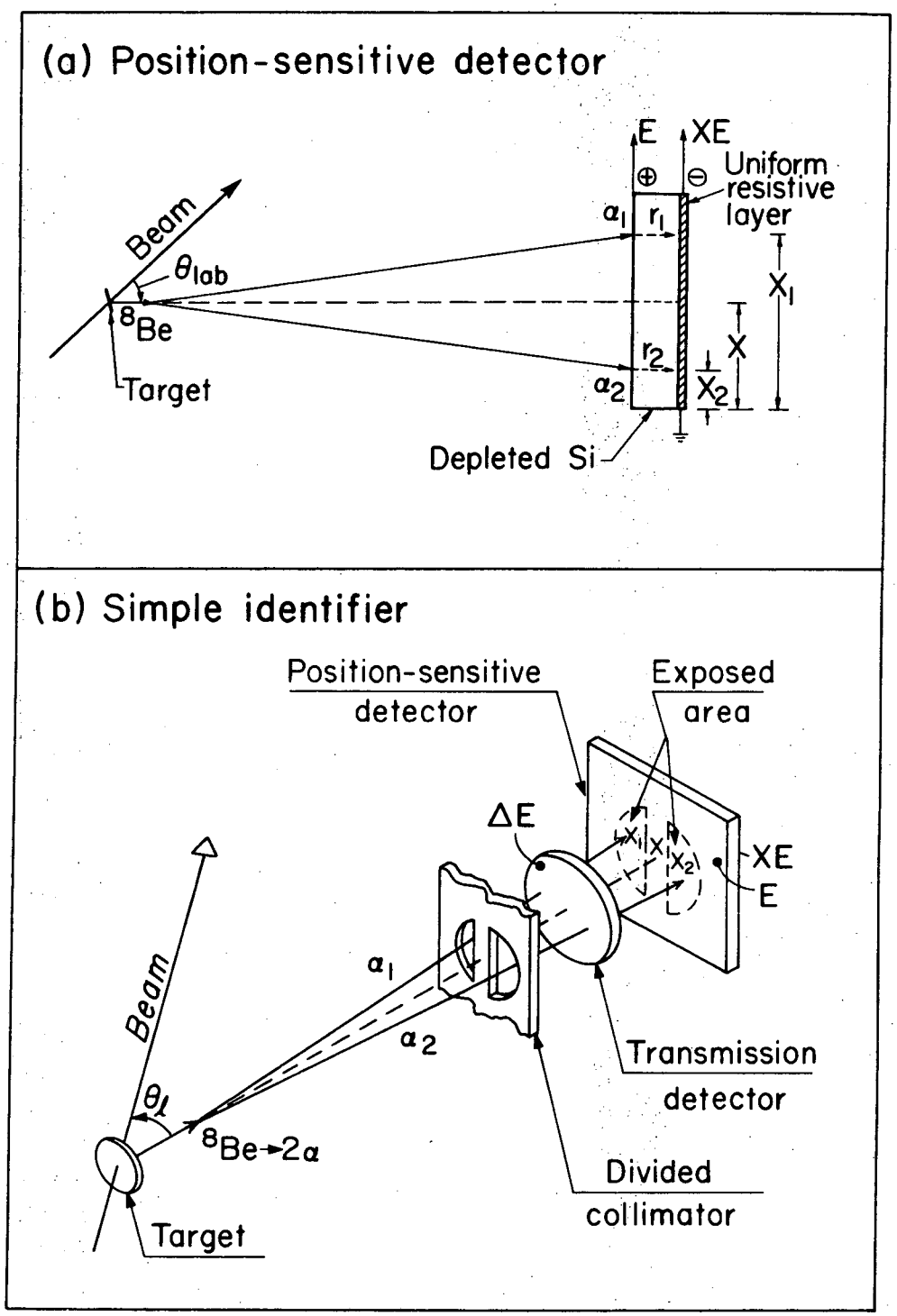

XBL 742-2323

Fig. 2-3. a) Determination of the ^{8}Be event's energy and direction using a PSD. See discussion in text. b) A schematic diagram of the simple ^{8}Be identifier showing the divided collimator, transmission detector and PSD.

As can be seen from Fig. 2-3a, this average position establishes the direction of the ^{8}Be event (θ_{lab}), and substantial kinematic broadening can therefore be avoided by gating the energy signals with position signals corresponding to a small angular range.

It is implied in the above derivation that the expression for X holds only to the extent that $E_1 = E_2$ and $\beta_1 = \beta_2$, and therefore that the direction of the ^{8}Be event (θ_{lab}) is correspondingly uncertain. However, since the measured position of the ^{8}Be event is given by:

$$X' = (X_1E_1 + X_2E_2)/(E_1 + E_2), \tag{2-5}$$

and because $X_1 = X + r_1$ and $X_2 = X - r_2$, then

$$X' = [(r_1 + X)E_1 + (X - r_2)E_2]/(E_1 + E_2). \tag{2-6}$$

The deviation (ΔX) of the measured ^{8}Be direction (X') from the true direction (X) is given by:

$$\Delta X = X' - X = (r_1E_1 - r_2E_2)/(E_1 + E_2). \tag{2-7}$$

Since the α-particle with the lower energy has the larger β and hence larger r, and vice versa (see Fig. 2-1), the products r_1E_1 and r_2E_2 are nearly equal. Expressing r_1, r_2, E_1, and E_2 in terms of the more convenient quantities D, Q, E_8, and γ (see Fig. 2-1), one obtains the following expression:

$$\Delta X = 1/2(DQ/E_8) \sin 2\gamma. \tag{2-8}$$

However, this equation must be modified when applied to the ^{8}Be identifier. As mentioned above, a transmission (ΔE) detector is introduced in front of the position-sensitive detector to reduce background. The energy loss in this detector modifies the above expression to the following one:

$$\Delta X = 1/2\,[\,DQ/(E_8 - \Delta E)]\,(1 + 3\Delta E/E_8)\,\sin 2\gamma. \qquad (2\text{-}9)$$

This is a small uncertainty which corresponds to an average error in the angle θ_{lab} of 0.1° for high energy ^{8}Be events detected with a counter telescope employing a 100 μm ΔE detector. The average value of $\sin 2\gamma$ was calculated with the FORTRAN program EFFICR (Je 74, see Section II-4).

2. Divided collimator

While good efficiency and energy resolution can be obtained with a position-sensitive detector alone, numerous particle-stable nuclei would also be detected, which would obscure ^{8}Be events except when these happened to be more energetic. To avoid this limitation, the high probability that the angular separation of the two breakup α-particles is close to its maximum value (~5°) is exploited to selectively detect ^{8}Be events. This selectivity is accomplished by using a divided collimator, which has a post subtending ~2°, to block out the central region of the position-sensitive detector, as is shown in Fig. 2-3b. Employing such a divided collimator eliminates particle-stable nuclei that are emitted within ~ ± 1° of the center of the detector. However, a subtantial fraction of the two α-particles from ^{8}Be nuclei emitted in this direction pass

one on either side of the post. As indicated in Fig. 2-3b, these events yield signals corresponding to the region of the position-sensitive detector masked by the post. Therefore, gating the energy signals by such position signals selects ^{8}Be events, while eliminating particle-stable nuclei.

3. Transmission detector

A divided collimator and a position-sensitive detector make a selective and efficient ^{8}Be detector. However, substantial background would arise at moderate counting rates (~15 kHz) from chance-coincident particles arriving within the pulse pair resolving time of the electronics. (All quoted counting rates give the number of counts in thousands averaged over one second.) The addition of a transmission detector reduces background in two ways. Because of the microscopic duty cycle of a cyclotron beam, the above background events can be categorized as originating from two different time regions. Inter-beam-burst pileup events are caused by chance-coincident particles produced by different beam-bursts occurring ~100 ns apart. Since energy signals from a position-sensitive detector have a slow and position-dependent risetime and thus poor timing characteristics, a transmission detector (see Fig. 2-3b) with a pileup rejector having a pulse pair resolving time of ~50 nanoseconds can eliminate inter-beam-burst background events.

Intra-beam-burst pileup events are not eliminated by the above pileup rejector since the beam-burst width of ~5 nanoseconds requires a pulse pair resolving time of <1 nanosecond to eliminate a substantial

fraction of these events. Although nearly all of these events are caused by particles which have sufficient energy to traverse the depleted depth of the PSD, most of them can not be eliminated by using a reject detector because commercially available PSDs have such thick undepleted back layers that a large fraction of these particles would fail to traverse the PSD. However, many of these intra-beam-burst background events can be eliminated by performing particle identification (PI) with the ΔE and E signals from the transmission and position-sensitive detectors. For nuclei stopping in the depleted depth of the PSD, an α-particle generates the following PI signal:

$$PI(\alpha) = (E_\alpha + \Delta E_\alpha)^{1.73} - E_\alpha^{1.73}, \qquad (2\text{-}10)$$

while two α-particles generate the following signal:

$$PI(2\alpha) = (E_{\alpha_1} + E_{\alpha_2} + \Delta E_{\alpha_1} + \Delta E_{\alpha_2})^{1.73} - (E_{\alpha_1} + E_{\alpha_2})^{1.73}. \qquad (2\text{-}11)$$

This particle identification signal which is generated by two α-particles that are simultaneously detected in a counter telescope can be expressed in terms of the one which is generated by a single α-particle and the fraction f of the total energy($E_T(2\alpha)$) carried by this α-particle ($E_1(\alpha)$):

$$PI(2\alpha) \approx 2^{1.73}\, PI(\alpha)/(4f(f-1)), \text{ where } f = E_1(\alpha)/E_T(2\alpha). \qquad (2\text{-}12)$$

The function f(f-1) has a single maximum at f = 1/2 (corresponding to equal energy α-particles) and thus PI(2α) has a single minimum and is larger for all other values of f. It should be noted that the condition that both α-particles traverse the ΔE detector restricts f to be larger

than $E_{min}/E_T(2\alpha)$, where E_{min} is the energy corresponding to an α-particle range equal to the thickness of the ΔE detector, which for a 100 μm ΔE detector corresponds to $f > 0.25$ for $E_T(2\alpha) < 50$ MeV.

On the other hand the fraction of the total energy carried by an α-particle produced by the decay of a high energy ^{8}Be nucleus is even more restricted ($0.45 \leq f \leq 0.55$) by the small breakup Q-value. As $f(f-1)$ is extremely slow varying (±1%) in this region near its maximum,

$$PI(^8Be) = PI(2\alpha)_{f = 0.50 \pm 0.05} = 2^{1.73}\ PI(\alpha) \qquad (2\text{-}13)$$

and therefore ^{8}Be events identify as a peak in the particle identification output.

Only a small fraction of the intra-beam-burst-pileup events correspond to two α-particles stopping in the depleted region of the PSD and because of the experimental broadening of the PI signal, most of these events generate PI signals which fall inside a gate set around PI (^{8}Be). However, the great majority of pileup events are caused by coincidences between high energy elastically and inelastically scattered α-particles where one or both traverse the depleted depth of the position-sensitive detector. Since an α-particle loses a substantial fraction of its total energy near the end of its range, one stopping in the undepleted region of the PSD will generally deposit a substantial amount of charge in this region which will not be collected. Thus α-α pileup events, where one or both of the α-particles stop in the undepleted region, give rise to particle identification signals ($PI(2\alpha)'$) which depend strongly on the fraction of the total energy (f') lost in the undepleted region, as can be seen by examining the following expression:

$$PI(2\alpha)' \approx [PI(^8Be)/(4f(f-1))][1-f'] \qquad (2\text{-}14)$$

Since the factor $f(f-1)$ is slowly varying and f' increases rapidly due to the end of the range effect, the latter dominates for most of these pileup events, causing $PI(2\alpha)'$ to be substantially smaller than $PI(^8Be)$. Therefore a large fraction of these pileup events (where one or both α-particles traverse the counter telescope) can be eliminated by setting a gate around the ^8Be PI peak. This results in a substantial background reduction at moderate counting rates. (This PI gate will also eliminate most of the intra-beam-burst-pileup events caused by one α-particle stopping in the ΔE detector and the other traversing it.)

4. Detection efficiency

When using the simple identifier, the magnitude of the acceptance solid angle (Ω_{acc}) for detecting ^8Be events is restricted to the solid angle subtended by the post of the divided collimator. (It should be noted that for experiments using the simple identifier, Ω_{acc} is defined (or limited) by a position gate which is always less than the post width.) Only a certain fraction of the ^8Be events emitted into Ω_{acc} are detected. This fraction is defined to be the detection efficiency (ϵ), and the product of ϵ and Ω_{acc} yields the effective solid angle ($\Omega_{eff}=\epsilon\cdot\Omega_{acc}$) for detecting ^8Be events.

By increasing the vertical size of the post of the divided collimator, both the acceptance solid angle and the efficiency are increased. The efficiency increases because ϵ is the average efficiency over the entire extent of the acceptance solid angle. This solid angle is

(Ω_{coll}). The ratio, $\Omega_{eff}/\Omega_{coll}$, is called the relative efficiency (ϵ_{rel}). Because of the finite extent of the breakup cone, there is an optimum diameter of the divided collimator for maximum relative efficiency. As can be seen from Fig. 2-4b this maximum is obtained for $\mathcal{D} \sim 1.5$ d_m. Over a restricted range of kinetic energies (35 - 70 MeV), the size of the breakup cone varies by only a small amount ($d_m \propto (E_8)^{-1/2}$), thus a fairly energy-independent and large ϵ_{rel} can be achieved. A rectangular divided collimator can also be used and similar considerations apply as for a circular one.

C. Modified Identifier

1. Twin transmission detectors

A substantial improvement to the simple identifier can be made by using, instead of a single ΔE detector, two ΔE detectors diffused side by side on a single silicon wafer (see Fig. 2-5). An order-of-magnitude reduction of intra-beam-burst pileup can then be achieved by making a subnanosecond coincidence between these detectors. Further reduction in background is possible through a comparison of the energy loss in each detector.

2. Intra-beam-burst pileup rejection

When ^{8}Be decays, the two breakup α-particles generally have different energies, and so different arrival times at the twin ΔE detectors. The maximum time difference (Δt_{max}) is given by:

$$\Delta t_{max} = 1.24\ D/E_8 \text{ nsec}, \qquad (2\text{-}15)$$

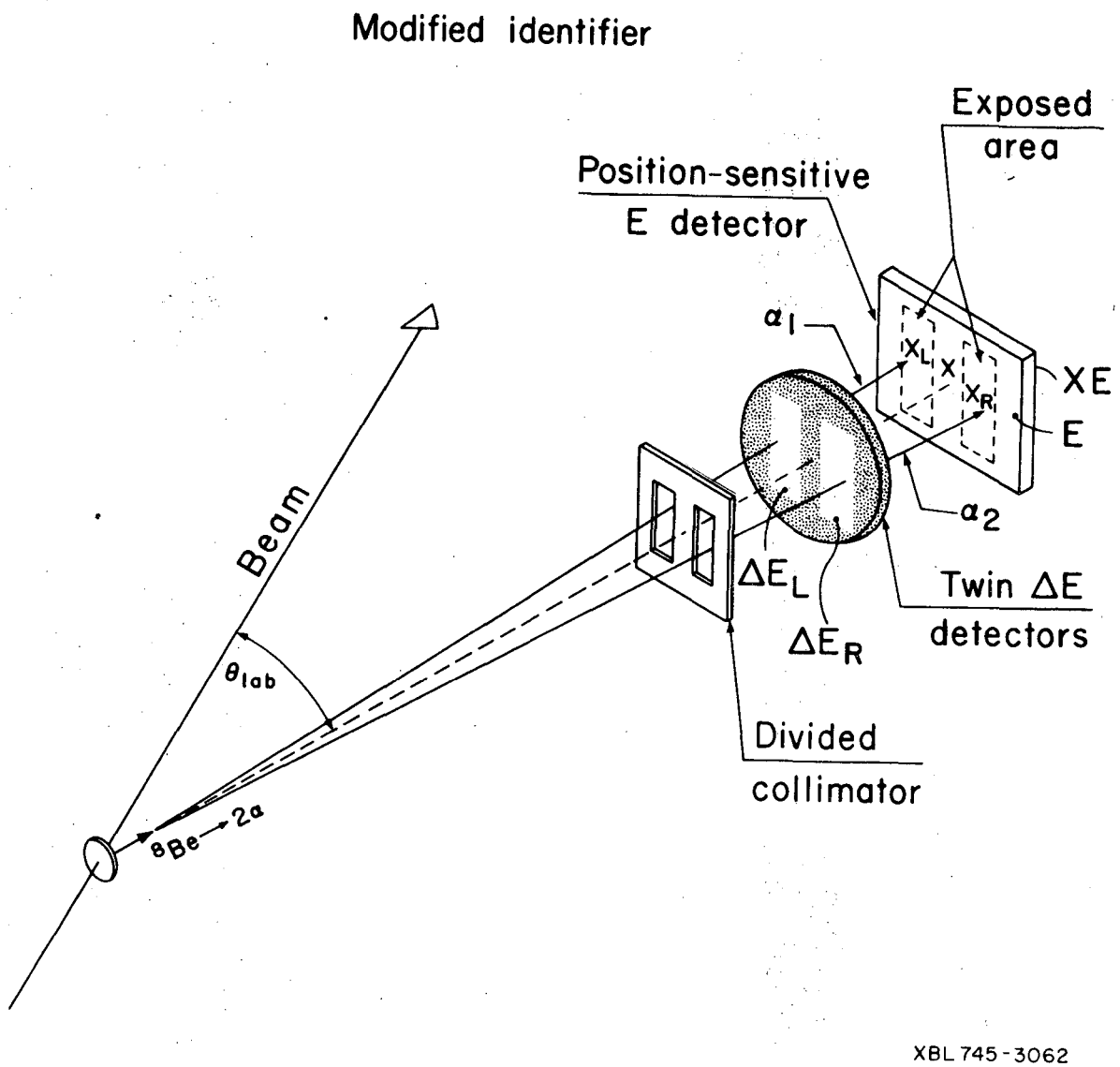

Fig. 2-5. A schematic diagram of the modified ^{8}Be identifier showing the divided collimator, twin transmission detectors and PSD.

where D is the distance from the target to the ΔE detector, and E_8 is the energy of the ^{8}Be event. For $E_8 > 35$ MeV and $D = 11.8$ cm, Δt_{max} is less than 0.42 nanoseconds. Therefore by performing a sub-nanosecond coincidence, the background can be reduced by a factor of ten, since the typical beam-burst width at the Berkeley 88-inch cyclotron is approximately five nanoseconds (at a frequency of 9 MHz).

3. Ratio requirement

Since both breakup α-particles from a ^{8}Be event have similar energies, the energy loss of α_1 in ΔE_L is approximately equal to that of α_2 in ΔE_R. By calculating the ratio $R = \Delta E_L/(\Delta E_L + \Delta E_R)$, ^{8}Be events are characterized by a ratio signal close to 1/2. Because two chance coincident particles will generally have different energies, setting an SCA about the ^{8}Be ratio peak will eliminate some intra-beam-burst pileup events.

4. Detection efficiency

When using the modified identifier, a ^{8}Be event can be characterized by a fast coincidence between the ΔE detectors, rather than by a position signal corresponding to the masked region of the E(PSD), and therefore the post need only be wide enough to cover the dead region between the detectors. (In the limit of a post width of zero, the acceptance solid angle (Ω_{acc}) would be restricted to the solid angle subtended by half the width of the "divided" collimator.) As the acceptance angle (Ω_{acc}) is no longer restricted by that of the post width, one can attain larger acceptance solid angles than were possible with the simple identifier.

To illustrate the dependence of Ω_{eff} on the collimator dimensions, a rectangular "divided" collimator with a line post (P = 0) is considered. In Fig. 2-6a the dependence of Ω_{eff} on the collimator width (W) is shown for two different values of the collimator height (H). The effective solid angle increases rapidly with W until a width equal to twice the size of the breakup cone diameter is reached whereupon it levels off. This flattening out is due to the necessity of having the breakup α-particles fall on either side of the central vertical dividing strip in the twin transmission detector in order to give a coincidence signal. Both Ω_{acc} and Ω_{eff} continue to increase as the height (H) of the collimator is increased. As for the simple identifier, Ω_{eff} is experimentally defined by the setting of the position gate.

The dependence of the detection efficiency (ϵ, solid curve) and the relative efficiency (ϵ_{rel}, dashed curve) on the collimator width (W) is shown in part b of Fig. 2-6. Both ϵ and ϵ_{rel} have a broad maximum at a collimator width of approximately one and one half times the breakup cone diameter and they have similar dependence on H as does Ω_{eff} for $H > d_m$.

In Fig. 2-6c a plot of the differential efficiency ($d\epsilon/dW$) illustrates the restriction of ^{8}Be events to a central vertical strip ($\pm$ W/4) of the collimator (corresponding to Ω_{acc}). Outside of this strip the detection efficiency is zero to the extent $\beta_1 = \beta_2$. Note that while the maximum value of $d\epsilon/dW$ is 50%, the average value (ϵ) is about 30%. Although the amplitude of the differential efficiency varies with the ^{8}Be energy, the shape is quite energy independent. Thus if an observed

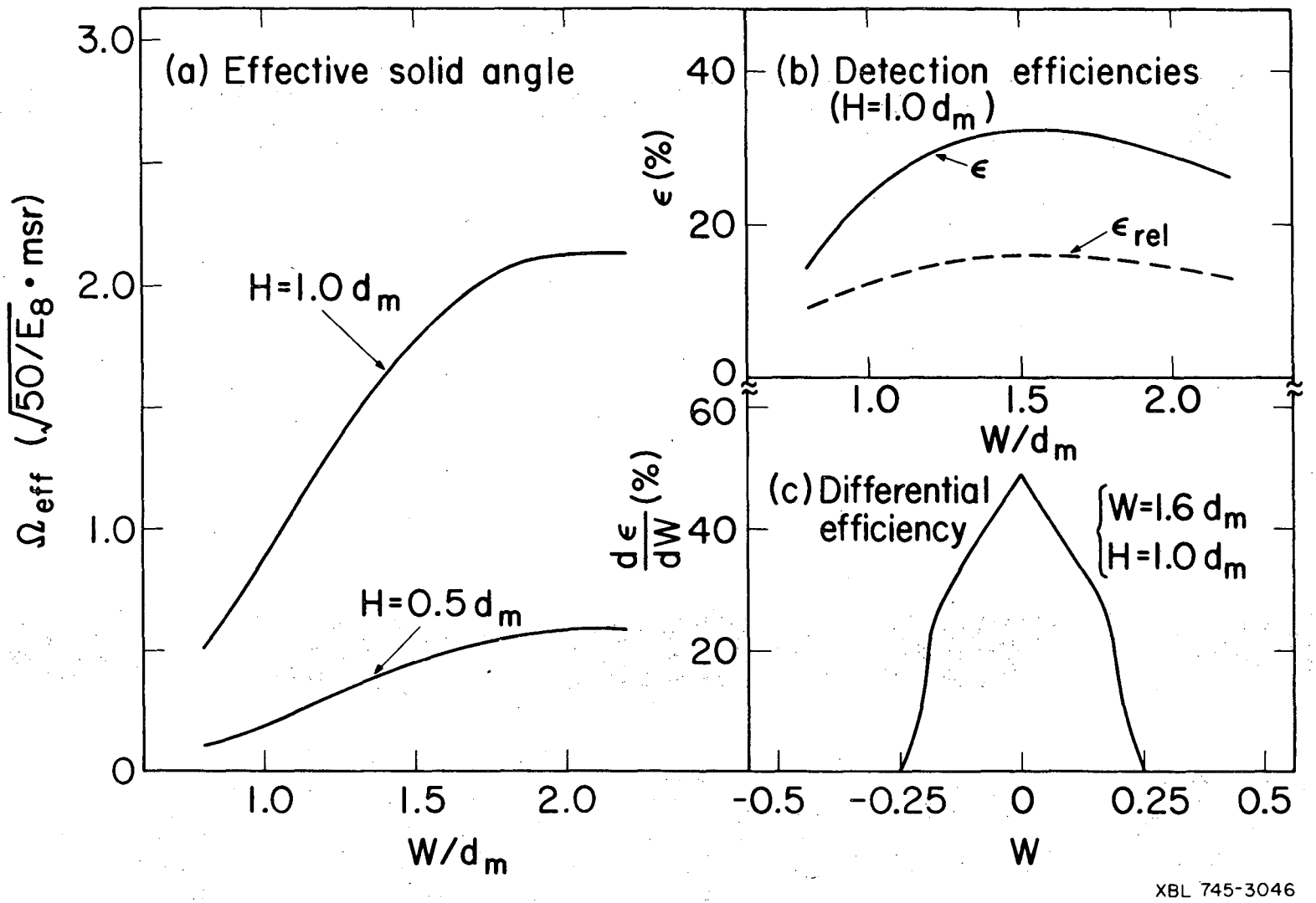

Fig. 2-6. a) The dependence of Ω_{eff} on the width (W) and height (H) of a rectangular "divided" collimator having a line post. E_8 is the energy of the ^{8}Be event in MeV and d_m is the diameter of its breakup cone. b) Calculated ϵ and ϵ_{rel} for collimators of different widths. c) A plot of the differential efficiency ($d\epsilon/dW$) across a PSD of width (W). Other symbols are defined in the text.

^{8}Be producing reaction has a constant differential cross section ($d\sigma/d\Omega$) across the acceptance angle (Ω_{acc}), the observed position spectrum should have a similar shape as the curve shown in part c of the above after folding in the position resolution. All the above considerations apply when considering a finite post width (P). (It should be noted that as in the case of the simple identifier for actual experiments Ω_{acc} is defined by the width of the position gates.)

The detector telescope was mounted on a platform inside the 0.51 meter scattering chamber. An aluminum housing with 1.5 mm thick tantalum shielding on the beam side enclosed the counter telescope and a 600 gauss permanent magnet was placed in front of it to deflect low energy electrons arising from projectile-electron collisions in the target. A turbomolecular pump with a liquid nitrogen cold trap to prevent the back streaming of pump oil kept the scatter chamber at a vacuum of 4×10^{-5} mm of Hg and an oil diffusion pump (see Fig. 3-1) maintained a vacuum of 5×10^{-6} mm of Hg in the beam line.

B. Targets

1. Solid targets

Self-supporting films of ^{10}B(98%), ^{11}B(98%), ^{12}C and SiO_2 were used as targets in these experiments. Up to seven targets plus an Al_2O_3 scintillator could be placed in a remotely controlled motor-driven target ladder. Target thicknesses were determined at the end of an experiment by placing a thin ^{212}Pb source behind the target and measuring the energy loss of the α-particles passing through it. In addition for targets of natural isotopic composition a 1 cm^2 central circular portion was weighed on a microbalance. Good agreement was obtained between these two methods so that the target thicknesses were known to ± 10%.

2. Gas targets

A gas target and recovery system which has been described previously (Br 69) was used for experiments with chemically pure

$^{14}N_2$, $^{16}O_2$ and isotopically enriched $^{15}N_2$(99%) gases at a pressure of one-third of an atmosphere. The gas pressures were measured with a mercury manometer and monitored remotely by a TV camera focussed on the mercury level. The 6.4 cm diameter gas cell consisted of two stainless steel disks supported by a 45° wedge between them. A 3.2×19.9 cm strip of 5 μm thick Havar[1] foil glued to the upper and lower disks formed a continuous 315° window.

To define the extent of the target from which ^{8}Be events could be observed, an unusual gas collimator was designed and built. This collimator could be used with either the simple or modified ^{8}Be identifiers (see Fig. 3-2, the ^{8}Be gas collimator is shown here with a modified identifier). In addition to the normal divided collimator immediately in front of the counter telescope, a second one is placed nearer to the gas cell. This front collimator defines the extent of the target (removing the possibility of detecting reaction products from the gas cell walls).

To reduce the singles counting rate in the twin ΔE detectors, a 0.5 millimeter tantalum partition connected the posts of the two collimators. This partition eliminated particles passing through different sides of the front and back collimators. The relative alignment of the left-right partition and the two divided collimators is important and was done to ± .03 mm on an optical comparator. To shield the counter telescope from seeing slit-scattered beam, two 1.3 mm thick aluminum plates were attached to and connected the outsides of the divided collimators (not shown in Fig. 3-2) on both sides of the gas collimator.

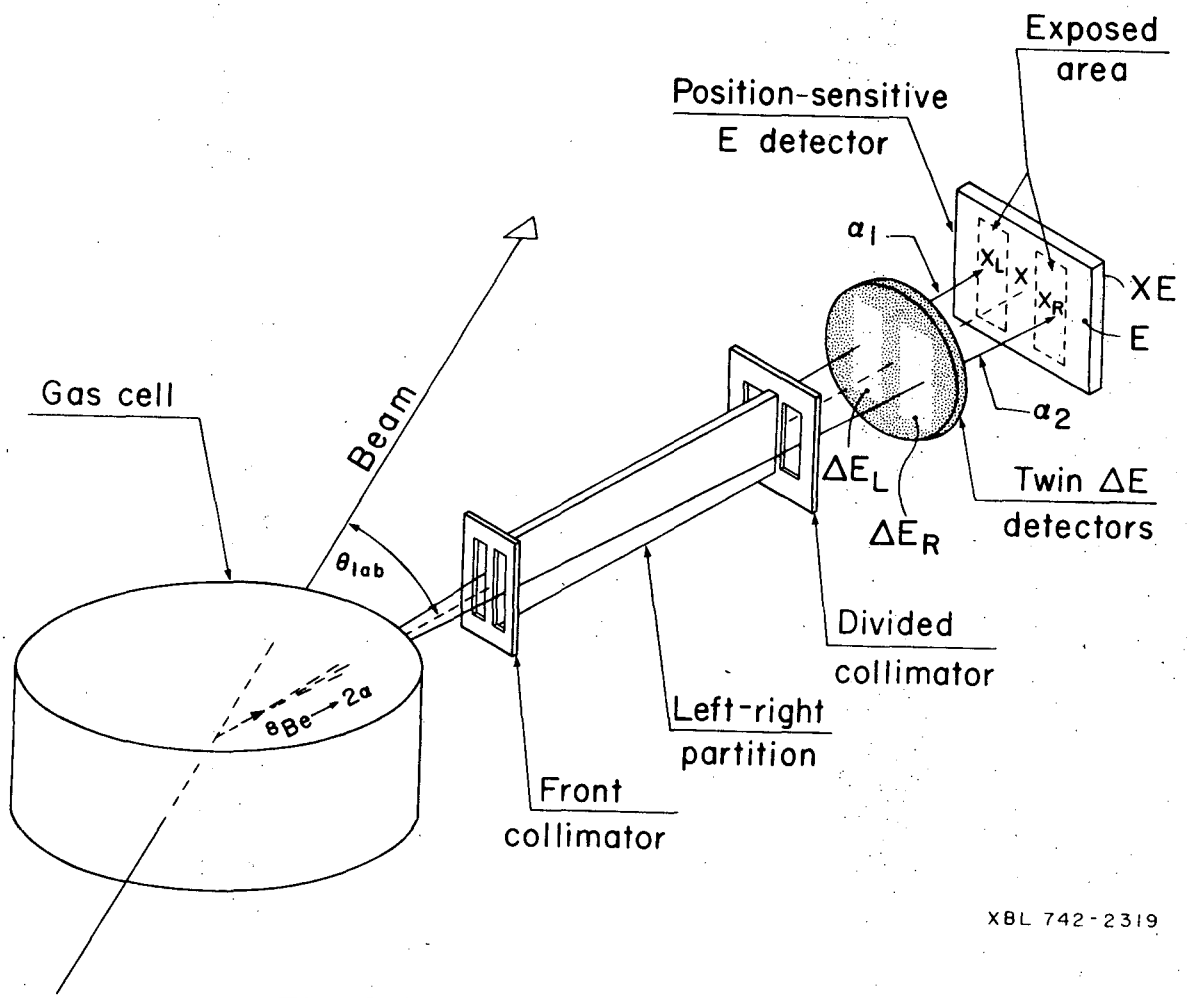

Fig. 3-2. A schematic diagram of a gas cell and the ^{8}Be gas collimator, here shown with a modified ^{8}Be identifier.

Previously described detection efficiency considerations have assumed a solid target although similar considerations apply for a gas target. The probability of detecting a ^{8}Be nucleus emitted from a gas target was determined by making a simple first order correction to the detection efficiency and by using oxygen gas and solid target data to normalize the gas target cross sections.

C. Simple Identifier

1. Detectors and equipment

A surface-barrier position-sensitive detector[2] having an active area of 10×50 mm and a 300 μm depletion depth was used in all experiments with the simple identifier. This PSD had a position resolution of 1% (~0.5 mm) of its length and an energy linearity of 7%. Only a 10×10 mm section (at the end from which the XE signal originated) was used. In this region the position resolution and linearity were 0.6 mm and 2%, respectively. The measured energy resolution and the observed change in pulse-height across the PSD were 70 keV FWHM and 100 keV, respectively, for 8.75 MeV α-particles.

Fully depleted phosphorus-diffused transmission detectors having depletion depths of 125 μm or 200 μm and circular (10 mm diameter) active areas were used depending on the experiment. Rectangular transmission detectors were also used. These were fabricated at LBL by making two 4.5×10 mm active areas separated by a two millimeter undiffused region in a 190 μm thick silicon wafer. These twin detectors act as a large area detector (10×11 mm) when the right and left signals are added. Since the same wafer is used for both ΔE_L

and ΔE_R, good uniformity and hence good particle identification is ensured. This technique takes advantage of the fact that the central region of the ΔE detector is not used since it is masked by the central post of the divided collimator.

In Fig. 3-3 is shown the housing for the simple identifier. It consisted of detector holders, shielding, a movable collimator, a remotely controlled electric motor, gearing and a helipot. This housing fitted into a vertically adjustable sleeve and was attached to the upper rotating ring of the scatter chamber through a horizontal sleeve which enabled the identifier to target distance to be changed (see Fig. 3-3).

The movable collimator defined the radial acceptance angle and contained five collimator patterns cut into a rectangular tantalum plate (on a common centerline to ±1 mil) which moved in a teflon slide. A fixed collimator recessed in the slide-backing defined the vertical acceptance angle and immediately behind it were mounted the ΔE and E (PSD) detectors. Relative alignment of the counter telescope components was accomplished by adjusting the detectors and the fixed collimator's positions. Final alignment of the counter telescope was performed in the scatter chamber by observing it with a transit at $\theta_{lab} = 180°$ and placing the identifier in the median scattering plane by adjusting its height in the vertical sleeve. Each collimator pattern was then centered in the median plane and its position noted by a DVM reading of the voltage drop across the helipot attached to the motor-drive gear.

The movable collimator was usually placed seven and a half centimeters from the target and at this distance the divided collimator

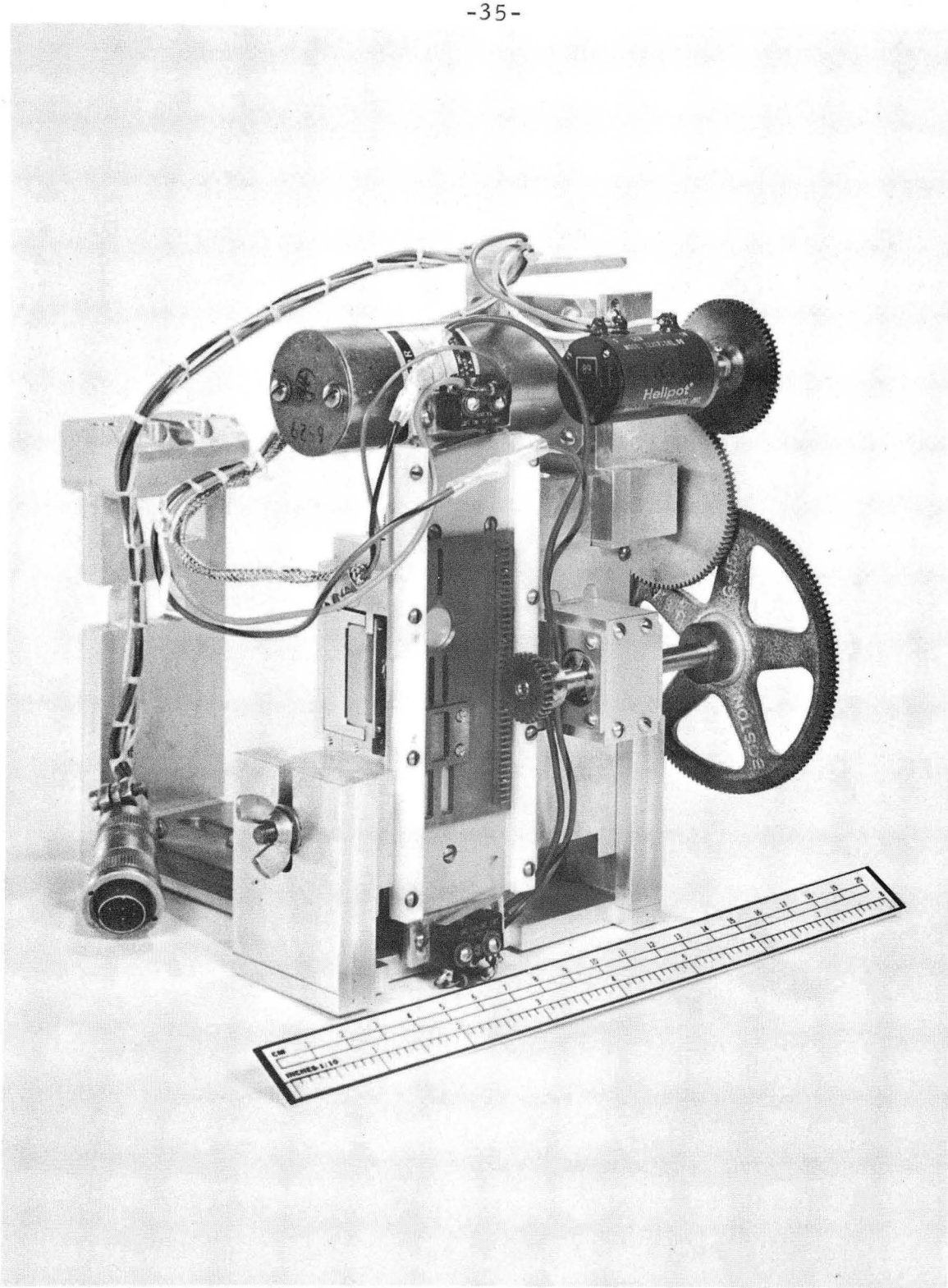

CBB 745-3082

Fig. 3-3. A photograph of the simple ^{8}Be identifier with a remotely-controlled and motor-driven movable collimator.

had a radial and vertical acceptance angle of six degrees and a central post width of two degrees. With this geometry, forward angle observations were possible to a minimum angle of twelve degrees, and near maximum relative efficiency (ϵ_{rel}) was attained for the range of ^{8}Be events stopped by the identifier (35-60 MeV). The beam spot size (1.5×2.0 mm) was equivalent to one degree and a one degree position gate was set. These conditions gave adequate energy resolution and detection efficiencies (ϵ) of 12-23% for 35-60 MeV ^{8}Be events emitted into the acceptance solid angle defined by a 1° central position gate. The intrinsic position resolution of the above detector was 1/2° and the two degree post width ensured the complete elimination of particle-stable nuclei from the central region of the position-sensitive detector.

2. Electronics

A block diagram of the electronics for the simple ^{8}Be identifier is shown in Fig. 3-4. Signals from the ΔE and E(PSD) fed three amplifier systems and a pileup rejector (PUR). This last unit established a coincidence (2τ = 50 ns) between the ΔE and E signals and inspected for pileup arising from different beam bursts over 1.5 microseconds. In the absence of such inter-beam-burst pileup, a valid-event signal was generated.

To minimize deadtime caused by the high counting rate in the ΔE detector, double-delay line shaping was used to provide short signal shaping times and fast baseline recovery. Because signals from the E(PSD) have a slow and position-dependent risetime, a linear amplifier with a two microsecond peaking time was used for both the E

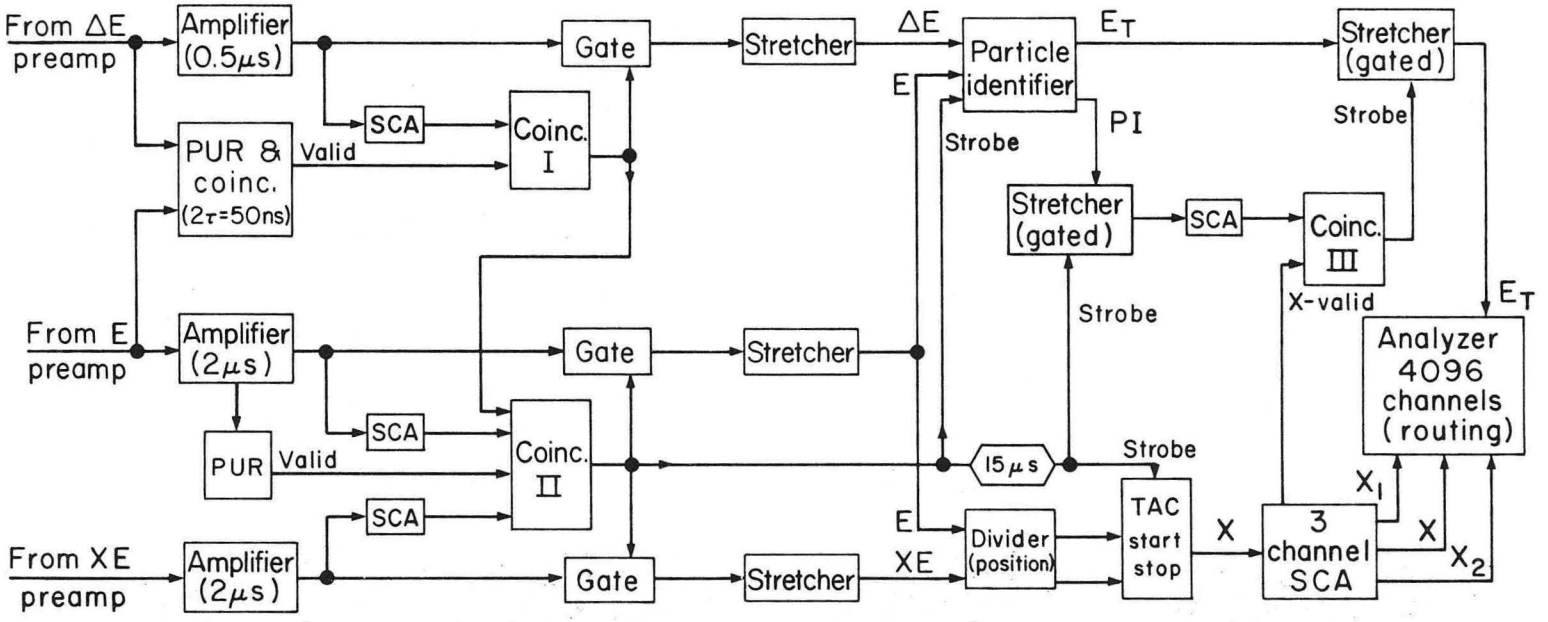

XBL 742-2321

Fig. 3-4. An electronic block diagram for the simple ^{8}Be identifier.

and the XE signals. A pulse from the E amplifier was used to feed a pileup rejector which inspected over the duration (~ 8 μs) of the E signal (the counting rate in the E(PSD) was typically a factor of four less than in the ΔE). The E and XE signals were connected to a divider, which converted the position information into a time difference, and a time-to- amplitude converter was used to give a voltage signal proportional to the position. The ΔE and E signals fed a particle identifier. Both particle identification (PI) and position gates were set with single channel analyzers (SCAs) and energy spectra, gated by these, were collected on a Nuclear Data 4096 channel analyzer. Gated and ungated PI and position spectra were monitored during experiments.

3. Position and particle identification

To calibrate the position spectra obtained with the simple identifier, the movable collimator was used to place before the counter telescope a collimator consisting of two narrow slits separated by approximately five degrees. The dimensions of this collimator were measured to ± 0.03 mm on an optical comparator before the experiment. In addition the target-to-movable collimator distance and its distance from the position-sensitive detector were measured to ± 0.3 mm.

In Fig. 3-5a is shown two position spectra obtained in sequential runs at different movable collimator settings. These spectra were collected at $\theta_{lab} = 15 \pm 3°$ during the bombardment of a carbon target with 65 MeV α-particles. The counting rate in the ΔE detector was 15 kHz. Only events satisfying the condition of no inter-beam-burst

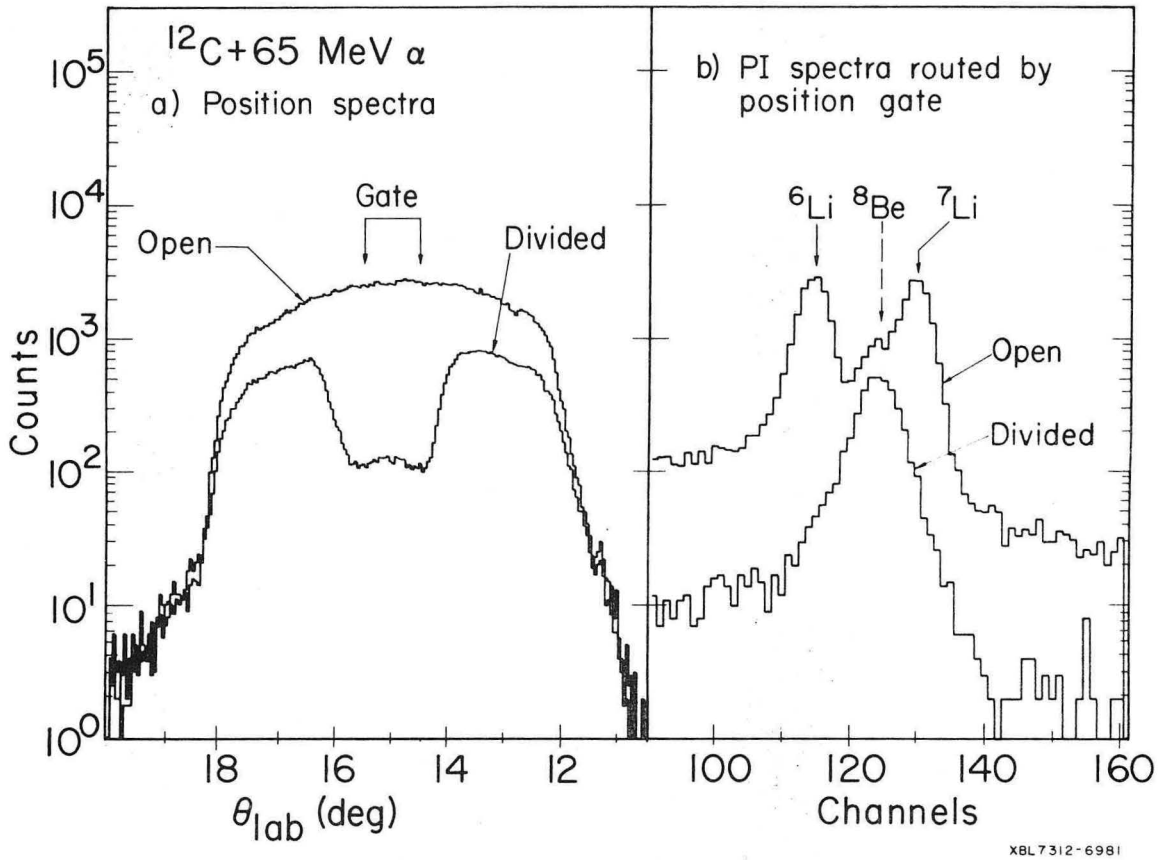

Fig. 3-5. Position (a) and particle identifier (b) spectra obtained with the simple ^{8}Be identifier. (See text).

pileup, a ΔE energy SCA (set to eliminate $Z = 1$ and 2 events) and an E-lower threshold of 8 MeV were recorded. The upper spectrum was taken with an open circular collimator, and the lower with a circular divided one. The elimination of particle-stable nuclei is illustrated in the lower spectrum. The counts in the central region of this lower spectrum are from ^{8}Be events with a small number from intra-beam-burst pileup events.

In Fig. 3-5b are shown PI spectra of events satisfying the one degree position gate indicated in part (a). The upper spectrum shows the identification of the particle-stable nuclei, ^{6}Li and ^{7}Li, with the relatively abundant ^{8}Be events appearing as a shoulder on the ^{7}Li peak. The lower spectrum, collected with the divided collimator, is characterized by the absence of lithium isotopes and the occurrence of a single peak (see Section II-B3) at the location predicted for ^{8}Be events by range-energy calculations (Wo 72). Nearly all background events seen above and below this peak correspond to intra-beam-burst α-α pileup. A relatively small fraction of these correspond to both chance coincident α-particles stopping in the sensitive region of the PSD and the PI signals for these events lie close to the position of the ^{8}Be peak. However, as the energy of one or both of the α-particles increases above the maximum capable of being stopped in the depleted region of the PSD, the PI signal for such a pileup event rapidly decreases in magnitude. As discussed in Section II-B3 this strong dependence of the PI signal on the fraction of the total energy deposited in the counter telescope is due to an end of the range effect. Consequently, at moderate

counting rates (15 kHz), nearly all pileup events are eliminated by setting a PI gate around the ^{8}Be peak.

Energy spectra (see Fig. 3-6) of the ^{11}B(α, ^{7}Li)^{8}Be and ^{11}B(α, ^{8}Be)^{7}Li reactions at θ_{lab} = 15 and 16.5 degrees, respectively, and E_{α} = 65 MeV were accumulated in two hours with a simple identifier. A 100 μg/cm^{2} ^{11}B target (enriched to 98%) was used and an experimental resolution of 600 keV was obtained at a counting rate in the ΔE detector of 19 kHz, which caused a 9% deadtime. One can clearly see from comparing part (a) with part (b) of Fig. 3-6 that there is total discrimination in the (α, ^{8}Be) data against ^{7}Li events. Transitions populating the ground and second excited states (Se 74) of ^{7}Li are seen. Preferential population of these states is expected on the basis of calculated α-particle structure factors (Ku 73). The measured cross-section to the ^{7}Li$_{gs}$ is 3.2 μb/sr c.m. at this angle, which, after allowing for the detection efficiency (21%), corresponds to an absolute cross-section of 15 μb/sr c.m. No contribution from the (α, ^{8}Be*(2.9 MeV)) reaction (Ro 73, see also Cr 73 for a discussion of a method for detecting ^{8}Be* events) was observed, which is in agreement with the low calculated detection efficiency (~ 0.5%) for ^{8}Be* events. The moderately low level of counts above the ^{7}Li$_{gs}$ peak is due to intra-beam-burst chance coincident events that fall within the ^{8}Be PI gate. This level of background is indicative of the background contribution to spectra taken at 19 kHz with the simple identifier, and is equivalent to an absolute differential cross section limit of ~1 μb/sr c.m.

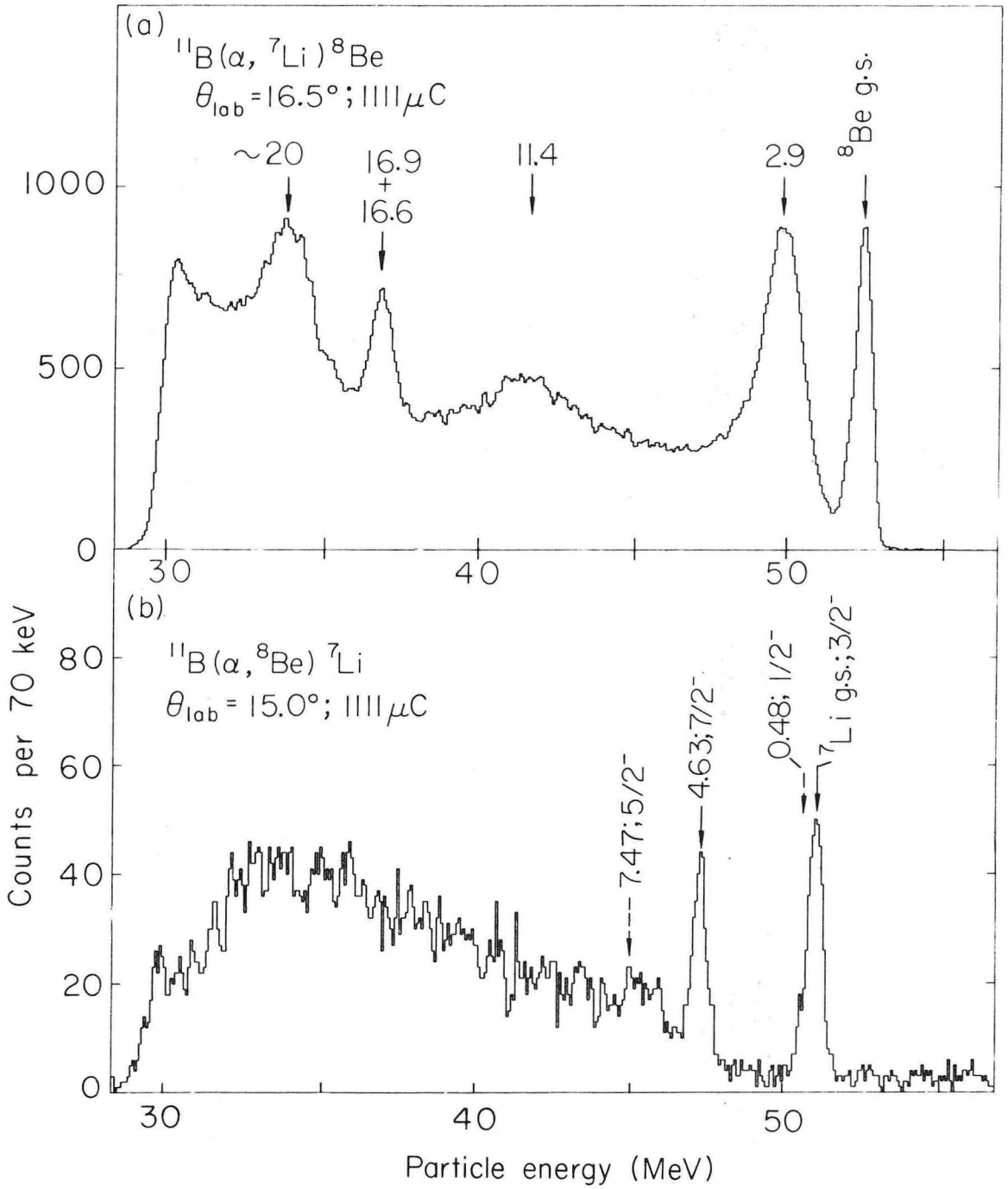

Fig. 3-6. Energy spectra taken at 65 MeV bombarding energy with the simple ^{8}Be identifier. (a) ^{7}Li and (b) ^{8}Be energy spectra, obtained concurrently by setting appropriate PI and position gates, from the reactions $^{11}B(\alpha, {}^{7}Li)^{8}Be$ and $^{11}B(\alpha, {}^{8}Be)^{7}Li$, respectively, after 1111 μC.

D. Modified Identifier

1. Detectors and equipment

In the modified identifier, besides requiring a fast coincidence and comparing the relative energy loss in the twin transmission detectors, larger area detectors were used. These allowed the identifier to be placed farther from the target while subtending the same solid angle as before, and hence maintaining good detection efficiency. At this greater distance (D = 11.8 cm), more forward angles could be studied and the contribution of the beam spot size to the energy resolution was decreased.

A 13×20 mm position-sensitive detector[2] was used which had a position resolution of 0.1 mm, (≡ 0.1°) and an energy linearity of better than 1%. Its 500 μm depletion depth, in conjunction with a 110 μm twin ΔE detector, enabled up to 70 MeV ^{8}Be events to be detected. The twin ΔE detector consisted of two fully depleted phosphorus-diffused transmission detectors, ΔE_L and ΔE_R, having 5.5×12 mm active areas separated by a one millimeter undiffused region.

The experimental setup constructed for the modified identifier is shown in Fig. 3-7. It consisted of a fixed collimator holder followed by a ΔE and a E(PSD) holder all of which were attached to an aluminum plate fastened to the lower rotating ring of the scatter chamber. The telescope housing, shielding and electron-suppression magnet are not shown here. To the right of the counter telescope is shown one of the twin transmission detectors with low inductance strip leads. Alignment of the counter telescope components relative to each other and of the telescope itself in the median scattering plane was accomplished in

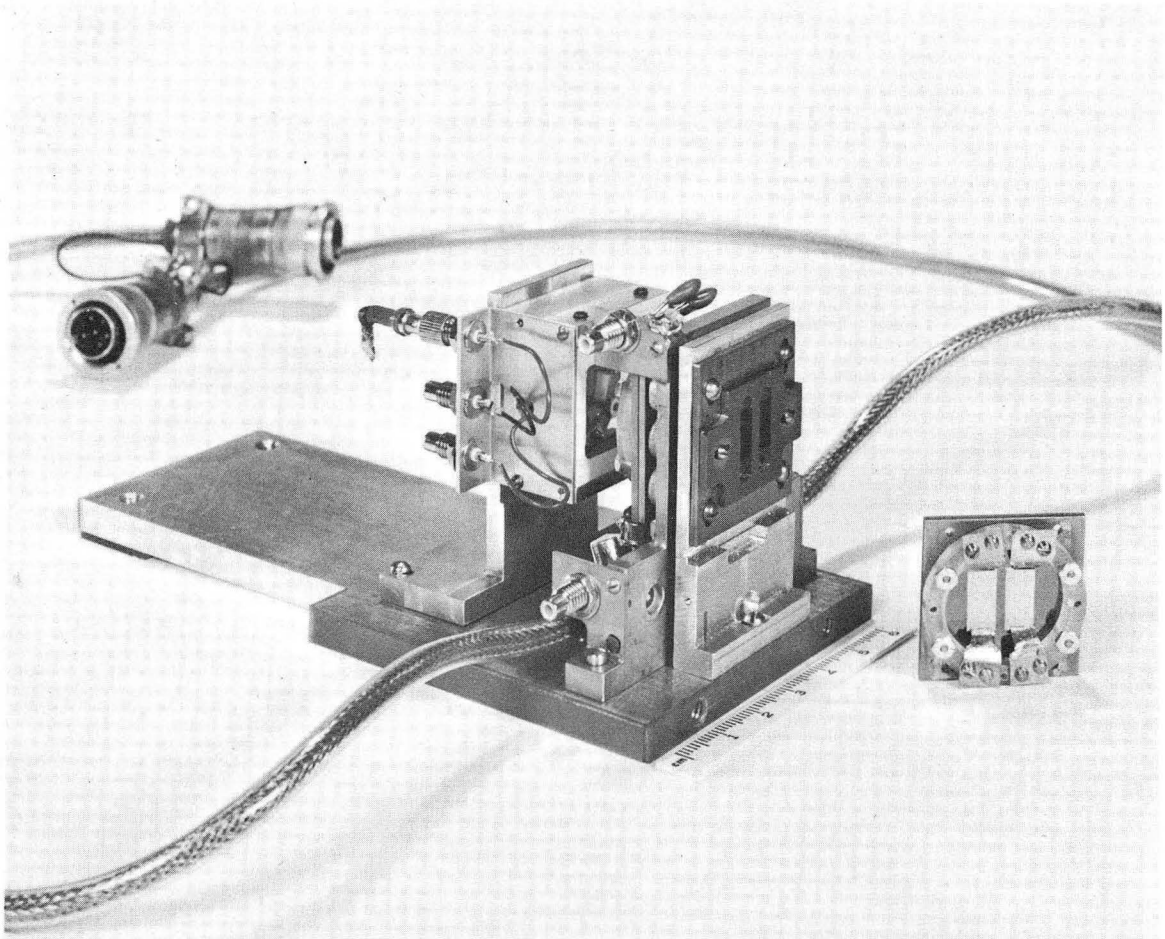

CBB 745-3084

Fig. 3-7. A photograph of the modified ^{8}Be identifier showing the divided collimator, twin transmission detectors and fast preamp head as an integral part of the detector holder, and the PSD and its holder. To the right of the identifier is a twin transmission detector (without the preamp head) mounted in a holder with strip-contact leads for the pulser (upper) and the output signal (lower).

a similar manner to that described above for the simple identifier.

2. Electronics

To measure the difference in the flight times (ΔTOF) of the two α-particles from ^{8}Be decay, two fast preamplifiers are used, whose first stages are mounted on the holder for the twin ΔE detectors. These preamplifiers are similar to the one described by Butler et al. (Bu 70), but with a charge-sensitive (slow) output added to give greater energy stability. The FET in the first stage of the preamplifier is connected by a low inductance strip to the surface of the detector. This detector is made with a low sheet resistance ($< 10\ \Omega/cm^2$) and the short direct coupling produces very fast risetime pulses (< 2 ns).

The 110 μm twin transmission detectors have a low capacitance (~ 70 pF), which gives a good signal to noise ratio, and they hold a voltage gradient (2 volts/μm), which ensured fast (< 1 ns) collection of the deposited charge. As indicated in the block diagram of the electronics for the modified identifier (see Fig. 3-8), the fast outputs of the ΔE_L and ΔE_R preamplifiers feed two constant-fraction discriminators (CFD), which are connected to a time-to-amplitude converter (TAC). The range of energy deposited in the ΔE detectors by α-particles varied between 4 and 11 MeV, but no time-walk-with-amplitude compensation is required for good time resolution, since ^{8}Be events generate ΔE_L and ΔE_R signals of approximately equal amplitude. By injecting charge on the detector surface with a fast pulser (< 1 ns rise-time), a simulated ^{8}Be event ($\Delta E_L = \Delta E_R = 8.75$ MeV, $E_8 = 32$ MeV) gave a time resolution of 140 picoseconds FWHM. The division of the ΔE_L amplitude

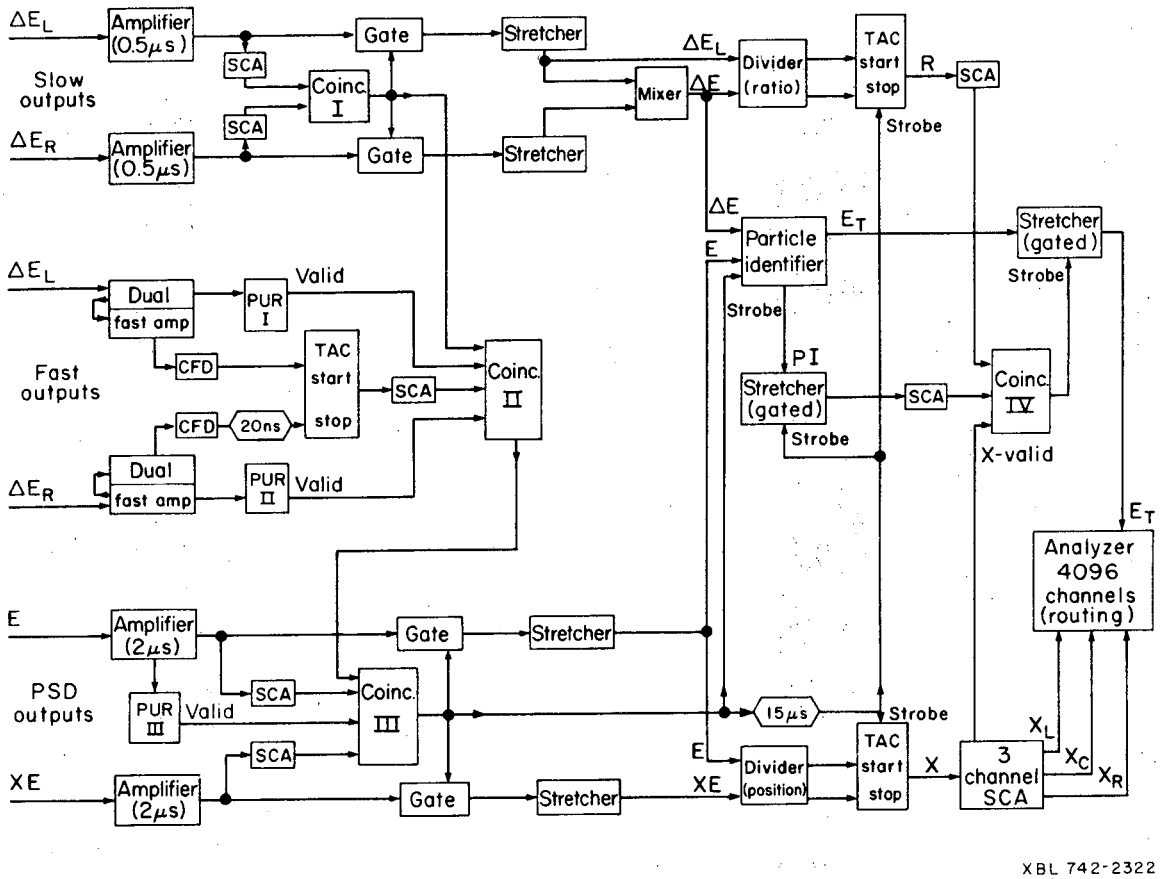

Fig. 3-8. An electronic block diagram for the modified ^{8}Be identifier.

by the summed ΔE_L and ΔE_R amplitudes to yield the ratio R is carried out in a similar manner to the XE/E division (see Fig. 3-4). Particle identification (PI), position (X), ratio (R) and time of flight (ΔTOF) gates are set with single channel analyzers (SCAs) and energy spectra, gated by these, are collected on a Nuclear Data 4096 channel analyzer. Gated PI, position, ratio and ΔTOF spectra are monitored during experiments.

3. Background reduction

Figure 3-9 presents a ΔTOF spectrum (ΔE_L(start) - ΔE_R(stop)) of events originating from the same beam burst. These events, from the bombardment of a ^{10}B target with 72.5 MeV α-particles, were detected with the modified identifier at $\theta_{lab} = 24°$. The symmetric double peak is due to ^{8}Be events. Background counts are caused by fragmentation reactions and random chance coincident events associated with the high counting rate of 25 kHz in each of the ΔE detectors (intra-beam-burst rate 500 kHz). The full width at the base of the ΔTOF peak (~1 ns) reflects the minimum energy (~30 MeV) ^{8}Be event that could be detected, and the central dip is the effect of collimation on the breakup α-particle velocity distribution. If the identifier had 100% detection efficiency and perfect time resolution, then the ΔTOF peak would be rectangular with a width of $2\Delta t_{max}$. This is most closely realized for ^{8}Be nuclei emitted toward the center of the identifier. However, for those emitted off center, the first part of the breakup cone that is lost through collimation is the edge. Therefore, most of the ^{8}Be events emitted into the acceptance solid angle, that are not detected, correspond to the breakup α-particles

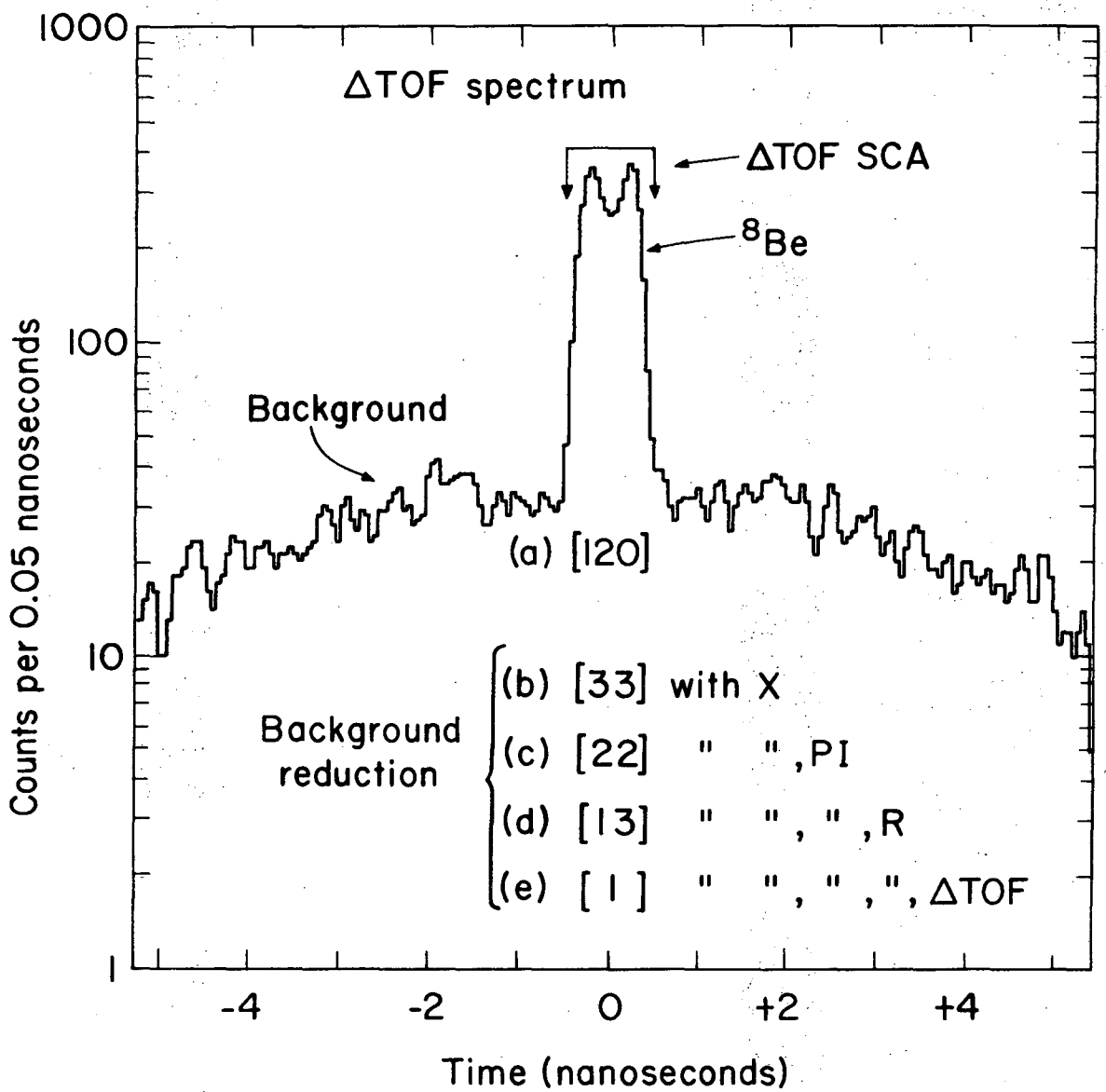

XBL 742-2318

Fig. 3-9. A ΔTOF spectrum, ΔE_L(start) -ΔE_R(stop), of events originating from the same beam burst. The ratio of the total background to ^{8}Be events decreases from 120% to 1% as various SCA requirements are introduced.

having approximately equal velocities, and therefore equal time-of-flights, hence the central dip in the ΔTOF spectrum.

In the spectrum shown in Fig. 3-9, only events depositing more than 10 MeV in the E detector, and satisfying a ΔE_L - ΔE_R inter-beam-burst coincidence (2τ = 50 ns) and ΔE energy SCAs (set to eliminate Z = 1 and 3 particles), were recorded. The total number of intra-beam-burst background counts, expressed as a percentage of the number of ^{8}Be events, is 120% for the above conditions (see (a) in Fig. 3-9). As further SCA requirements are made: (b), (c), (d), and (e), the background decreases considerably with only a 25% loss in the number of ^{8}Be events which is almost entirely due to the setting of a restricted X gate ($X \equiv X_L + X_C + X_R$, see Fig. 3-10b). The lowest background is achieved when the position signal is restricted to fall within the ^{8}Be acceptance angle (X SCA); the PI falls in the calculated region for ^{8}Be events (PI SCA); the ratio is close to one-half (R SCA); and the ΔTOF signal corresponds to a time difference $\leq \Delta t_{max}$ (ΔTOF SCA). All these conditions are characteristic of ^{8}Be events. With these requirements the total background in a ^{8}Be energy spectrum is 1% of the number of ^{8}Be events, at a counting rate of 25 kHz in each ΔE detector.

4. X, PI, R, and ΔTOF spectra

Figure 3-10 shows a particle identification and a position spectrum obtained with the SCA conditions discussed above, except that their respective SCAs were not required. In Fig. 3-10a the PI spectrum is dominated by a single peak occuring in the expected location for ^{8}Be events (Wo 72) with very little background above and below

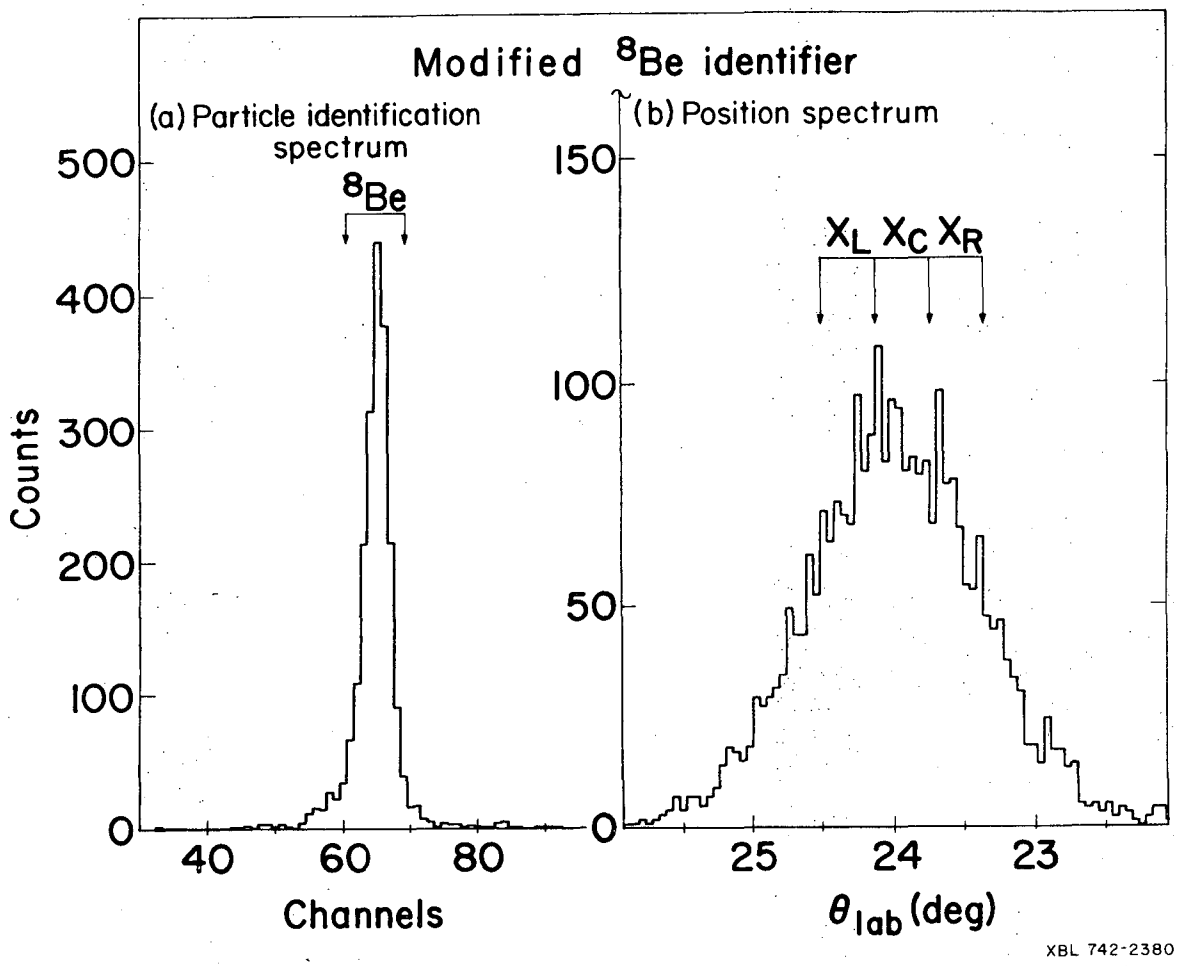

Fig. 3-10. Particle identification (a) and position (b) spectra obtained with the modified ^{8}Be identifier.

this peak. (The ΔE_L - ΔE_R coincidence requirement eliminates particle stable nuclei.) The peaking of the position spectrum, shown in Fig. 3-10b, at 24° (the angle of the center line of the divided collimator's post) arises because ^{8}Be nuclei emitted in this direction have the largest probability of yielding breakup α-particles which satisfy the ΔE_L - ΔE_R coincidence condition.

A ratio spectrum, with the above PI and X SCA requirements, is given in Fig. 3-11b. The double peaking in this spectrum corresponds to that seen in the ΔTOF spectrum shown in Fig. 3-9. If the lower velocity alpha from a ^{8}Be event traverses ΔE_L and the higher velocity one traverses ΔE_R, this corresponds to a negative time difference in the ΔTOF spectrum. It also corresponds to a higher ΔE_L energy loss ($dE/dx \propto E^{-1}$), and therefore a ratio greater than one-half. This equivalence is demonstrated in Fig. 3-11c (ii).

In Fig. 3-11c (i) a ΔTOF spectrum, routed by the wider R SCA, is shown. The shape of this peak is closely predicted as can be seen from the calculated peak shapes for 45 and 65 MeV ^{8}Be events given in part (a). These ΔTOF spectra were calculated with the program EFFICR. (The asymmetry in the experimentally observed ΔTOF peak of Fig. 11c (i) is due to a slight asymmetry in the position gates.)

The relationship between the amplitude of the ratio (R) and that of the ΔTOF (T), illustrated in Fig. 11c (ii), demonstrates that further background reduction is possible. Expressing $R = R_o + \Delta R$ and $T = T_o + \Delta T$, where R_o and T_o corresponds to a ratio of one-half and to a time difference of zero, respectively, yields:

$$\Delta R \propto -\Delta T \cdot (E_8)^{1/2}. \qquad (3\text{-}1)$$

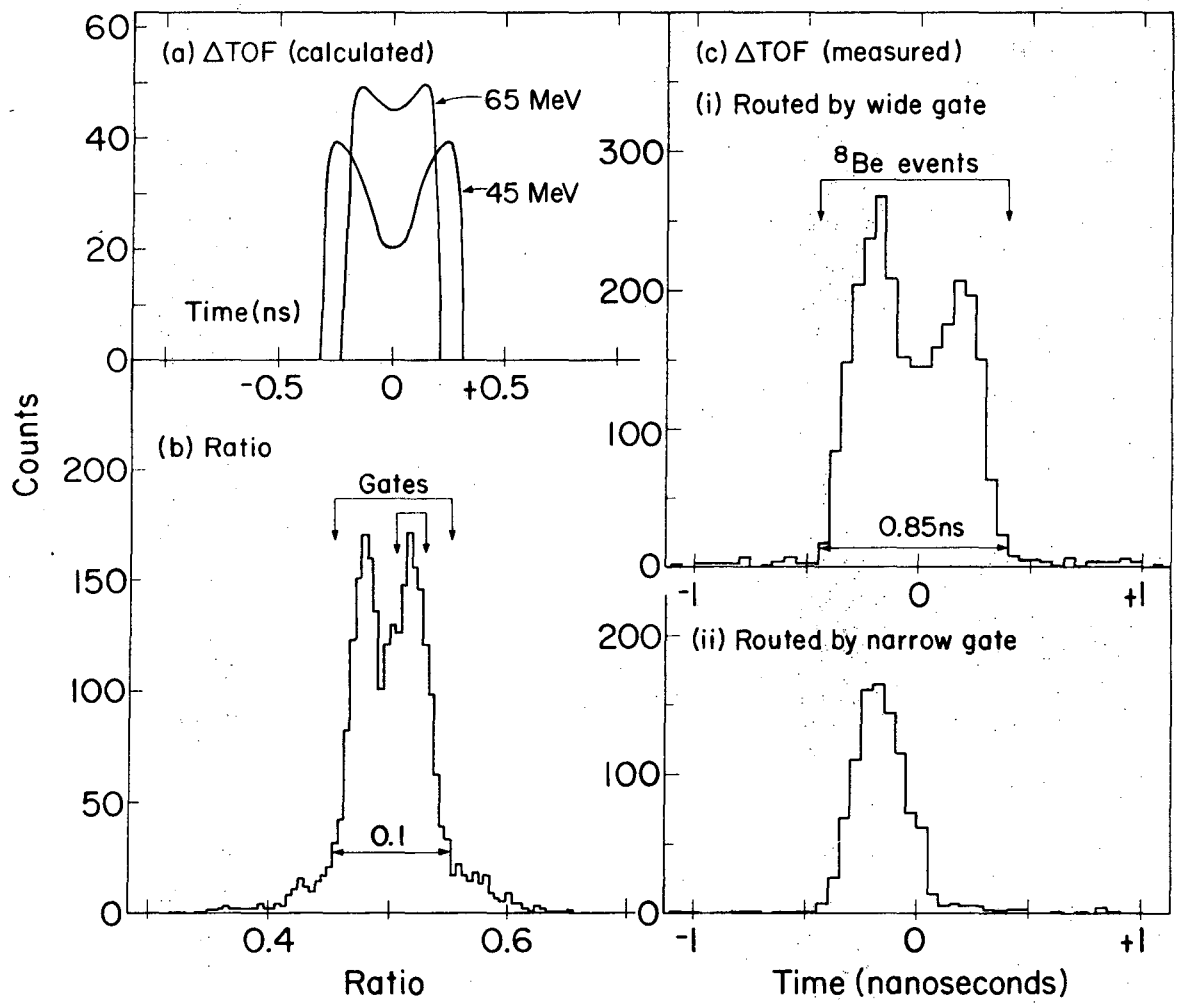

Fig. 3-11. a) Calculated ΔTOF spectra, ΔE_L(start) - ΔE_R (stop), showing the effect of the divided collimator's shape on the relative velocity distribution. b) A ratio spectrum, $\Delta E_L/(\Delta E_L + \Delta E_R)$, collected with the PI and X gates shown in Fig. 3-10. c) Measured ΔTOF spectra routed by the ratio gates shown in part b).

This relationship could be calculated using a computer. Alternatively, a good analogue approximation would be to set an SCA about the sum of R and T, since the variation in $(E_8)^{1/2}$ is small for 35-70 MeV ^{8}Be events.

To reduce the effect of kinematic broadening on the ^{8}Be energy resolution, three narrow position gates (X_L, X_C, X_R) were set (see Fig. 3-10b). Each was equivalent to 0.4° and the summed gate (1.2°) had a detection efficiency (ϵ) of 20-36% for 35-70 MeV ^{8}Be events. In addition, a thin target (100 μg/cm^2) was used and rotated to reduce the combined effect of the differential energy loss in the target and the beam spot size.

A ^{8}Be energy spectrum accumulated in two hours from the ^{11}B(α, ^{8}Be)^{7}Li reaction at θ_{lab} = 20° and E_α = 72.5 MeV is shown in Fig. 3-12. This spectrum was obtained by summing the kinematically corrected energy spectra corresponding to the three position gates. Over 25 MeV of excitation in ^{7}Li is observed, and the main transitions to the ground and second excited states are seen with better energy resolution and lower background than was obtained with the simple identifier (see Fig. 3-6b). Also indicated are transitions to the 7.47 MeV; $5/2^-$ and the 0.48 MeV; $1/2^-$ states (the latter only partially resolved). The $5/2^-$ and $1/2^-$ states are expected to be less strongly excited on the basis of calculated α-structure factors (Ku 73). The absolute cross section to the ground state is 18 μb/sr at this energy and angle. The observed energy resolution is 400 keV and the counting rate in each ΔE detector was 25 kHz. At this counting rate the deadtime (observed with a pulser triggered by a monitor counter) was 35%.

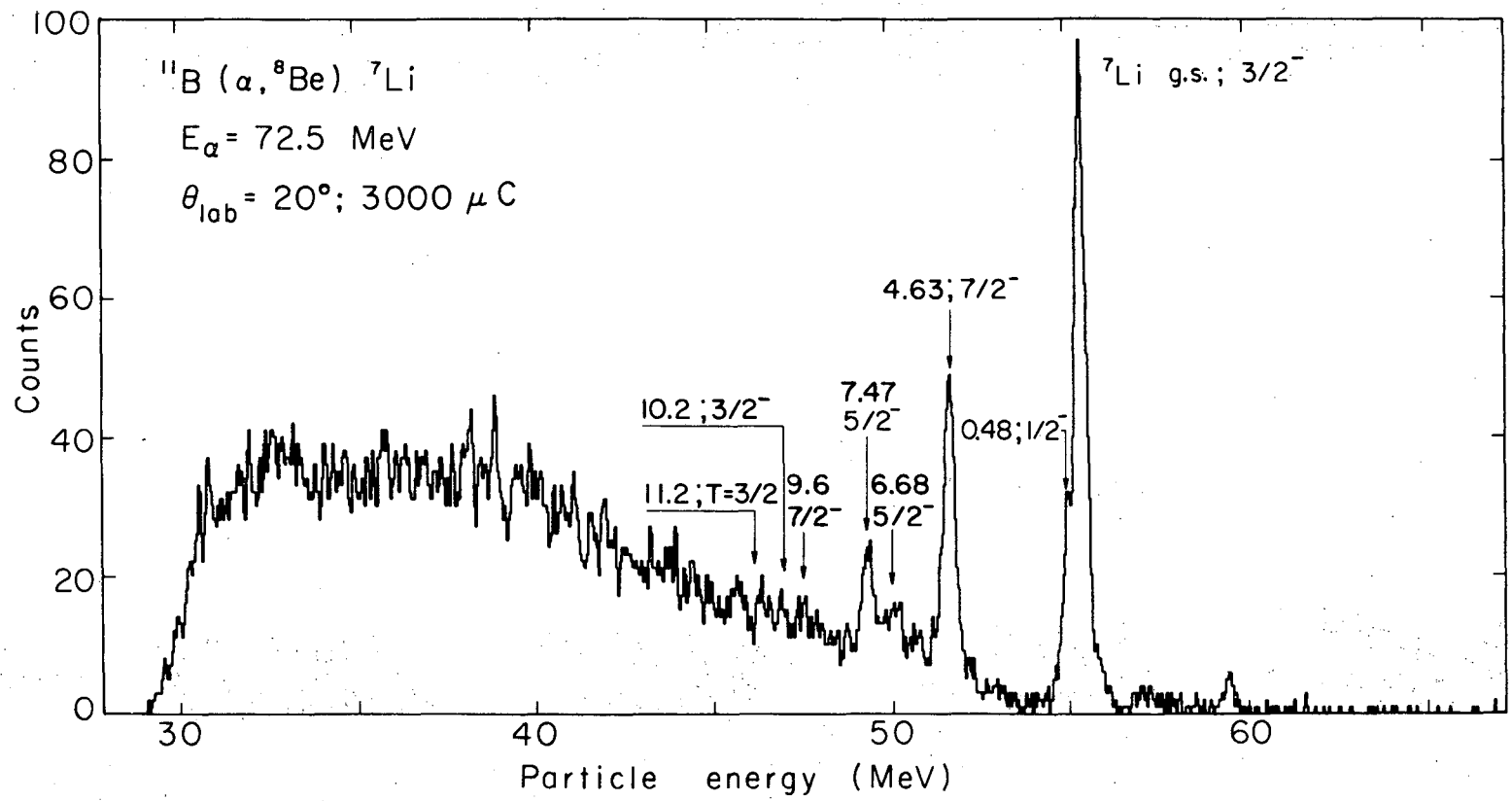

XBL742 - 2411

Fig. 3-12. A ^{8}Be spectrum from the ^{11}B(α, ^{8}Be) ^{7}Li reaction taken with the modified identifier. The locations of possible transitions to all states below 11 MeV are indicated (Se 74).

Using the modified identifier, data could be collected at twice the rate and with a lower background level than was possible with the simple identifier (compare Figs. 3-6b and 3-12). The average background level above the impurity peak in Fig. 3-12 corresponds to an absolute differential cross section limit of ~ 0.1 μb/sr c.m. Lower cross section limits could be achieved if necessary by reducing the counting rate. There is no background from $^{8}Be^{*}$ (2.9 MeV), when using a modified identifier, because its large breakup Q-value coupled with the restriction on the separation angle of the two α-particles imposed by the divided collimator causes α_1 and α_2 to have sufficiently different energies that the ΔTOF SCA and R SCA requirements eliminate $^{8}Be^{*}$ events from the energy spectra.

E. Data Acquisition and Analysis

During an experiment, energy spectra routed by up to four position gates were accumulated in four 1024 channel groups of a multichannel analyzer. At the end of a run these data would be transferred to a PDP-5 computer and written on magnetic tape. Upon completion of an experiment, analysis of these energy spectra was performed with the interactive, Gaussian peak-fitting program DERTAG, (Ma 71), on the SCC-660 computer. Centroids, widths and integrals were obtained for each peak. If energy spectra from a run were taken with adjacent position gates, these spectra were kinematically shifted and summed with the program SUMSHIFT on the SCC-660 computer. This summed spectrum was then analyzed with DERTAG and the results checked for consistency against the results from the unsummed spectra.

On light targets the low level density made it relatively easy to decide which energy levels in the product nucleus were populated. To check level assignments and determine excitation energies, the program LORNA (Ma 71) on the CDC 7600 was used to calculate the reaction kinematics, absorber losses and an energy scale from a least-squares fit to the experimental points. This version of LORNA was modified to calculate the ^{8}Be event's absorber losses which is accurately given by twice the sum of the absorber loss of an α-particle which carried one half the energy of the ^{8}Be nucleus emitted from the reaction plus one half of the breakup Q-value.

IV. Theoretical Considerations

In this section a simple diffraction model is considered and harmonic-oscillator wave functions are used to describe the bound state of the α-cluster in the target. Finite range and recoil effects are included and a simple expression is obtained for the cross section at high energies.

A. α-Cluster Transfer

Since single-nucleon pickup calculations have been successfully used to investigate single-particle aspects of nuclear structure, it is natural to attempt to obtain corresponding information about correlated four-particle clusters in the same theoretical framework. Thus one hopes that in spite of the a priori complexity of the four-nucleon pick-up reaction (α, ^{8}Be), its main features could be understood by assuming that the four nucleons are transferred as a single cluster having the internal quantum numbers of a free α-particle. Since the incident α-particle picks up an α-cluster from the target nucleus B, only the component of the target wave function which has the form B = A + α is treated as relevant.

The "α-transfer approximation" implies that the α-cluster in the target and in ^{8}Be are identical and the same as a free α-particle. For ^{8}Be which is well described by two α-particles with zero relative binding energy, this should be a good assumption. If the α-cluster in the target is different from a free α-particle because it is bound to A, the dependence of this phenomenon on the α-separation energy can be

investigated with target nuclei having different separation energies.

B. Selection Rules

Since the projectile, the transferred cluster and ^{8}Be all have zero spin and positive parity, quite simple selection rules apply to the (α, ^{8}Be) reaction. The transferred intrinsic angular momentum (spin) ΔS and the transferred isospin ΔT are zero:

$$\Delta S = \Delta T = 0. \tag{4-1}$$

The total angular momentum $\vec{J}$ transferred between an initial ($\vec{J}_i$) and final state ($\vec{J}_f$) by four nucleons coupled to zero spin and isospin is given by the transferred orbital angular momentum $\vec{L}$ and can be expressed as

$$\vec{J}_f = \vec{J}_i + \vec{L}. \tag{4-2}$$

As the parity change is given by

$$\Delta\pi = (-1)^L, \tag{4-3}$$

only natural parity states can be populated in the final nucleus.

If the four transferred nucleons are restricted to originating from the 1p shell, then L can have only even values (0, 2, 4) and the parity of states in the final nucleus is the same as that of the ground state of the target nucleus. For target nuclei having ground state spins of 0 or 1/2, the transferred angular momentum (L) is a unique value for transitions to any state in the final nucleus. This result makes the study of these target nuclei particularly interesting so as to determine whether different transferred L values give rise to

characteristic angular distributions.

C. Direct Reaction Theory

The theory adopted in this work has been advanced and developed entirely by others and a number of excellent and detailed accounts exist elsewhere (Au 70, Gr 69, Gr 66, Bu 66, Hu 65, Hu 69, Hu 70, Do 65, Do 70, Vi 68, Co 73). In particular Nagarajan (Na 74) has adapted this approach to the (α, ^{8}Be) reaction. A brief review of this theoretical development is given below.

1. Transfer to an unbound final state

At first glance the (α, ^{8}Be) reaction has the apparent complication that the exit particle is unbound. However, this problem can be handled by well known theoretical techniques and in fact the particle-instability of ^{8}Be considerably simplifies the theoretical description of this reaction. Huby et al. (Hu 65, Hu 69, Hu 70, Co 70) and others (Vi 68, Be 68, Ba 69) have formulated the theory of nucleon transfer leading to unbound states in light ion induced reactions. The method that has been used is either to describe the unbound state as a quasi-bound one or, if it is in the vicinity of a resonance, to describe it as a Gamov state. Both of these methods lead to an expression for the transition amplitude which resembles the one for transfer to bound states.

Nagarajan (Na 74) has extended this theory to include heavy ion induced transfer reactions leading to weakly bound (or unbound) final states. This treatment can also be applied to reactions where

the transferred particle is in a resonant state in the final system. An example of this is the (α, ^{8}Be) reaction where ^{8}Be is composed of two α-particles in a s-wave resonance at about 92 keV above the threshold. The relative motion of the two α-particles at large separation distances can be described by a radial wave function which is more or less constant over all space.

Since ^{8}Be has a very extended wave function, it can interact with the target at large distances where nuclear distortion effects are small. In Fig. 4-1 are shown calculated bound state wavefunctions (Φ) for an α-cluster bound to a ^{12}C core and for two α-clusters bound together by 100 keV. This latter wave function should be a good representation of the ^{8}Be ground state one as it is not very sensitive to small binding energies. Fig. 4-1 illustrates that there will be substantial overlap of these two wave functions when the two mass centers are separated by 10 fermis and even at larger distances due to the long tail of the ^{8}Be wave function.

Because of the strong absorption in the exit channel and the large size of ^{8}Be, one would expect that the α-cluster transfer would occur in the asymptotic region of the ^{8}Be wave function. In fact the extended size of ^{8}Be requires that it be formed at large distances from the target nucleus. This can be seen by considering that if ^{8}Be is formed near the target nucleus, it will almost certainly be absorbed before it can escape. Because of this effect only α-particles with large impact parameters in the entrance channel will contribute to the (α, ^{8}Be) reaction. This reaction therefore takes place at large distances (~10 fm) from the target where nuclear distortion effects are small.

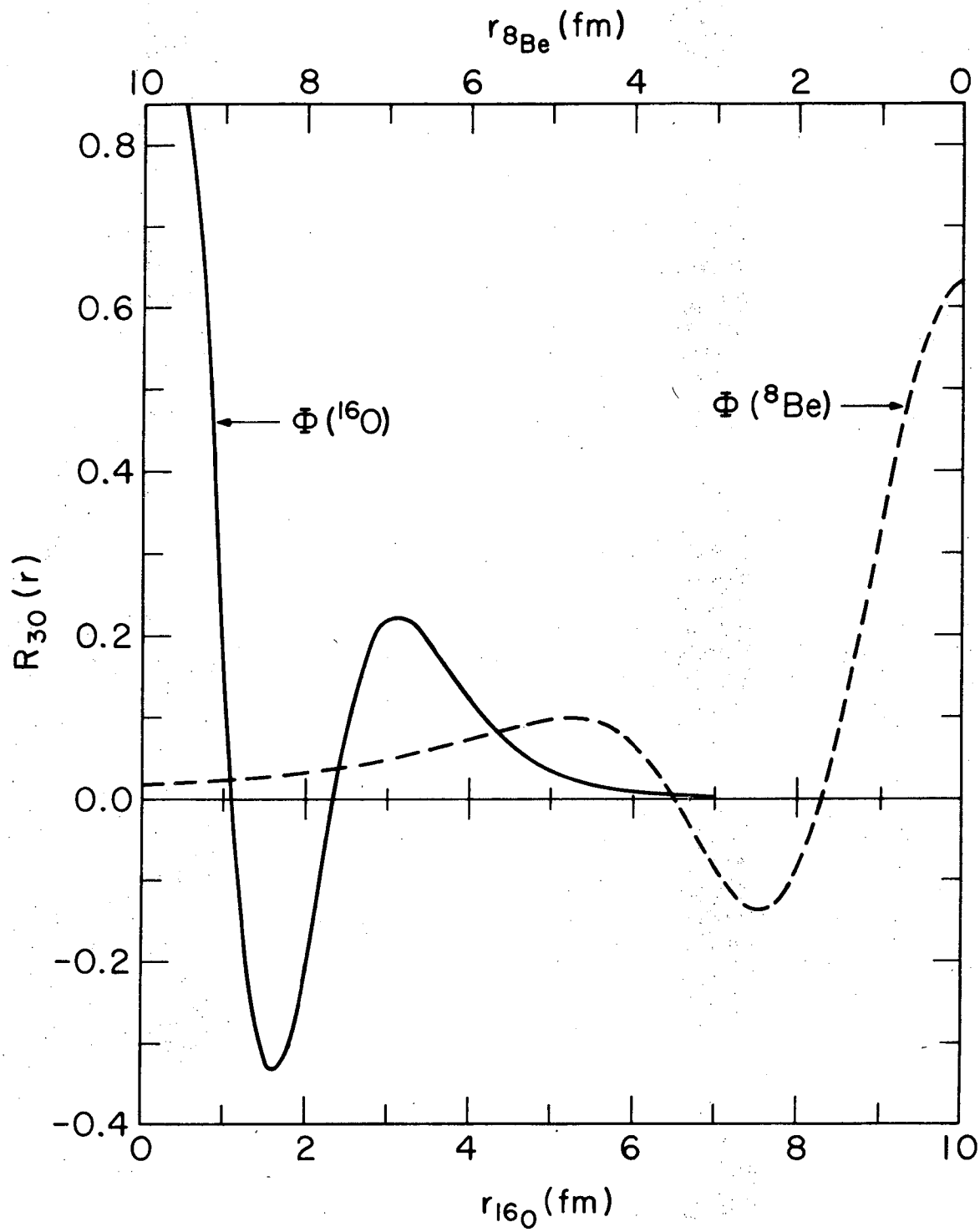

XBL 748-3784

Fig. 4-1. A plot of the α-cluster radial wave functions (R_{NL}) of ^{16}O and ^8Be which shows the large overlap of their wave functions when their centers of mass are separated by 10 fermis. The ^{16}O wave function was calculated for an L = 0 α-cluster in a Woods-Saxon well of radius 3.1 fermis and with the depth adjusted to obtain the known binding energy. The ^8Be wave function was calculated by the same method with a well radius of 4.0 fermis and an assumed ^8Be binding energy of 100 keV. See discussion in text.

Although at these distances the amplitude of the wave function of the bound α-cluster in the target is small, the long tail of the ^{8}Be wave function ensures a sizable probability for this reaction channel.

2. Born approximation

The (α, ^{8}Be) reaction can be represented as

$$(A + \alpha_2) + \alpha_1 \rightarrow A + (\alpha_1 + \alpha_2) \tag{4-4}$$

where a direct reaction mechanism is assumed. Schematically, this process is depicted in Fig. 4-2 where all coordinates are in the center of mass system. The entrance channel consists of α_1 approaching B along $\vec{r}_i$ where

$$\vec{r}_i = \vec{r} - \frac{M_\alpha}{M_B} \vec{r}_1 . \tag{4-5}$$

In its initial state α_2 is bound to the core A (internal coordinate $\vec{r}_1$) forming the target nucleus B. The two α-particles approach each other along $\vec{r}_2$ where

$$\vec{r}_2 = \vec{r}_1 - \vec{r} \tag{4-6}$$

and $\vec{r}$ is the coordinate connecting α_1 and A. In the exit channel $\vec{r}_2$ is fixed and equal to the α-α separation distance in ^{8}Be. This system recedes from A along $\vec{r}_f$ where

$$\vec{r}_f = 1/2\ (\vec{r} + \vec{r}_1). \tag{4-7}$$

The above reaction process depends on the probability that α_1 scatters from B with a final momentum $\vec{k}_f/2$ (one half of the momentum

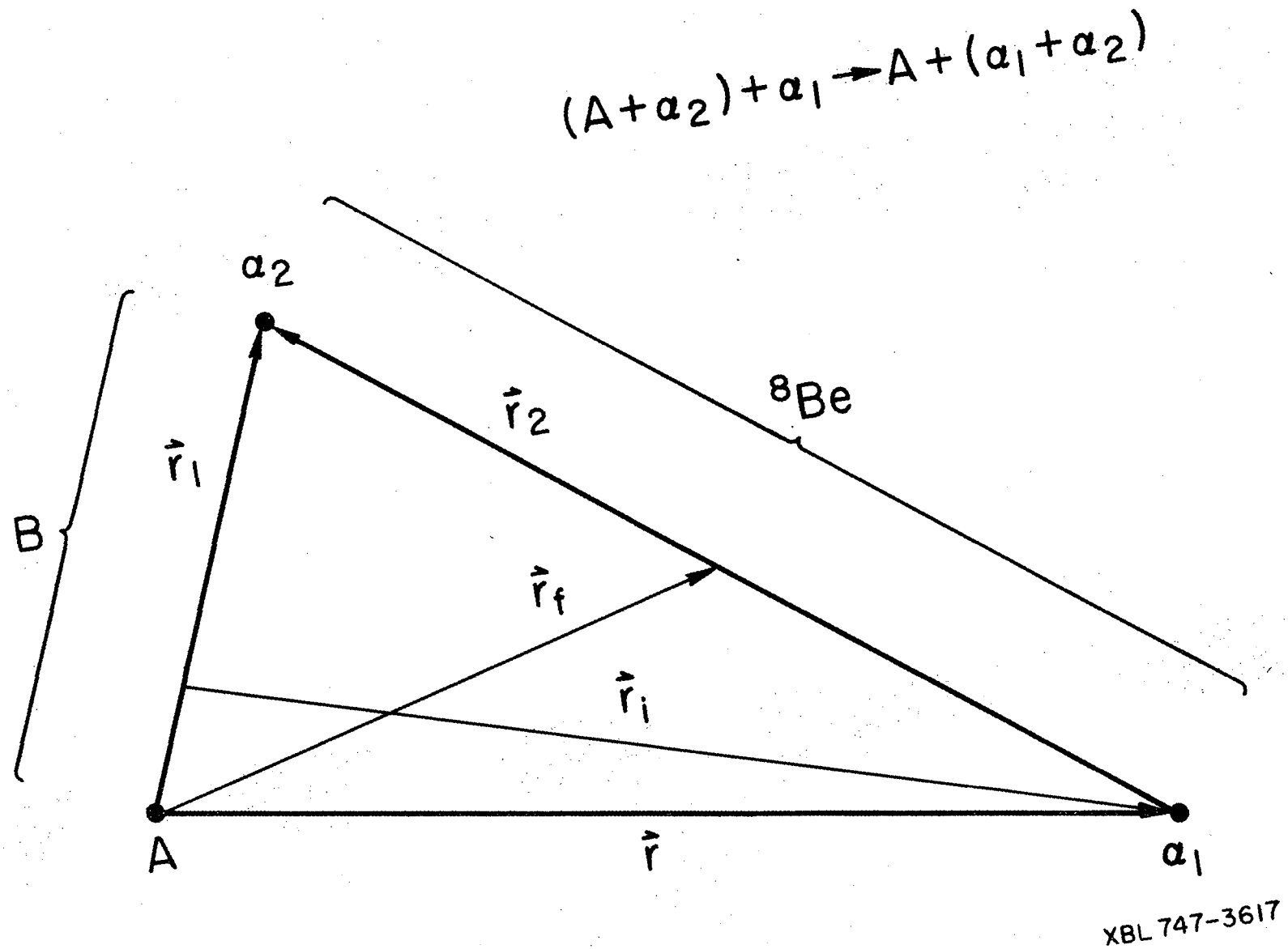

Fig. 4-2. Diagram of the coordinate system for the α-induced α-particle transfer reaction (α, ^{8}Be). The relationships between the various vectors are described in the text.

carried by ^{8}Be). If the target α-cluster also has the momentum $\vec{k}_f/2$, then there is a probability that the two α-particles will travel along together in the same direction forming ^{8}Be. The reaction probability therefore depends on the chance that α_2 has a momentum of $\vec{k}_f/2$ in its initial bound state which depends on the binding energy of α_2 to A.

In the distorted-wave Born approximation, the transition matrix element (see Gr 69) for the three body process depicted by equation (1) is given by

$$T_{A\alpha}(\vec{k}_i, \vec{k}_f) = \int d\vec{r}_f \int d\vec{r}_i \, \chi_f^{(-)}(\vec{k}_f, \vec{r}_f) \langle \Phi_A \Phi_{8_{Be}} | V_{\alpha A}(\vec{r}_1) | \Phi_B \Phi_\alpha \rangle \times \chi_i^{(+)}(\vec{k}_i, \vec{r}_i). \tag{4-8}$$

The above expression is a six dimensional integral and the potential ($V_{\alpha A}$) which causes the direct reaction is the interaction in the entrance channel between the bound α-particle (α_1) and its core (A). The distorted waves $\chi_i^{(+)}$ and $\chi_f^{(-)}$ describe the scattering in the entrance and exit channels and the nuclear wave functions Φ are eigen-functions of the initial and final state nuclear Hamiltonians. The applicability of the Born approximation is based largely on the assumption of a direct mechanism. That is, the interaction responsible for the transition is assumed to occur only once and to last $\sim 10^{-22}$ seconds (the nuclear transit time for a bombarding α-particle).

3. Diffraction model

To make the above integral a more tractable one, advantage is taken of the fact that nuclear and Coulomb distortion effects are expected

to be small. Because of the high-energy incident ($E_\alpha \sim 65$ MeV) and exit particles (since $Q \sim -8$ MeV), it is assumed that a diffraction model employing plane-waves would give an adequate description of the entrance and exit channels. This assumption was borne out by several full-recoil DWBA calculations using the program LOLA(De 73) which gave similar results to the plane-wave calculations (see Section V-I).

For simplicity the diffraction model of Dodd and Greider (Do 69) which avoids a partial-wave expansion is used. Because of the strong nuclear absorption or scattering of complex nuclei well above the Coulomb barrier, the distorted wave $\chi_i^{(+)}$ (or $\chi_f^{(-)}$ is represented in configuration space by a plane-wave which vanishes inside a sphere of radius R. For the exit channel of ^{8}Be +A this should be a very good representation. Thus the elastic scattering wave functions are described by

$$\chi_i^{(+)}(\vec{k}_i, \vec{r}_i) \simeq \exp(i\,\vec{k}_i \cdot \vec{r}_i)\,\theta(\vec{r}_i) \tag{4-9}$$

and

$$\chi_f^{(-)}(\vec{k}_f, \vec{r}_f) \simeq \exp(-i\,\vec{k}_f \cdot \vec{r}_f)\,\theta(\vec{r}_f)\,. \tag{4-10}$$

The momentum dependence of these θ coefficients is neglected and the effect of strong absorption in the optical potential is included by setting them equal to unity outside a sphere of radius R and zero inside. The cutoff radius R is determined by requiring that angular momentum is matched in the entrance and exit channels and is given by

$$R = 2k_i/k_f\,(R_\alpha + R_B) \tag{4-11}$$

where k_i and k_f are the linear momentum in the initial and final channels, respectively.

The above approximation allows one to factor the transition matrix element $T_{A\alpha}$ into the product of two integrals. Ignoring the dependence of $\theta_i(\vec{r}_i)$ and $\theta_f(\vec{r}_f)$ on the vectors $\vec{r}_i$ and $\vec{r}_f$,

$$T_{A\alpha}(\vec{k}_f, \vec{k}_i) \simeq \beta_o(\vec{q})\, G_{fi}(\vec{r}) \tag{4-12}$$

where the first factor $\beta_o(\vec{q})$ is the distorted wave integral

$$\beta_o(\vec{q}) = \int d\vec{r}\ \theta_i(r)\ \theta_f(r)\ e^{i\vec{q}\cdot\vec{r}} \tag{4-13}$$

and the second one $G_{fi}(\vec{r}_i)$ is the form factor

$$G_{fi}(\vec{r}) = \int \langle \Phi_A \Phi_{8_{Be}} | e^{-i\vec{k}_R \cdot \vec{r}_1}\ V_{\alpha A}(r_1) | \Phi_B \Phi_\alpha \rangle\ d\vec{r}_1 . \tag{4-14}$$

The linear momentum transfer $(\vec{q})$ and recoil momentum $(\vec{k}_R)$ are defined as

$$\vec{q} = \vec{k}_i - (1/2)\,\vec{k}_f \tag{4-15}$$

and

$$\vec{k}_R = (M_\alpha/M_B)\,\vec{k}_i + 1/2\,\vec{k}_f \tag{4-16}$$

where M_α and M_B are the masses of the α-particle and the target nucleus, respectively. Physically, $\vec{q}$ is the difference between the initial and final momenta of the projectile, whereas $\vec{k}_R$ is the sum of the latter quantity plus the momentum of the α-particle bound inside the target nucleus. The finite mass of the transferred cluster is

taken into account by the inclusion of a recoil phase factor in the transfer function G_{fi}.

The first factor $\beta_o(\vec{q})$ in the transition matrix element is a radial integral (see 4-13) over the scattering waves in the entrance and exit channels which can be evaluated using the technique of Vincent (Vi 68) or Huby (Hu 65). Its value can be expressed as

$$\beta_o(\vec{q}) = -4\pi[\cos(qR)]/q^2R^2 \tag{4-17}$$

and its phase is determined by the product of the cutoff radius R and the transferred momentum q.

Assuming that the target nucleus $(A+\alpha)$ can be described by a single-particle state of a three-dimensional harmonic oscillator, one can make the following parentage expansion

$$\langle \Phi_A | \Phi_B \rangle = \sum_{L_1 M_1} \beta_{J_A L_1 J_B} \langle J_A M_A L_1 M_1 | J_B M_B \rangle \times R_{L_1}(r_1)\, Y_{L_1 M_1}(\vec{r}_1). \tag{4-18}$$

The factors $R_{L_1}(r_1)$ and $Y_{L_1 M_1}(\vec{r}_1)$ are the radial wave function and the spherical harmonic function, respectively, which describe the bound state of the target α-cluster. Furthermore the ^{8}Be wave function can be written (see Na 74) as

$$\langle \Phi_{^8Be} | \Phi_\alpha \rangle \simeq \theta_0 \frac{\sin(k_2 r_2 + \delta)}{k_2 r_2} \tag{4-19}$$

which satisfies an addition theorem (Na 74) yielding as a final result

$$\langle \Phi_{^8Be} | \Phi_\alpha \rangle \simeq \frac{\theta_o}{\sqrt{4\pi}} \times \text{constant} \tag{4-20}$$

where θ_o^2 is the $^8Be \rightarrow 2\alpha$ spectroscopic factor. Utilizing equations (4-18) and (4-20) the form factor becomes

$$G_{f,i}(\vec{r}) \simeq \frac{C\theta_o}{\sqrt{4\pi}} \sum_{L_1 M_1} \beta_{J_A L_1 J_B} \langle J_A M_A L_1 M_1 | J_B M_B \rangle$$
$$\times \int d\vec{r}_1 \, e^{-\vec{k}_R \cdot \vec{r}_1} V_{\alpha A}(r_1) R_{L_1}(r_1) Y_{L_1 M_1}(\vec{r}_1). \tag{4-21}$$

For p-shell nuclei, the four nucleons in the α-cluster have a total energy of

$$\epsilon = 4(5/2 \ \hbar\omega) = 10 \hbar \omega. \tag{4-22}$$

Since the internal state of the α-cluster is assumed to be in its lowest state and because it has three degrees of freedom,

$$E_{int} = 3\left(\frac{3}{2} \hbar\omega\right) = \frac{9}{2} \hbar \omega. \tag{4-23}$$

Hence the energy carried by the center-of-mass of the α-cluster is

$$E_{CM} = 11/2 \ \hbar\omega = (2N + L - \frac{1}{2}) \hbar \omega. \tag{4-24}$$

Thus an α-cluster having angular momentum of 0, 2, 4 relative to the core is described by 3S, 2D, and 1G wave functions, respectively.

The integral in the expression for the form factor given in (4-21) is defined as

$$F_L(k_R) = \int_0^\infty r_1^2 dr_1 \, e^{-k_R \cdot r_1} V_{\alpha A}(r_1) R_{L_1}(r_1) Y_{L_1 M_1}(\vec{r}_1). \qquad (4\text{-}25)$$

Since $V_{\alpha A}(r_1)$ is the potential which yields the α-cluster radial wave function R_L as a solution of the Schrodinger equation

$$(T + V) R_L = - \epsilon R_L, \qquad (4\text{-}26)$$

this permits one to write this integral in the following form

$$F_L(k_R) = -\int_0^\infty r_1^2 dr_1 \, (T + \epsilon) \, e^{-k_R \cdot r_1} R_L(r_1) Y_{L_1 M_1}(\vec{r}_1). \qquad (4\text{-}27)$$

Integrating by parts

$$F_L(k_R) = \frac{-\hbar^2}{2\mu} (k_R^2 + \gamma^2) \int_0^\infty r_1^2 \, e^{-k_R \cdot r_1} R_{L_1}(r_1) Y_{L_1 M_1}(\vec{r}_1). \qquad (4\text{-}28)$$

where

$$\mu = M_\alpha \cdot M_A / M_B \qquad (4\text{-}29)$$

and

$$\gamma^2 = 2\mu\epsilon/\hbar^2 \qquad (4\text{-}30)$$

and ϵ is the binding energy of the α-cluster in the target.

The above integral is the Fourier transform of the target bound state wave function and it gives the probability amplitude that the bound α-cluster has a momentum k_R. Thus the possibility that an α-cluster in the target will be picked up by an incident α-particle is dependent on the momentum distribution of that cluster in its initial bound state.

A more useful expression for the form factor is the following

$$F_L(k_R) = -(\hbar^2/2\mu)(k_R^2 + \gamma^2) \, Y_{L_1 M_1}(k_R) R_{L_1}(k_R) \qquad (4\text{-}31)$$

where $R_L(k_R)$ is the Fourier transform of the radial wave function

(see Ta 63) of the bound α-cluster in the target nucleus with respect to the recoil momentum and is given by

$$R_{L_1}(k_R) = \sqrt{\frac{2}{\pi}}\,(i)^L \int_0^\infty r_1^{\,2}\, dr_1\, j_{L_1}(r\cdot k_R)\, R_{L_i}(r_1). \tag{4-32}$$

$R_{L_1}(k_R)$ can be evaluated using harmonic oscillator radial wave functions (see Ta 63). Employing equation (4-31), the form factor can be rewritten as

$$G_{fi} \simeq \frac{-C\theta_o}{\sqrt{4\pi}} \sum_{L_1 M_1} \beta_{J_A L_1 J_B} \langle J_A M_A L_1 M_1 | J_B M_B \rangle \left(\frac{\hbar^2}{2\mu}\right) (k_R^{\,2} + \gamma^2) \times Y_{L_1 M_1}(k_R)\, R_{L_1}(k_R). \tag{4-33}$$

Summing over the initial and averaging over the final magnetic substates and invoking the orthonormality of the spherical harmonics yields the following simple expression for the form factor

$$G_{fi} \simeq \frac{-C\theta_o}{\sqrt{4\pi}}\, \frac{\hbar^2}{2\mu} (k_R^{\,2} + \gamma^2) \sum_L N_L \times R_L(k_R). \tag{4-34}$$

The quantity N_L is the probability amplitude (α-structure amplitude) that the target (A + α) appears in the form of a nucleus A and an α-particle with relative angular momentum L.

With the aid of the above expression for the form factor the square of the transition matrix element is written as

$$T_{A\alpha}^{2} \simeq \frac{C^2}{4\pi}\beta_o^2(q)\left(\frac{\hbar^2}{2\mu}\right)^2(k_R^2+\gamma^2)^2\,\theta_o^2\sum_L N_L^2\,|R_L(k_R)|^2. \tag{4-35}$$

Since the differential cross section can be expressed as,

$$d\sigma/d\Omega = \frac{\mu_i\mu_f}{(2\pi\hbar^2)^2}\,\frac{k_f}{k_i}\,T_{A\alpha}^{2}, \tag{4-36}$$

utilizing equations (4-35) and (4-17) yields the following simple form for the reaction cross section:

$$d\sigma/d\Omega \simeq \frac{\mu_i\mu_f}{\mu^2}\,\frac{k_f}{k_i}\,(k_R^2+\gamma^2)^2\cdot C^2\cdot\theta_o^2\cdot\pi^{-1}$$
$$\times\left|\frac{\cos(qR)}{q^2R^2}\right|^2\times\sum_L N_L^2\,|R_L(k_R)|^2. \tag{4-37}$$

The two dominant factors in determining the shape and magnitude of the cross section are cos (qR), which is a function of the transferred momentum (q), and the probablity $R_L(k_R)$ that the target α-cluster has a momentum k_R. The minima of the cross section are given by the zeros of cos (qR) and this envelope is modulated by the region of $R_L(k_R)$ that the reaction is probing.

Since the bound α-cluster in these experiments consists of four 1p- shell nucleons, the 3S, 2D and 1G harmonic oscillator wave functions describe the α-cluster as having relative angular momenta of L = 0, 2 and 4, respectively. In Fig. 4-3 the probability amplitudes of these wave functions are plotted against the square of the recoil momentum (k_R) divided by the square of the oscillator parameter (ν) where

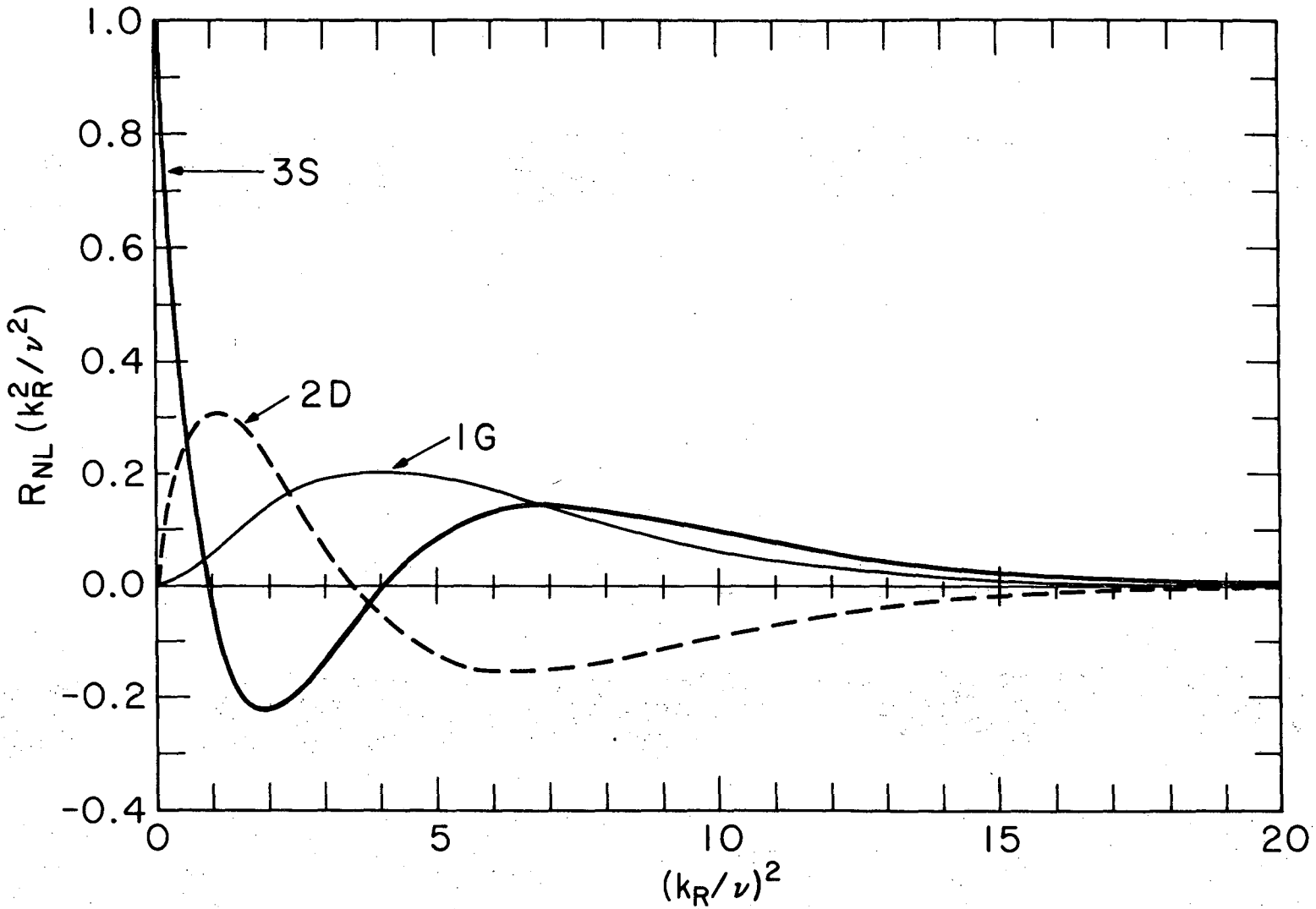

XBL748-3785

Fig. 4-3. A plot of the probability amplitude that a bound α-cluster in the target will have a momentum (k_R) for 3S(L = 0), 2D(L = 2) and 1G(L = 4) harmonic oscillator wave functions. The abscissa is in units of the square of the recoil momentum normalized by the oscillator strength function. See discussion in text.

$$\nu^2 = M_\alpha \cdot \omega/\hbar \,. \tag{4-38}$$

Since k_R is a function of the bombarding energy and the reaction angle (θ_{cm}), it is clear from the shape of these curves that the magnitude of the cross section depends on the region of the probability amplitude that the reaction is probing.

In summary, the above diffraction model includes recoil effects and takes advantage of the fact that the α-cluster is transferred at large distances from the target nucleus where distortion effects are small. Thus plane waves can be used to describe the scattering in the entrance and exit channels which greatly simplifies the calculations. (One should note that it is assumed implicity that the core A (to which α_2 is bound) is particle stable; hence the theory might not be expected to correctly describe transitions to unbound states of A.)

V. Experimental Results and Discussion

The (α, ^{8}Be) reaction was studied on both solid and gas targets with reaction Q-values typically of ~ -8 MeV. The 1p shell nuclei discussed in this section were bombarded with α-particle beams of 63.2-72.5 MeV from the Berkeley 88-inch cyclotron. A summary of the experiments is tabulated in Table V-1. In general the same relative population of final states was observed at the different incident energies although at some energies weak transitions were obscured by background not eliminated by the simple ^{8}Be identifier. Qualitative as well as quantitative comparisons with theoretical predictions are discussed below as well as a comparison with (α, 2α) results at $E_\alpha = 90$ MeV. In addition, evidence for a direct reaction mechanism is presented.

A. ^{8}Be Breakup Distribution

In studying the (α, ^{8}Be) reaction, we indirectly measure the number of ^{8}Be nuclei emitted at a particular angle by detecting the decay products. For the measured cross sections to be free of a systematic bias, it is important to verify that the events detected correspond to ^{8}Be. In this spirit several tests were carried out to confirm the isotropic decay of ^{8}Be and the kinematic focussing of the decay α-particles.

By measuring the relative efficiency for monoenergetic ^{8}Be events from the ^{12}C(α, ^{8}Be)^{8}Be reaction for collimators of different area, one can determine whether the detected α-particles have a

Table V-1. Summary of the targets and angular ranges studied with the (α, ^{8}Be) reaction plus relevant Q-values, beam energies and observed final states.

Target	Q(α, ^{8}Be) (MeV)	Beam energy (MeV)	^{8}Be Identifer	Angular range studied ($\theta_{c.m.}$)	Final nucleus	Observed energy levels (MeV)
^{12}C	-7.4587	72.5	modified	39°	^{8}Be	0.0, 2.9, 11.4
^{12}C	-7.4587	67.3	simple	30° - 70°	^{8}Be	0.0, 2.9
^{12}C	-7.4587	66.6	simple	30° - 50°	^{8}Be	0.0, 2.9
^{12}C	-7.4587	65.8	simple	30° - 50°	^{8}Be	0.0, 2.9
^{12}C	-7.4587	65.2	simple	20° - 75°	^{8}Be	0.0, 2.9
^{12}C	-7.4587	63.2	simple	30° - 50°	^{8}Be	0.0, 2.9
SiO_2	-7.2536	72.5	modified	29°, 34°	^{12}C	0.0, 4.4. 7.6, 9.6, 14.1
$^{16}O_2$ gas	-7.2536	72.1	simple	25° - 45°	^{12}C	0.0, 4.4, 7.6, 9.6, 14.1
SiO_2	-7.2536	65	simple	20° - 80°	^{12}C	0.0, 4.4, 9.6, 14.1
^{10}B	-4.5521	72.5	modified	25° - 70°	^{6}Li	0.0, 2.2
^{11}B	-8.7576	72.5	modified	34°	^{7}Li	0.0, 0.5, 4.6, 6.7, 7.5
^{11}B	-8.7576	65	simple	20° - 70°	^{7}Li	0.0, 0.5, 4.6, 7.5
$^{14}N_2$ gas	-11.7054	72.1	simple	25° - 45°	^{10}B	0.0, 0.7, 2.1, 3.6, 4.8, 6.0
$^{15}N_2$ gas	-11.0830	72.1	simple	20° - 55°	^{11}B	0.0, 2.1, 4.4, 5.0, 6.7

radial distribution across the breakup cone consistent with the expected one. To carry out these measurements, remotely movable collimation was employed which could place any of five different collimators machined in a single piece of tantalum in front of the simple identifier. Even though the simple identifier was used, a divided collimator was not necessary, because the (α, ^{8}Be) Q-value is more positive than that of the (α, ^{7}Li) reaction on ^{12}C or ^{13}C. Since the differential efficiency ($d\epsilon/dX$) is more uniform across the 1° position gate for an open collimator than for a divided one, an open collimator is the best one to employ so as to minimize position resolution effects. (An open collimator has approximately twice the efficiency (ϵ) of a divided one. However, it has only an ~20% larger relative efficiency than a divided collimator with a similar dependence of ϵ_{rel} on E_8 and D.)

In Fig. 5-1 are presented measured efficiency (ϵ) points taken with open circular collimators compared with calculated ones, using a 1° position gate. The good agreement between the experimental and calculated values for two different ^{8}Be energies confirms the isotropic decay of ^{8}Be.

The kinematic focussing of the α-particles from the decay of ^{8}Be nuclei causes the α-particles to be confined to a cone. To establish this focussing, transitions to the ground and first excited states of ^{8}Be produced by the ^{12}C(α, ^{8}Be)^{8}Be reaction at E_α = 65 MeV and θ_{lab} = 25° were utilized. These transitions produce ~47 MeV ^{8}Be nuclei which have a calculated apex angle for their breakup cone of 5.1° ± 0.1°. Spectra collected using two different <u>divided</u> collimators of

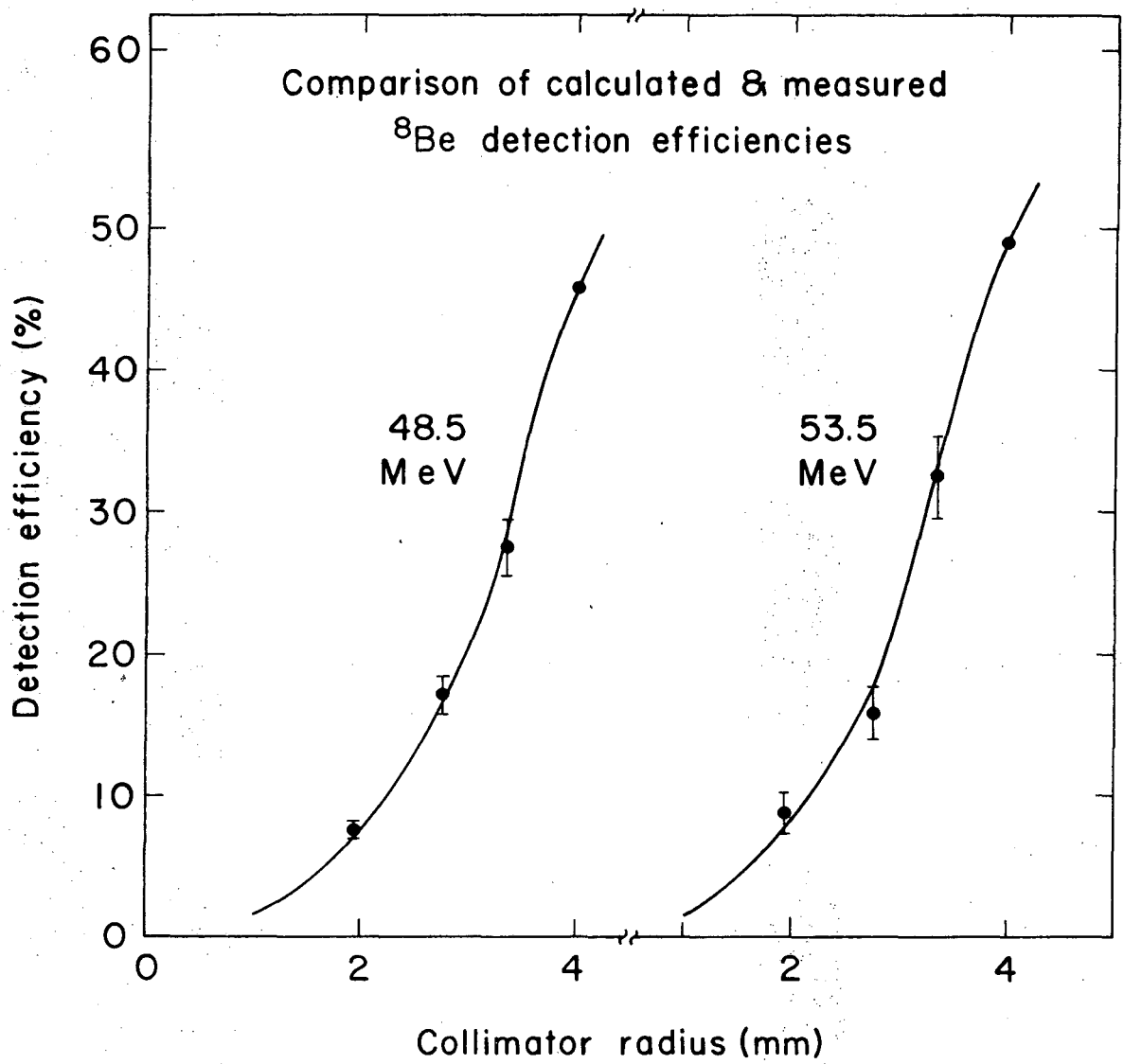

XBL 742-2316

Fig. 5-1. ^{8}Be detection efficiencies at two ^{8}Be energies for open circular collimators of different radii. The experimental points are normalized to the calculated curves at r = 4 mm; statistical error bars are shown.

equal open area and with post widths of 5.4° and 3.6°, respectively, are shown in Fig. 5-2. These spectra, accumulated for an equal number of μC, confirm the kinematic focussing of the two α-particles following ^{8}Be decay. The inserts show the collimator dimensions relative to the size of the ^{8}Be breakup cone. The above spectra were collected with a simple identifier, a ΔE counting rate of 20 kHz, and a 2° central position gate.

B. The ^{12}C(α, ^{8}Be) ^{8}Be Reaction

1. Excitation function

To conclusively determine the direct nature of the (α, ^{8}Be) reaction near 65 MeV bombarding energy, an excitation function of the ^{12}C(α, ^{8}Be) ^{8}Be(gs) reaction was obtained. Measurements in small angular steps were taken over the maximum in the angular distribution at $\theta_{c.m.} \simeq 35°$ (Wo 73) to see if the shape or magnitude changed substantially with bombarding energy. Data measured at E_{α} = 63.2, 65.2, 65.8, 66.6, 67.3 MeV are shown in Fig. 5-3. The angular width of each data point is ~1°, and the error bars shown are entirely statistical. Upon examining Fig. 5-3, it is clear that the magnitude of the differential cross section is a smooth and slowly decreasing function of the bombarding energy. The shape of the two observed maxima seems to also vary slowly with the incident energy.

The above behavior is in marked contrast to that observed at incident energies of 35.5-41.9 MeV (Br 65) for the differential cross sections for the ^{16}O(α, ^{8}Be)^{12}C reactions to the ground and first excited state of ^{12}C. In the latter case, both the shapes and magnitudes

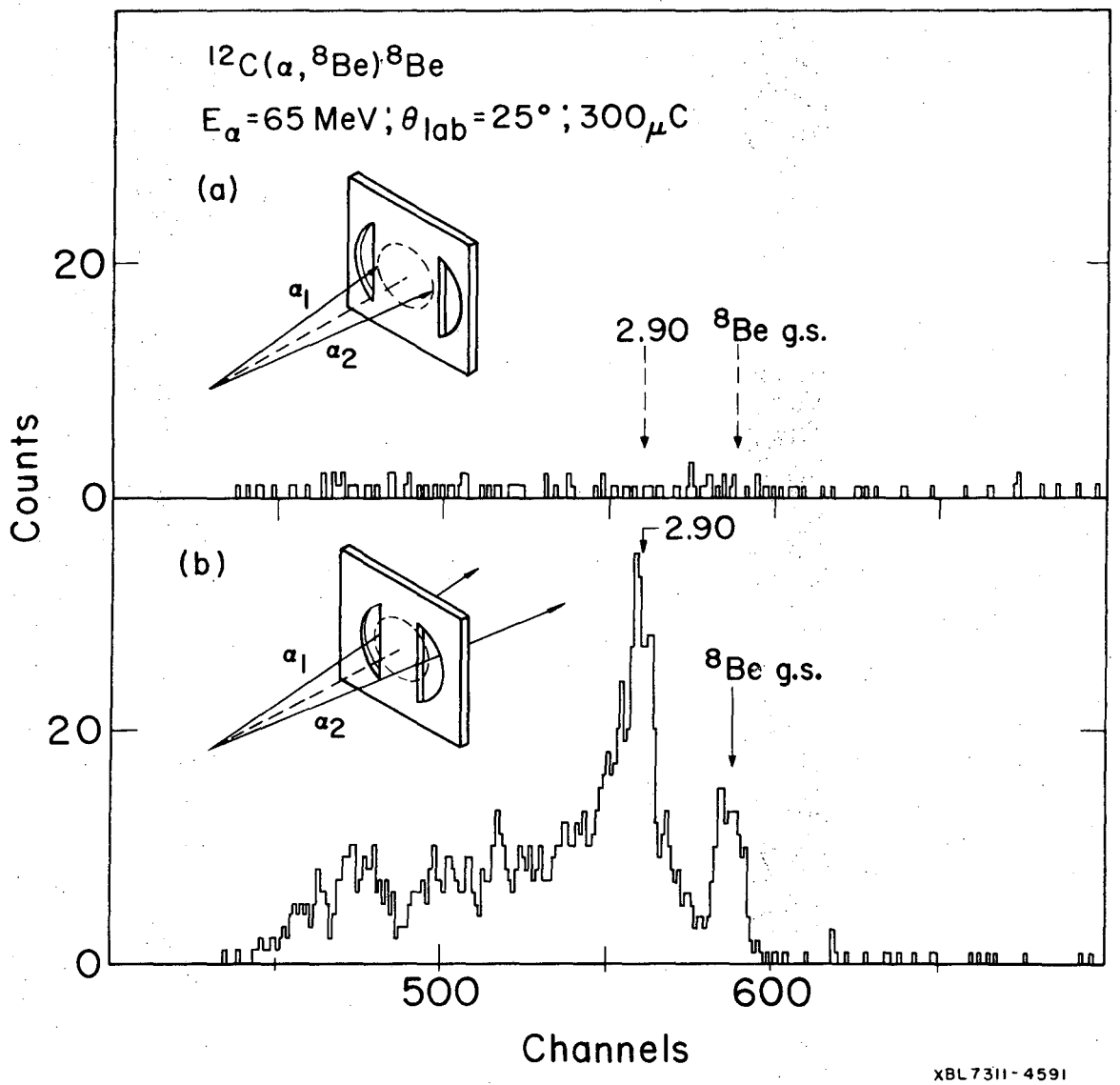

Fig. 5-2. Energy spectra from the $^{12}C(\alpha, {}^{8}Be)^{8}Be$ reaction taken with two different divided collimators to illustrate the kinematic focussing of the breakup α-particles. Depicted in the respective inserts is the size of the breakup cone relative to that of the divided collimator.

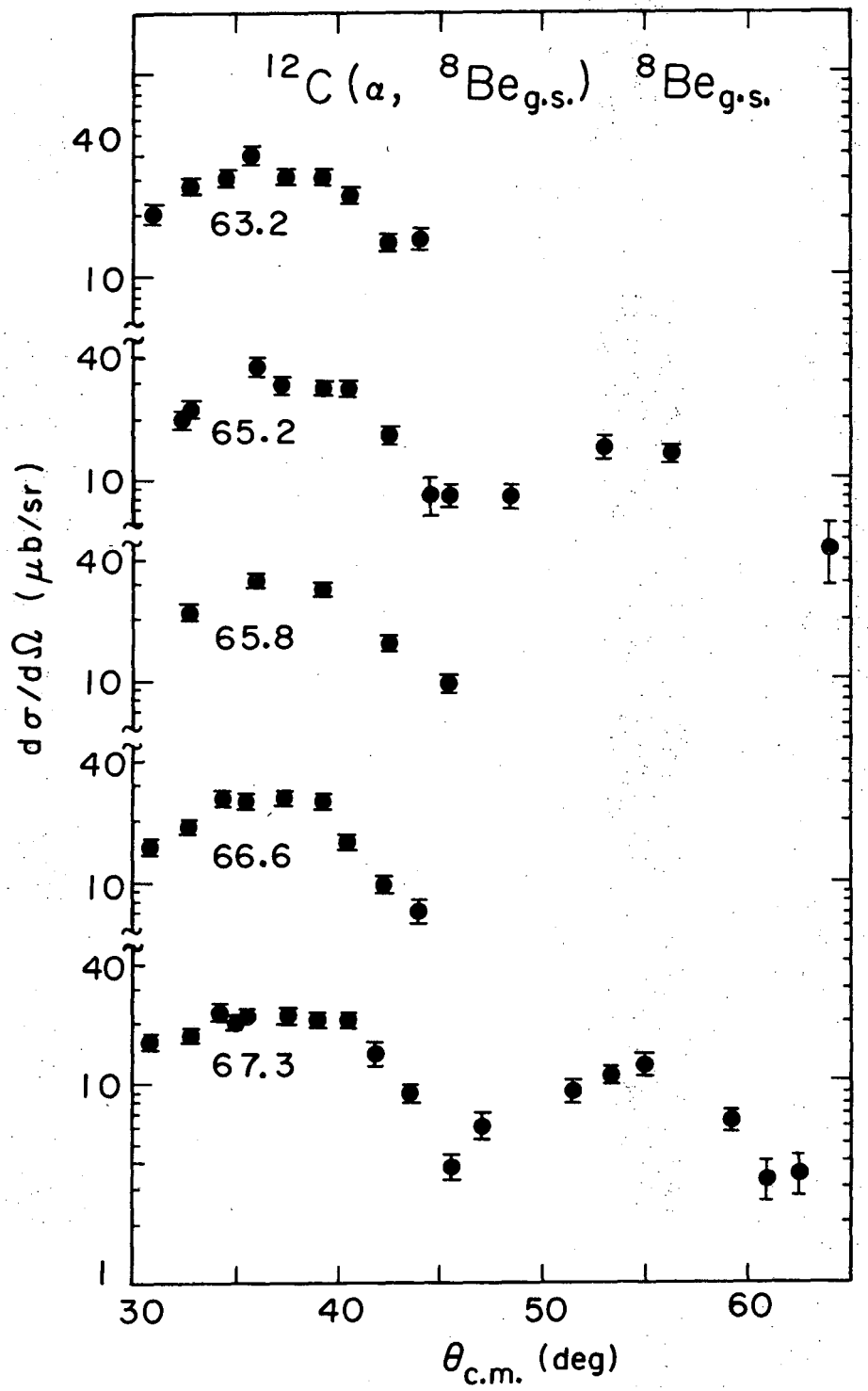

XBL744-2825

Fig. 5-3. Angular distributions of ^{8}Be nuclei emitted from the $^{12}C(\alpha, {}^{8}Be_{g.s.})^{8}Be_{g.s.}$ reaction leading to the ^{8}Be ground state at E_{α} = 63.2, 65.2, 65.8, 66.6, and 67.3 MeV.

of the cross sections changed substantially causing Brown et al. to conclude that in this energy region statistical processes dominated direct ones. At the low bombarding energies of 12-26 MeV the $^{12}C(\alpha, {}^{8}Be)$ ^{8}Be reaction also seems to be dominated by compound processes (Ch 67, Ma 72, Ja 73, Br 73).

In summary, it seems that in the region of 20-40 MeV incident energies compound processes are important for the $(\alpha, {}^{8}Be)$ reaction mechanism, but at higher energies a direct mechanism is the major process, substantiating the conclusion of an earlier study (Wo 73).

2. Observed energy levels

A ^{8}Be energy spectrum of the $^{12}C(\alpha, {}^{8}Be)^{8}Be$ reaction taken with the modified identifier at $\theta_{lab} = 24°$ is shown in Fig. 5-4. This spectrum was obtained by bombarding a 300 $\mu g/cm^2$ carbon target with 72.5 MeV α-particles and by summing the kinematically corrected energy spectra from the three position gates. The observed energy resolution of the ^{8}Be ground state peak in Fig. 5-4 is 450 keV(FWHM). Transitions can be clearly seen to the 0^+ ground and 2^+ first excited states. Evidence is also seen for the population of the broad (FWHM ~ 7 MeV) 4^+ level at 11.4 MeV.

At a bombarding energy of 65 MeV angular distributions (Wo 73) were measured of the transitions to the ground and first excited states of ^{8}Be between $\theta_{cm} = 20 - 80°$. These data were taken with the simple identifier and at this bombarding energy only transitions to 0^+ ground and 2^+ first excited states were observed. Transitions to the 4^+ level at 11.4 MeV which were seen at 72.5 MeV were expected but

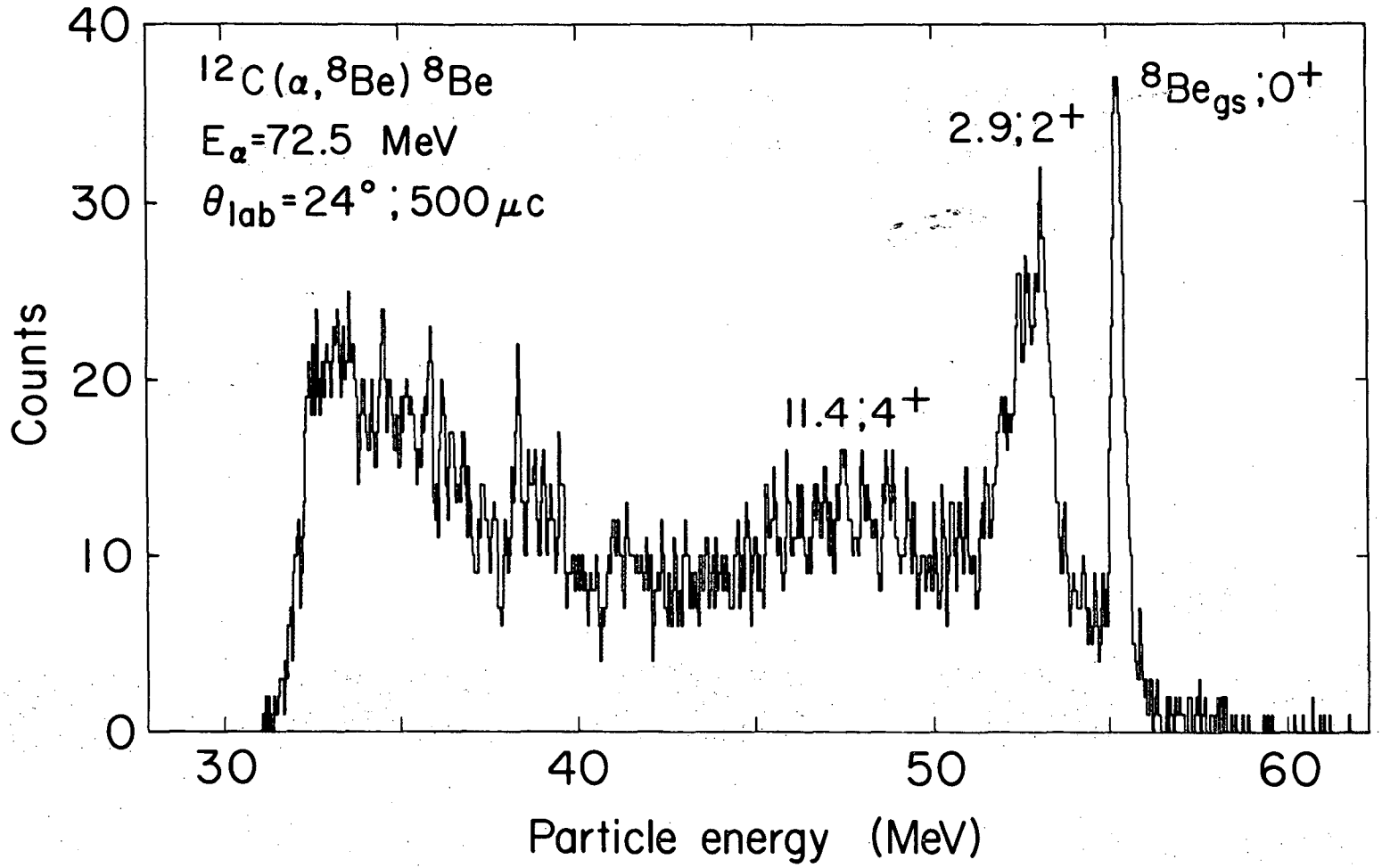

XBL 744-2833

Fig. 5-4. A ^{8}Be energy spectrum from the $^{12}C(\alpha, {}^{8}Be)^{8}Be$ reaction at θ_{lab} = 24°.

its broad width hindered their observation. Also, no population of the 2^+ (mixed isospin) states at ~ 16 MeV was seen.

Excitation energies, spins and parities of the levels populated in ^{8}Be were assigned by comparing the observed excitation energies (see Table V-2) to previously measured ones (Se 74). Kurath's calculated α-structure factors (Ku 73) predict approximately equal strengths for transitions to the first three members of the ground state band and the data are in excellent qualitative agreement as these levels are all made with the same intensity to within a factor of two. Intermediate-coupling calculations (Bo 64) indicate that the mixed isospin states at ~16 MeV have a dominant single particle nature. An upper limit of 20% of the ground state strength could be placed on the population of these mixed isospin levels which is consistent with their calculated relative α-structure factor of 0.1.

The above limit on the population of these mixed isospin states is in marked contrast to results obtained with the (d, ^{6}Li) and (^{3}He, ^{7}Be) reactions at incident energies of 55 MeV (Mc 71) and 120 MeV (Wo 74a), respectively. These reactions populated these mixed isospin states with an integrated cross section equal to that of the ground state. This large observed strength would argue the presence of substantial contributions from mechanisms other than a simple direct process in both the (d, ^{6}Li) and (^{3}He, ^{7}Be) reactions as these states should be populated very weakly by a direct α-cluster transfer.

Table V-2. Comparison of ^{8}Be levels observed in the $^{12}C(\alpha, {}^{8}Be)^{8}Be$ reaction with previously reported ones and with theoretical calculations.

Known levels[a]			Observed levels		Calculated levels[b]		Relative strength[c] at experimental first maximum	Relative α-spectroscopic factors	
MeV	J^{π}	T	MeV	±keV	MeV	J		Theory[b]	This work
0.0	0^{+}	0	0.0	50	0	0	1.00 (30)[d]	1.00	1.00
2.94	2^{+}	0	2.96	70	3.41	2	2.00	1.28	1.81
11.4	4^{+}	0	11.1	300	11.29	4	2.2[e]	1.39	---
16.63 16.91	2^{+} 2^{+}	0+1 0+1	---		14.43	2	<0.2	0.10	---

a) These excitation energies are from Se 74.

b) Ku 73.

c) These quantities were measured at E_{α} = 65 MeV, unless otherwise noted.

d) The quantity in parenthesis is the absolute differential cross section in μb/sr of the ground state transition at its experimental first maximum in the center of mass.

e) This relative cross section was determined at E_{α} = 72.5 MeV.

3. Angular distributions

Experimental angular distributions of transitions to the ground and first excited states of ^{8}Be at $E_{\alpha} = 65$ MeV are shown in Fig. 5-5. The L = 0 transfer to the ground state has a shape which shows the forward peaking and oscillatory behavior characteristic of a direct reaction. The L = 2 transfer also shows an oscillatory behavior with a slightly different phase than that of the L = 0 transfer. Only statistical error bars are shown and the absolute cross sections could be uniformly in error as much as 20%. The large error bars on the small angle points for the L = 2 distribution are caused by a strong background from the $^{12}C(\alpha, {}^{8}Be)\, 2\alpha$ process.

Diffraction model fits (solid curves) to the data are also given in Fig. 5-5. The L = 0 fit was normalized to the experimental points at their second maximum and a cutoff radius (R) of 8.8 fm was required to reproduce the phase of the distribution. A radius parameter (R_o) of 1.40 was used to calculate the form factor of the α-cluster inside ^{12}C. It should be noted that the amplitude of the third maximum is closely predicted and that the overall agreement with the L = 0 transfer data is good except for the two forward angle points.

For the fit to the L = 2 transfer, R was reduced by 7% to reproduce the position of the first maximum of the distribution. This adjustment introduced no amplitude change as is discussed later in Section V-C. A theoretical relative spectroscopic factor ($N_L^2(2^+/g.s.)$) of 1.3 (Ku 73) was used for the L = 2 fit otherwise all parameters were the same as those used in the above L = 0 fit. Assuming that the diffraction model correctly calculates the kinematic factor, then better

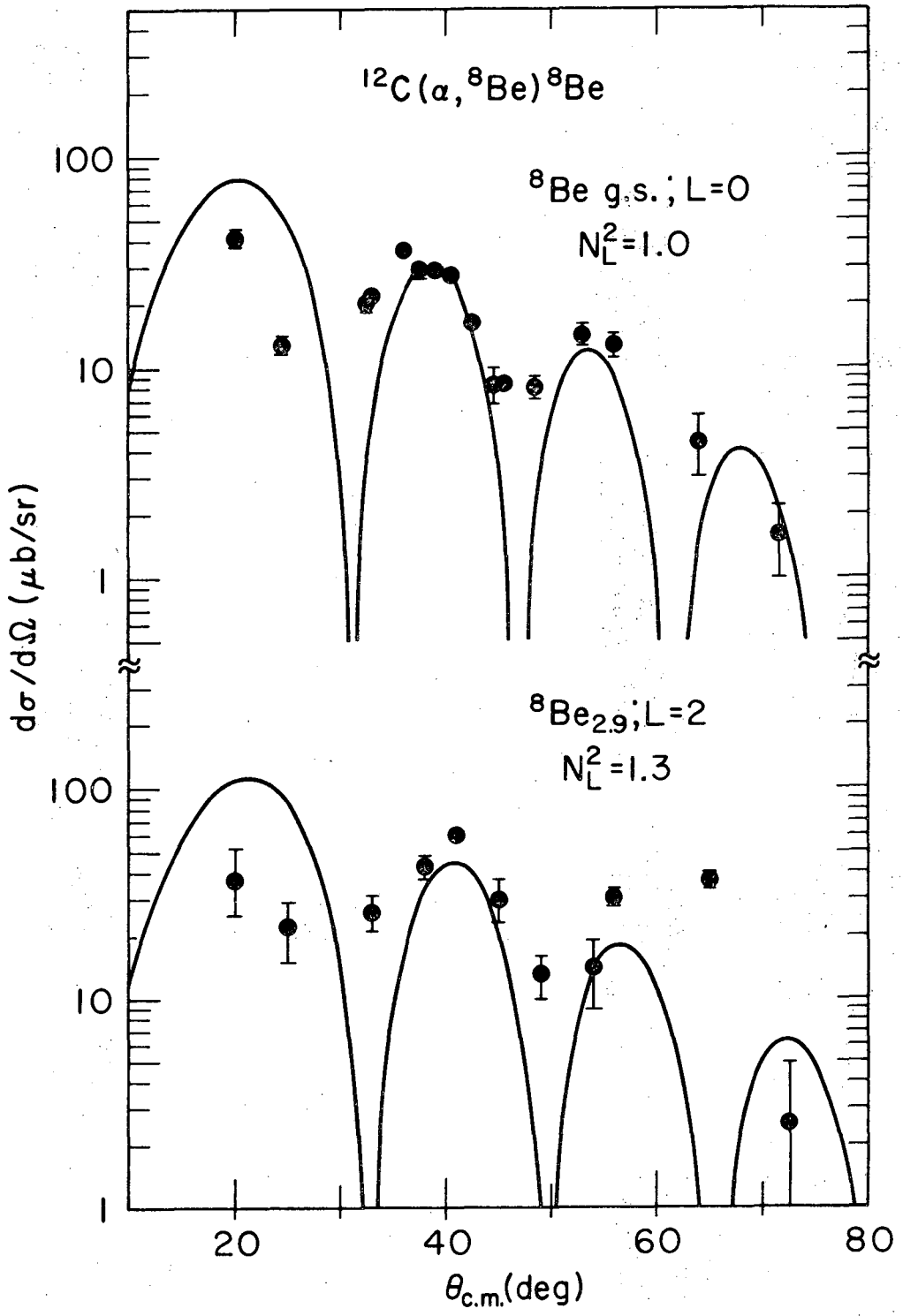

XBL 747-3616

Fig. 5-5. Cross section data for (α, ^{8}Be) transitions to the ground and first excited states of ^{8}Be at E_α=65 MeV with diffraction model fits (solid curves). See discussion in text.

agreement with the data would require a spectroscopic factor for the 2^+ state relative to the ground state of 1.8 (instead of the 1.3 used in Fig. 5-5) which is ~40% larger than the theoretical one. The agreement between the experimental and theoretical α-structure factors is fair considering that the ^{8}Be(2.9 MeV) state is unbound by ~3 MeV and that the theory can not be expected to well describe this unbound final state.

C. The ^{16}O(α, ^{8}Be)^{12}C Reaction

1. Observed energy levels

The ^{16}O(α, ^{8}Be)^{12}C reaction was investigated at two bombarding energies (65 and ~ 72 MeV, see Table V-1) with the bulk of the data taken at E_α = 65 MeV. At an incident energy of ~ 72 MeV both SiO_2 and oxygen gas targets were used and contributions from ^{28}Si impurities in the solid target were determined to be small. A ^{8}Be energy spectrum from a 220 μg/cm^2 SiO_2 target is shown in Fig. 5-6.

The observed energy resolution in Fig. 5-6 is 400 keV (FWHM) and transitions can be clearly seen to the ground and first three excited states of ^{12}C. Several small peaks due to ^{12}C and ^{28}Si impurities in the target appear in this spectrum in the region of the ^{12}C ground state and at excitation energies below 9 MeV and can be taken as an indication of their contribution to the spectrum at higher excitation energies. The 4^+ 14.08-MeV level in ^{12}C is weakly populated at this angle, however, it was seen with large strength at other angles as is shown in Fig. 5-7. This energy spectrum was obtained with a gas target at θ_{lab} = 23° and a gas pressure of 0.28 atmospheres. The

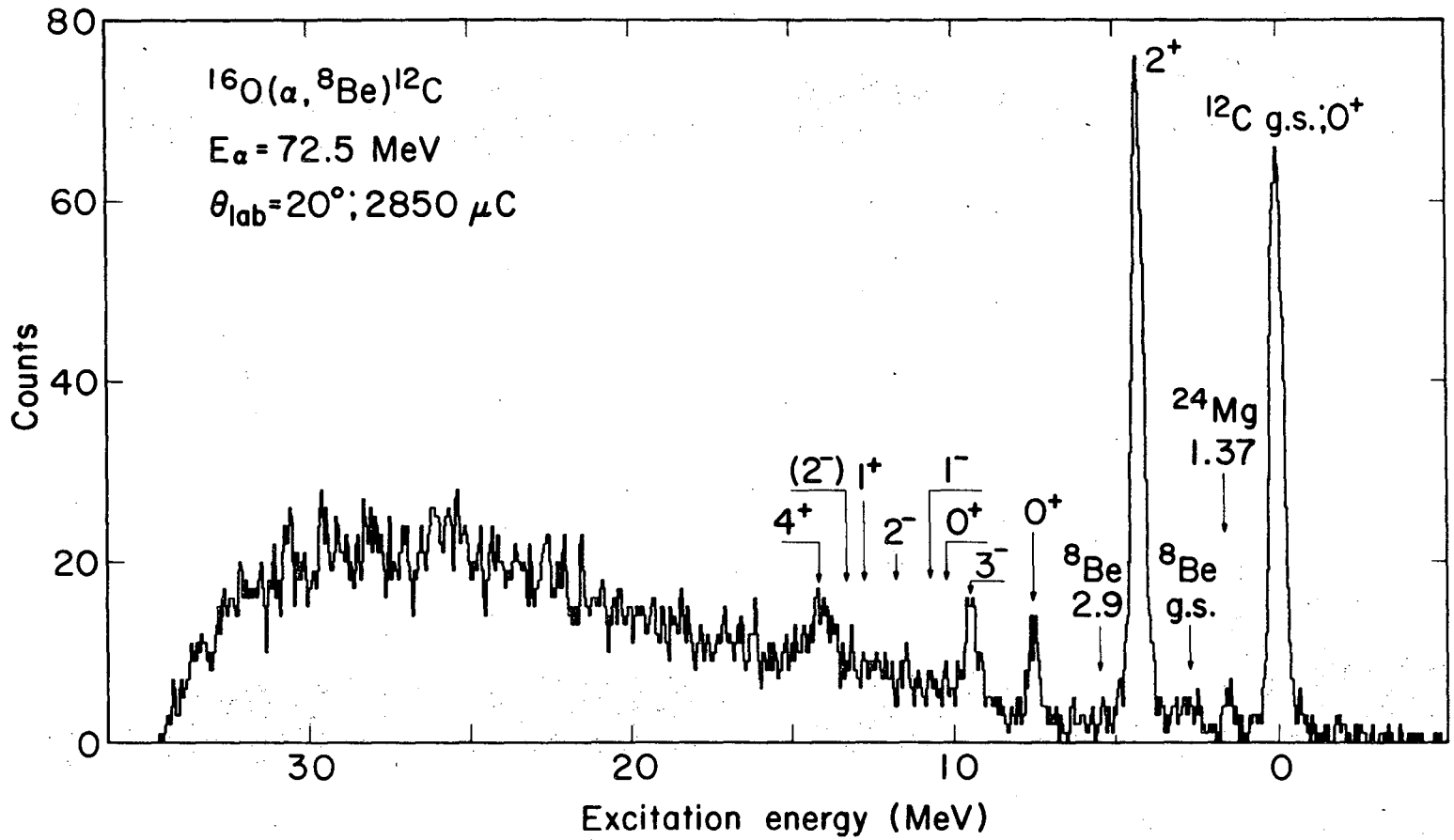

Fig. 5-6. An energy spectrum from the $^{16}O(\alpha, {}^{8}Be)^{12}C$ reaction at $\theta_{lab} = 20°$. The locations of possible transitions to all final states in ^{12}C below 14 MeV excitation are indicated. This spectrum was obtained with a SiO_2 target and the locations of several transitions from ^{28}Si and ^{12}C target impurities are also shown.

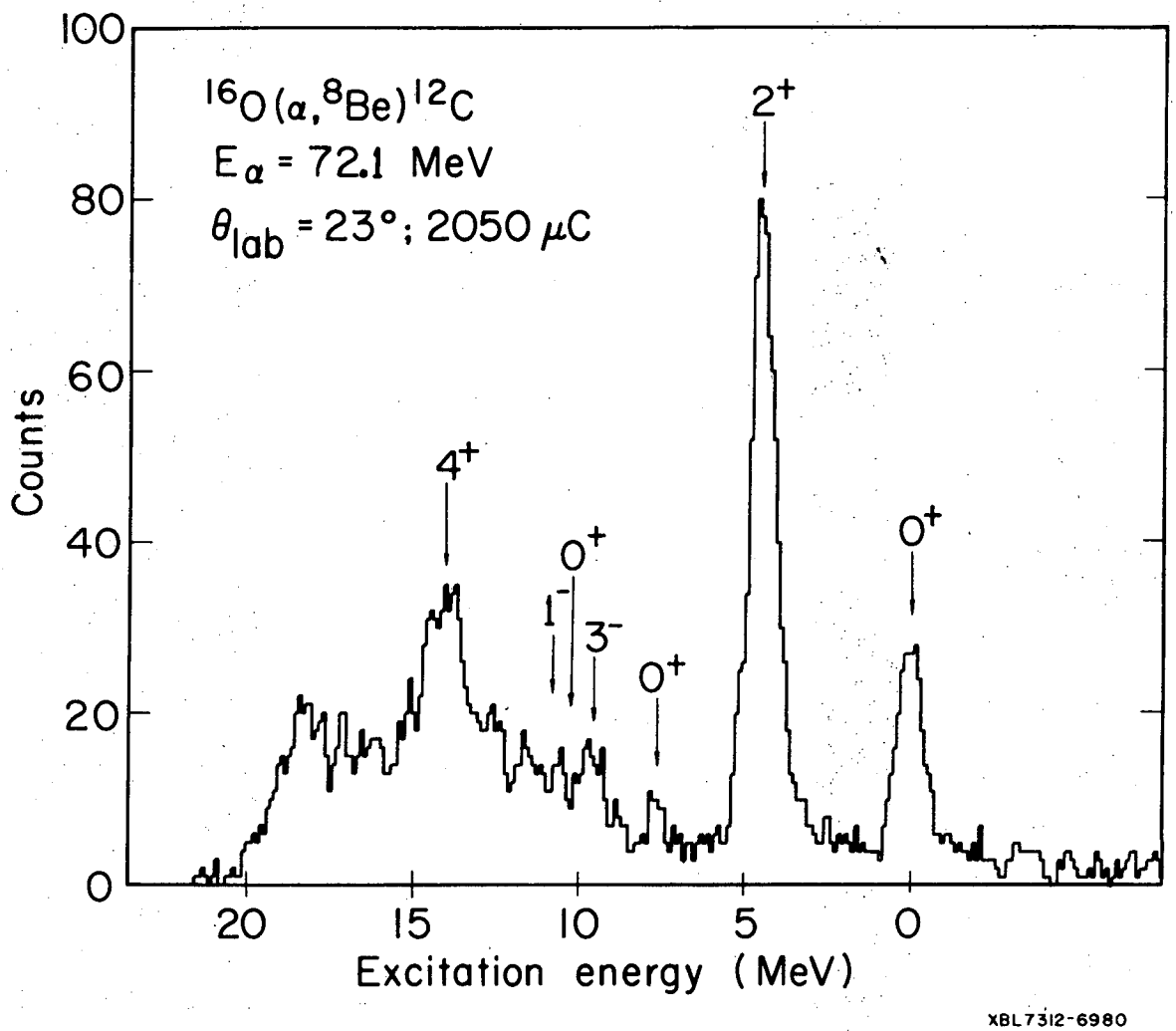

Fig. 5-7. An energy spectrum from the $^{16}O(\alpha, {}^{8}Be)^{12}C$ reaction at $\theta_{lab} = 23°$. This spectrum was obtained with a gas target and the locations of transitions to all natural parity states in ^{12}C below 14 MeV are indicated.

observed energy resolution was ~850 keV FWHM and was typical of the poorer resolution obtained with gas targets. An upper limit of 5% of the observed ground state strength at $E_\alpha \sim 72$ MeV was set for transitions to the five known levels between 10 and 14 MeV excitation energy in ^{12}C. Possible weak transitions to these levels were obscured by a rising continuum background and either a) possible impurity states from the solid target or b) the poor resolution obtained with the gas target.

The $^{16}O(\alpha, {}^8Be)^{12}C$ reaction was also studied at a bombarding energy of 65 MeV and angular distributions were measured of the transitions to the ground and first excited states of ^{12}C between $\theta_{cm} = 20° - 80°$. A 255 $\mu g/cm^2$ SiO_2 target and the simple identifier were used. At this beam energy as at the higher one, only the 0^+ ground, 2^+ first excited and 4^+ 14.08-MeV states were observed to be strongly populated. The 3^- 9.64-MeV state was weakly populated whereas the 0^+ 7.65-MeV level (observed with weak strength at $E_\alpha \simeq 72$ MeV) was obscured by background not eliminated by the simple identifier and by a significant contribution from a ^{12}C impurity in the target. To determine the possible contribution to the SiO_2 data arising from ^{24}Mg states populated by the $(\alpha, {}^8Be)$ reaction on ^{28}Si at this bombarding energy, a natural silicon target was irradiated and this contribution was determined to be small. The above data indicate that the $(\alpha, {}^8Be)$ reaction on an ^{16}O target is quite selective in which final states of ^{12}C it populates strongly.

Excitation energies, spins and parities of the levels populated by the $(\alpha, {}^8Be)$ reaction were assigned by comparing the observed

Table V-3. Comparison of ^{12}C levels observed in the $^{16}O(\alpha, {}^{8}Be)^{12}C$ reaction with previously reported ones and with theoretical calculations.

Known levels[a]			Observed levels		Calculated[b] levels		Relative strength[c] experimental first maximum	Relative α-spectroscopic factors	
MeV	J^{π}	T	MeV	±keV	MeV	J		Theory[b]	This work
0.0	0^+	0	0.0	40	0	0	1.00 (17)[d]	1.00	1.00
4.44	2^+	0	4.42	40	4.6	2	1.94	5.56	3.4
7.65	0^+	0	7.67	50	13.5	0	~.13[e]	.25	
9.64	3^-	0	9.65	50	---		~.14[e]	---	
10.3	(0^+)	0	---		---		<.05[e]	---	
10.84	1^-	0	---		---		<.05[e]	---	
11.83	2^-	0	---		---		<.05[e]	---	
12.71	1^+	0	---		---		<.05[e]	---	
13.35	(2^-)	0	---		---		<.05[e]	---	
14.08	(4^+)	0	14.06	100	13.5	4	.44[e]	10.19	
					15.7	2	---	.25	
					18.1	2	---	.27	
					23.7	4	---	1.15	

a) These excitation energies are from Se 68.

b) Ku 73.

c) These relative strengths are measured at E_{α} = 65 MeV unless otherwise noted.

d) The quantity in parenthesis is the absolute differential cross section in μb/sr of the ground state transition at its experimental first maximum in the center of mass.

e) These relative strenghts were measured at $E_{\alpha} \simeq$ 72 MeV.

excitation energies to known ones (see Table V-3). If the (α, ^{8}Be) is a good a-transfer reaction, then the states that it populates strongly should be connected to the target nucleus's ground state by a large α-structure factor. A qualitative comparison of observed strengths to calculated α-structure factors will be given below.

In Table V-3 are tabulated transition strengths relative to that of the ground state at their experimental first maxima. To facilitate comparing cross sections on different targets, the absolute differential cross section for the ground state transition at its experimental first maximum is given in parenthesis in the relative strength column of Table V-3. The last column in this table gives the theoretical α-structure factors calculated by Kurath (Ku 73) relative to that of the $^{12}C_{gs}$. Comparing this column with that of the experimental relative strengths, one sees that there is reasonable qualitative agreement. Of the four levels which Kurath predicts to have relative α-structure factors greater than unity, the first three are populated strongly by the (α, ^{8}Be) reaction. The fourth level, which was not observed and is experimentally unknown, is a 4^+ level predicted to occur at ~24 MeV. Since this level is far above the α-particle emission threshold at 7.4 MeV excitation, it is almost certain to have a broad width and thus be difficult to experimentally observe. It should be noted that the 4^+-14.08 MeV state is populated a factor of 20 less than Kurath's α-structure amplitude would predict. Some of this weak relative strength can be accounted for by the fact that the cross section decreases with the binding energy of the picked-up cluster (see De 70), that is with the excitation energy of the residual nucleus. The 0^+ level

predicted by Kurath to occur at 13.5 MeV probably corresponds to the known 0^+ level at 7.65 MeV which is populated at a level consistent with its calculated α-structure factor.

The population of the 3^- 9.64 MeV state requires an L = 3 transfer for the case of pure α-particle pickup. Such a transfer is impossible if all four transferred particles are in the 1p-shell. However, this state may be formed via known 2p-2h and 4p-4h admixtures (Lo 66) in the ground state wave function of ^{16}O. Both the (d, ^6Li) and (^3He, ^7Be) reaction also populate this state with an appreciable fraction of the ground state strength (see Co 72, Mc 71, De 70). Alternatively, since the 3^- state could be made in a two-step process, the relative strength of this state can be taken as an upper limit of the contribution of such a mechanism to the α-cluster transfer.

The above observations are in qualitative agreement with earlier work (Br 65) on the reaction $^{16}O(\alpha, {}^8Be)^{12}C$ at $E_\alpha = 35.5$-41.9 MeV for the relative strengths of transitions to the ground and first excited states. However, at $E_\alpha = 41.9$ MeV the 3^- state was populated with roughly the same strength as the ground state at the angles studied. In contrast at our bombarding energy of ~ 72 MeV, the yield to the 3^- state was ~14% of the ground state yield. If the population of the 3^- state is taken as a measure of the contribution of 2-step processes, then this contribution is substantially less at high bombarding energies.

2. Angular distributions

The experimental points for transitions to the ^{12}C ground and first excited states are shown in Fig. 5-8. (The small open circles

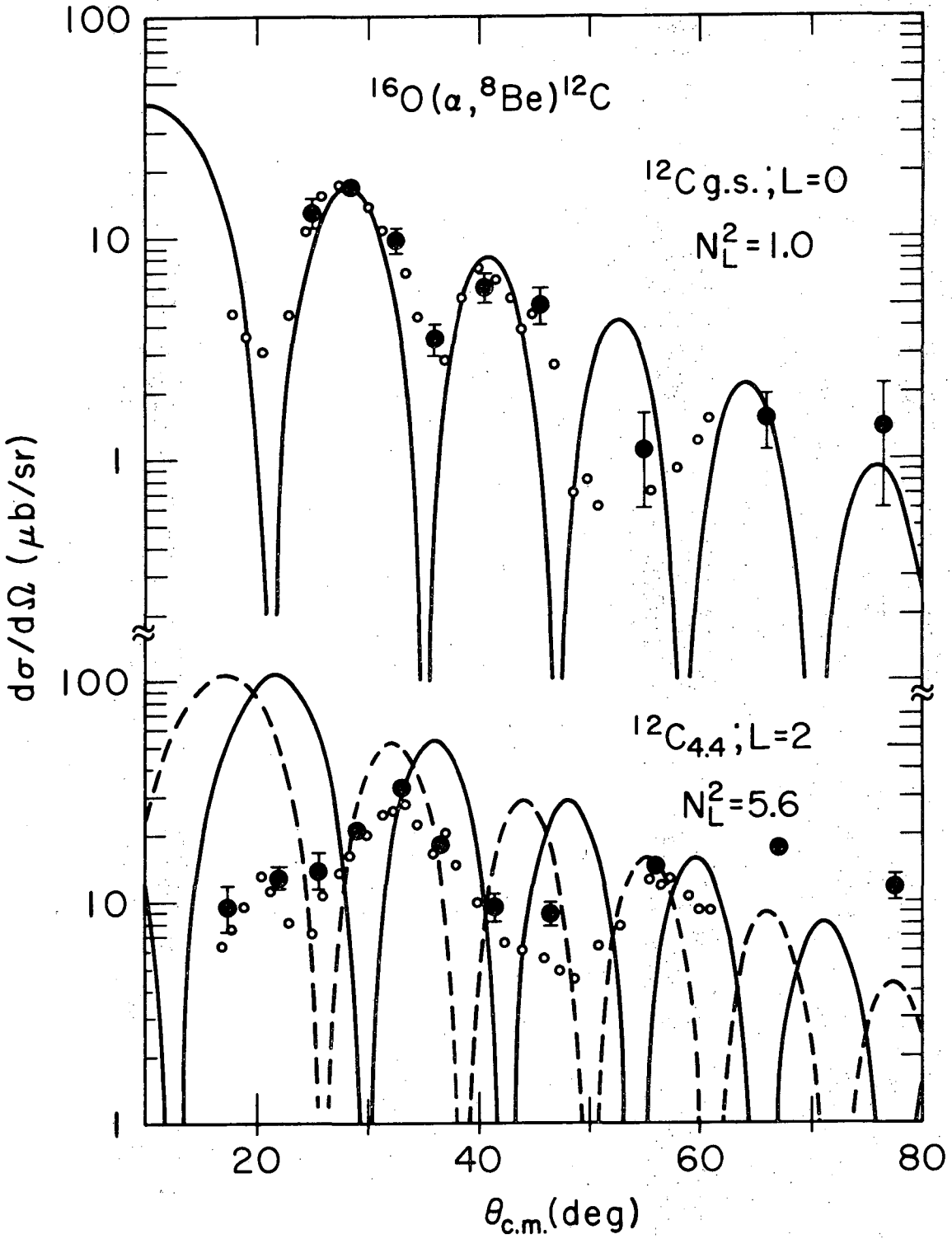

XBL 747-3615 a

Fig. 5-8. Cross section data for (α, ^{8}Be) transitions to the ground and first excited states of ^{12}C at $E_\alpha = 65$ MeV with diffraction model fits (solid curves). The small open circles are preliminary results from a recent experiment. See discussion in text.

are preliminary results from a recent experiment.) The L = 0 angular distribution shows the typical characteristics of a direct reaction. It has an oscillatory pattern and is forward peaked, falling off a factor of ten from 30° to 60°. The L = 2 angular distribution for the transfer to the 2^+, 4.44 MeV state is less characteristic of a direct reaction. It shows evidence of two oscillations separated by a broad dip. At back angles the L = 2 cross section is an order of magnitude larger than the L = 0 one.

Diffraction model fits to the data are also shown in Fig. 5-8. The L = 0 fit was normalized to the data at the first maximum of the distribution and a cutoff radius (R) of 9.8 fm was chosen to correctly reproduce the phase. A radius parameter (R_o) of 1.20 which correctly gives the size of ^{16}O was used to calculate the form factor of the α-cluster inside ^{16}O. It should be noted that the amplitude of the second maximum is predicted well and that the overall agreement is fair.

Two L = 2 fits to the 2^+-4.44 MeV data are shown. The solid curve was calculated using the same R and R_o as was used for the L = 0 fit. The L = 2 fit predicts the observed maximum further back in angle than is experimentally observed. Increasing R by 7% correctly predicts this maximum (dashed curve) with virtually no change in amplitude. The amplitude of the calculated differential cross section is insensitive to small changes in R.

Both of the L = 2 fits were calculated using the relative spectroscopic factor (N_L^2 (2^+/gs) = 5.6) predicted by Kurath (Ku 73) and the same normalization as was used for the L = 0 fit. Assuming that the diffraction model correctly calculates the kinematical factor for the

(α, ^{8}Be) reaction then the data indicate a spectroscopic factor of 3.4 which is 40% smaller than the theoretical one. It should be noted that a study of the ^{16}O(d, ^{6}Li)^{12}C reaction gave a ratio of the integrated cross sections for populating the 2^+ relative to that of the ground state of ~3. If the kinematic factors in that reaction were similar to those seen here, this ratio would also give a relative spectroscopic factor in agreement with that determined from the (α, ^{8}Be) reaction.

Although the 4^+ 14.08 MeV state in ^{12}C was only observed at a limited number of angles, its maximum differential cross section is well determined. Thus a relative α-structure factor ($N_L^2(4^+/gs)$) of 2.1 was extracted which is a factor of five smaller than the ratio predicted by Kurath.

D. The ^{10}B(α, ^{8}Be)^{6}Li Reaction

1. Observed energy levels

An investigation of the ^{10}B(α, ^{8}Be)^{6}Li reaction was carried out at 72.5 MeV with the modified identifier. In Fig. 5-9 is shown a typical ^{8}Be energy spectrum which was obtained at a laboratory angle of 24° by irradiating a 150 μg/cm^2 self-supporting ^{10}B(98%) target. The experimental energy resolution was 500 keV (FWHM).

The above spectrum is dominated by transitions to the 3^+ level which would be expected to be populated the strongest from calculated α-structure factors for ^{10}B (see Table V-4). No evidence for transitions to the 2^+ 4.30 MeV and 1^+ 5.7 MeV states or the T = 1 states at 3.65 MeV and 5.37 MeV was obtained. The predicted location of transitions to these states are indicated in Fig. 5-9. The former two states

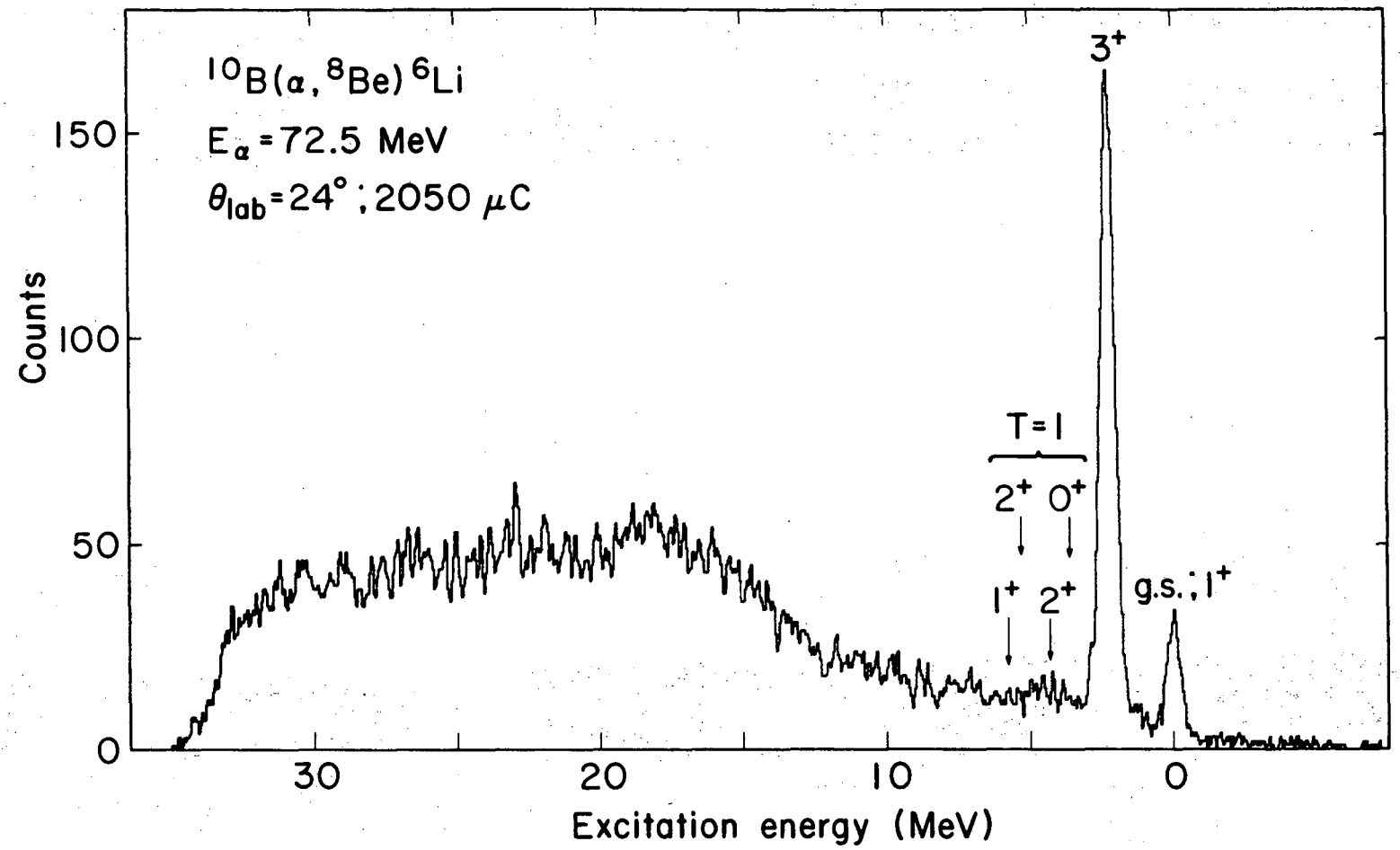

XBL 747-3619

Fig. 5-9. A ^{8}Be energy spectrum from the $^{10}B(\alpha, ^{8}Be)^{6}Li$ reaction at $\theta_{lab} = 24°$. The locations of possible transitions to the ^{6}Li ground and first five excited states are indicated. See discussion in text.

Table V-4. Comparison of ^{6}Li levels observed in the $^{10}B(\alpha, {}^{8}Be)^{6}Li$ reaction with previously reported ones and with theoretical calculations.

Known levels[a]			Observed levels		Calculated[b] levels		Average[c] relative strengths	Relative α-spectroscopic factors[b]			
MeV	J^{π}	T	MeV	±keV	MeV	J		N_0^2	N_2^2	N_4^2	ΣN_L^2
0.0	1^+	0	0.0	30	0	1	.22		<.001	.004	~.003
2.18	3^+	0	2.18	30	2.14	3	1.00(31)[d]	.304	.826	.339	1.00
3.56	0^+	1	---		---		---	---	---	---	---
4.30	2^+	0	---		5.33	2	---		.054	.033	.06
5.37	2^+	1	---		---		---	---	---	---	---
5.7	1^+	0	---		5.06	1	---		.001	.008	.01
26.1	4^-	1	---		---		---	---	---	---	---

a) These excitation energies were taken from Se 74.

b) Ku 73.

c) These relative strengths were determined at E_{α} = 72.5 MeV.

d) The quantity in parenthesis is the absolute differential cross section in the center of mass for this transition.

have small calculated α-structure factors while the latter two are forbidden by the $\Delta T = 0$ selection rule. An upper limit of 5% of the first excited state's strength was set on the population of these levels. An interesting feature of the above spectrum is the large reaction strength at high excitation energies (~ 15 MeV) which was observed at all angles studied.

As can be seen from Table V-4, good overall qualitative agreement with Kurath's predictions is observed. (Since multiple L-transfers are allowed, contributions arise from each allowed L-value. In Table V-4 Kurath's spectroscopic amplitudes (N_L^2) are tabulated as well as a sum over L of these quantities ($\Sigma_L N_L^2$) which have been normalized to 1.00 for the 3^+ 2.18 MeV state in ^{6}Li. (A very similar procedure is used for the ^{11}B and ^{14}N targets.) It should be noted, however, that the ground state is populated with approximately two orders of magnitude larger strength than is predicted by Kurath. A similar disagreement with Kurath's predictions was observed in investigations with the (d, ^{6}Li) and (^{3}He, ^{7}Be) reactions. Both reactions populated the ^{6}Li first excited state stronger than the ground state, at least one order of magnitude larger than the ratio of theoretical α-structure amplitudes in Table V-4. No evidence was seen in either reaction for transitions to other excited states in ^{6}Li which is in excellent agreement with the above (α, ^{8}Be) results.

2. Angular distributions

The angular distributions of the transfers to both the ground and first excited states of ^{6}Li are slowly varying and have an almost

constant amplitude (see Fig. 5-10). This lack of obvious direct features may be due to the fact that multiple L transfers are allowed (see Table V-4) because the ^{10}B ground state has a spin of 3. In fact these distributions show the same large back angle strength as the L = 2 transfers on ^{12}C and ^{16}O.

In the diffraction model described in Section IV, the contributions from different L values should add incoherently. Thus one would expect an oscillatory envelope for the cross section which is modulated by several form factors rather than one. These multiple form factors will cause some washing out of the oscillations from the individual L transfers. However, diffraction model calculations for the multiple L transfers to the ground and first excited states of ^{6}Li gave oscillatory cross sections which failed to reproduce the experimental points as is shown in Fig. 5-10 (solid and dashed curves). The magnitude of both curves were normalized to the forward angle data points and these calculations were performed using Kurath's α-structure factors, a radius parameter (R_o) of 1.4 and a cutoff radius (R) of 8.7 fermis. The calculated angular distribution for the ground state transition reproduces some of the observed back angle strength. This calculated back angle strength is due to the fact that the α-cluster inside ^{10}B is weakly bound (see Table V-1) and thus its wave function is more spatially extended than those of ^{12}C or ^{16}O.

(An alternative explanation of the back angle strength of the above transitions could arise from the (α, ^{6}Li) reaction considering this is such a light target. If this reaction has a large probability at back angles, then ^{8}Be's emitted in the forward direction will contribute

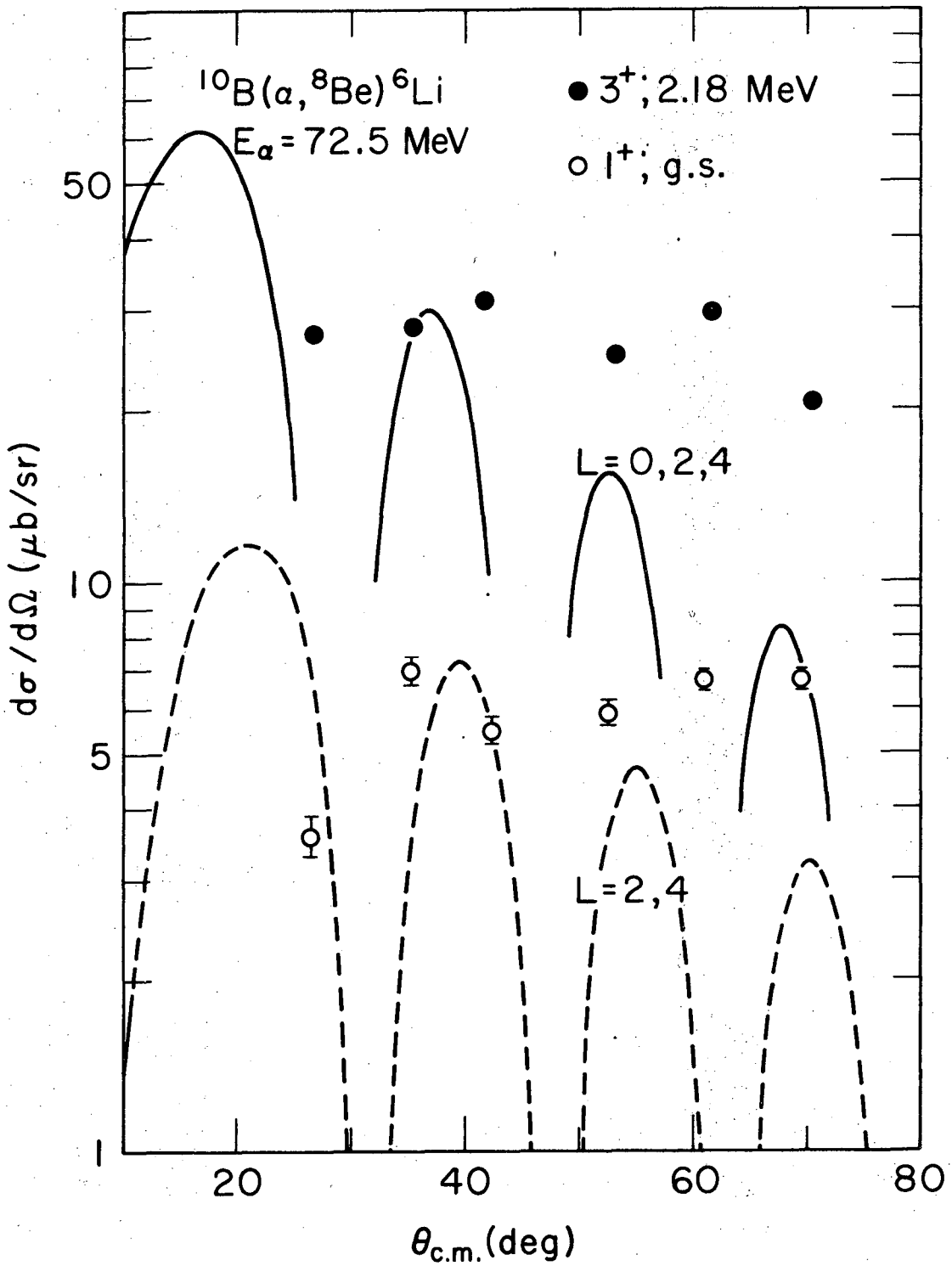

XBL 747-3621a

Fig. 5-10. Cross section data for (α, ^{8}Be) transitions to the ground and first excited states of ^{6}Li at E_α = 72.5 MeV with diffraction model fits. See discussion in text.

to the α-pickup cross section. (At forward angles and E_α = 46 MeV the (α, ^{6}Li) cross section is a factor of 50 larger than that of the (α, ^{8}Be) reaction (Ze 70).) This contribution should be small for ^{8}Be's emitted at forward angles and increase with $\theta_{c.m.}$. Thus the increasing contribution due to the (α, ^{6}Li) reaction added to the decreasing α-pickup component could give a flat angular distribution if the two contributions have similar magnitudes. However, at very forward angles most of the reaction strength should be due to the α-pickup process.)

E. The ^{11}B(α, ^{8}Be)^{7}Li Reaction

1. Observed energy levels

The ^{11}B(α, ^{8}Be)^{7}Li reaction was investigated briefly at E_α = 72.5 MeV with the modified identifier and more completely with the simple identifier at E_α = 65 MeV. Representative spectra obtained at these energies are shown in Figs. 3-6 and 3-12 of Section III. At 65 MeV, angular distributions were taken of the strong transitions populating the $3/2^-$ ground and $7/2^-$ 4.63-MeV second excited states of ^{7}Li. These distributions were rather structureless and quite flat (see Fig. 5-11). Weak transitions to the two $5/2^-$ states at 6.68 and 7.47 MeV were observed at only two angles, however, the large continuum background may have obscured these transitions at other angles.

At an incident energy of 72.5 MeV the ^{11}B(α, ^{8}Be)^{7}Li reaction was observed at a laboratory angle of 20° (see Fig. 3-12). Strong transitions to the $3/2^-$ ground and $7/2^-$ second excited states were observed and moderate ones to the $1/2^-$ first excited state and the two $5/2^-$ states at 6.68 and 7.47 MeV (see Table V-5). Due to the fact that

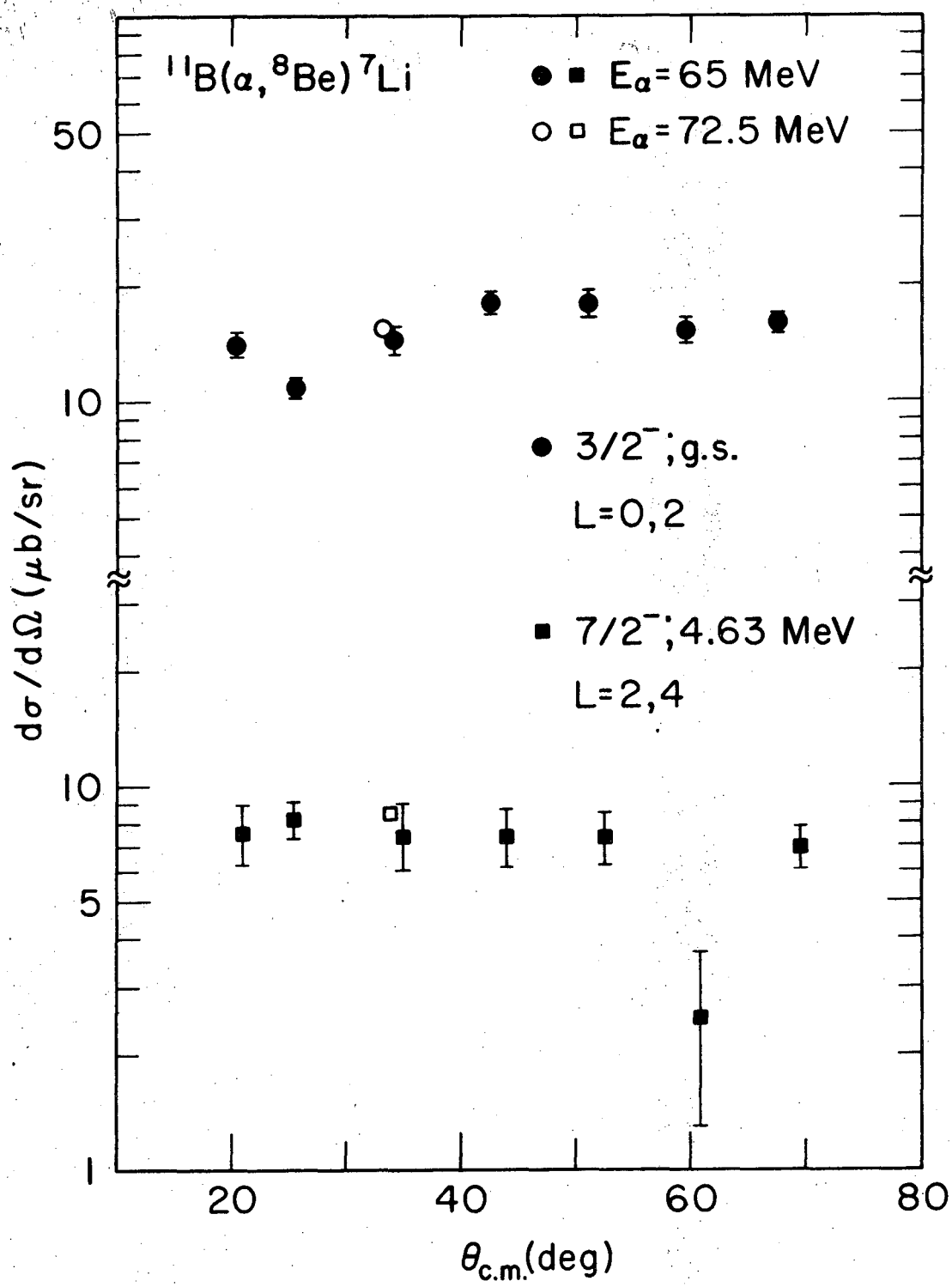

XBL 747-3622

Fig. 5-11. Cross section data for (α, ^{8}Be) transitions to the ground and second excited states of ^{7}Li at E_α = 65 MeV. See discussion in text.

that the ground and first excited state peaks were poorly resolved there is a large uncertainty on the strength of the transition to this latter state. No states were observed above 8 MeV excitation and an upper limit of ~ 7% of the ground state strength was placed on the population of such states. This limit is consistent with the small calculated α-structure factor for the $3/2^-$ 10.25 MeV state and the $\Delta T = 0$ selection rule which forbids populating the $3/2^-$, $T = 3/2$, 11.25 MeV state.

Comparisons between relative observed strengths with theoretical α-structure factors are somewhat difficult due to the allowed multiple L values. However, for ^{11}B the observed transition strengths are qualitatively in agreement with the summed calculated α-structure factors for the allowed L values except that the first excited state is populated much stronger than one would expect (see Table V-5).

The above observations for transitions to the ground and first two excited states are in agreement with a study of the $^{11}B(d, {}^6Li)^7Li$ reaction at 19.5 MeV. However, in contrast, the $(^3He, {}^7Be)$ reaction on this target populated both the ground and first excited states with equal intensity and only weakly populated the $7/2^-$ 4.63 MeV state at an incident energy of 36 MeV (Br 72) which is inconsistent with the calculated α-structure factors and also with the $(d, {}^6Li)$ and $(\alpha, {}^8Be)$ data.

2. Angular distributions

As was the case for the ^{10}B target which also involved multiple L transfers, the diffraction model calculations did not reproduce the observed angular distributions to the ^7Li ground and second excited states. The experimental angular distributions which are shown in Fig. 5-11 are generally to within a factor of two.

Table V-5. Comparison of the ^{7}Li levels observed in the $^{11}B(\alpha, {}^{8}Be)^{7}Li$ reaction with previously reported ones and with theoretical calculations.

Known levels[a]			Observed levels		Calculated[b] levels		Average[c] relative strengths	Relative α-spectroscopic factors[b]			
MeV	J^{π}	T	MeV	±keV	MeV	J		N_0^2	N_2^2	N_4^2	ΣN_L^2
0.0	$3/2^-$	1/2	-0.04	50	0	3/2	1.00(14.5)[d]	.453	.691		1.00
0.48	$1/2^-$	1/2	.52	50	1.07	1/2	.29[e]		.003		<.01
4.63	$7/2^-$	1/2	4.64	30	4.79	7/2	.57		.113	.742	.75
6.68	$5/2^-$	1/2	---		7.40		.21[e]		.059	.073	.12
7.47	$5/2^-$	1/2	7.46		9.15		.18[e]		.078	.045	.11
9.61	$7/2^-$	1/2	---		---		<.07[e]	---	---	---	---
10.25	$3/2^-$	1/2	---		10.87 11.82		<.07[e]		.003 .013	.006 .014	.03
11.25	$3/2^-$	3/2	---		---		<.07[e]	---	---	---	---

a) These excitation energies were taken from Se 74.

b) Ku 73.

c) These relative strengths were determined at $E_\alpha = 65$ MeV, unless otherwise noted.

d) The quantity in parenthesis is the absolute differential cross section in the center of mass for this transition.

e) These relative strengths were determined at $E_\alpha = 72.5$ MeV.

Data from the (d, ^{6}Li) and (^{3}He, ^{7}Be) reactions at 19.5 and 36 MeV, respectively, show angular distributions of the ground state transition that are forward peaked and fall off an order of magnitude from 10 - 60° in the c. of m. The fact that the (α, ^{8}Be) reaction yields rather flat angular distributions may be due to a strong (α, ^{7}Li) reaction strength in the backward hemisphere. Comparing parts a and b of Fig. 3-6, demonstrates that the ^{11}B(α, ^{7}Li)^{8}Be reaction has a cross section that is in fact 20 times larger than the ^{11}B(α, ^{8}Be)^{7}Li reaction at approximately the same forward angle.

F. The ^{14}N(α, ^{8}Be)^{10}B Reaction

1. Observed energy levels

A brief survey of the (α, ^{8}Be) reaction on a $^{14}N_2$ gas target was carried out at an incident energy of 72.1 MeV with the simple identifier. Three angles were studied between θ_{lab} = 18° - 28° and an energy resolution of ~800 keV (FWHM) was attained with a gas pressure of 0.33 atmospheres. Because the effective area of the PSD used was only 10×10 mm, it was necessary to place the counter telescope close to the gas cell wall to attain a large detection efficiency. This restriction plus straggling in the cell walls and the extended target caused poor energy resolution.

In Fig. 5-12 is shown an energy spectrum taken at θ_{lab} = 18° with the predicted locations of transitions to T = 0 states indicated. No evidence was observed for the excitation of the T = 1 states occuring at 1.74 and 5.17 MeV in accordance with the ΔT = 0 selection rule. Strong transitions were observed to the 3^+ ground, 1^+ 2.15 MeV, 2^+ 3.59 MeV

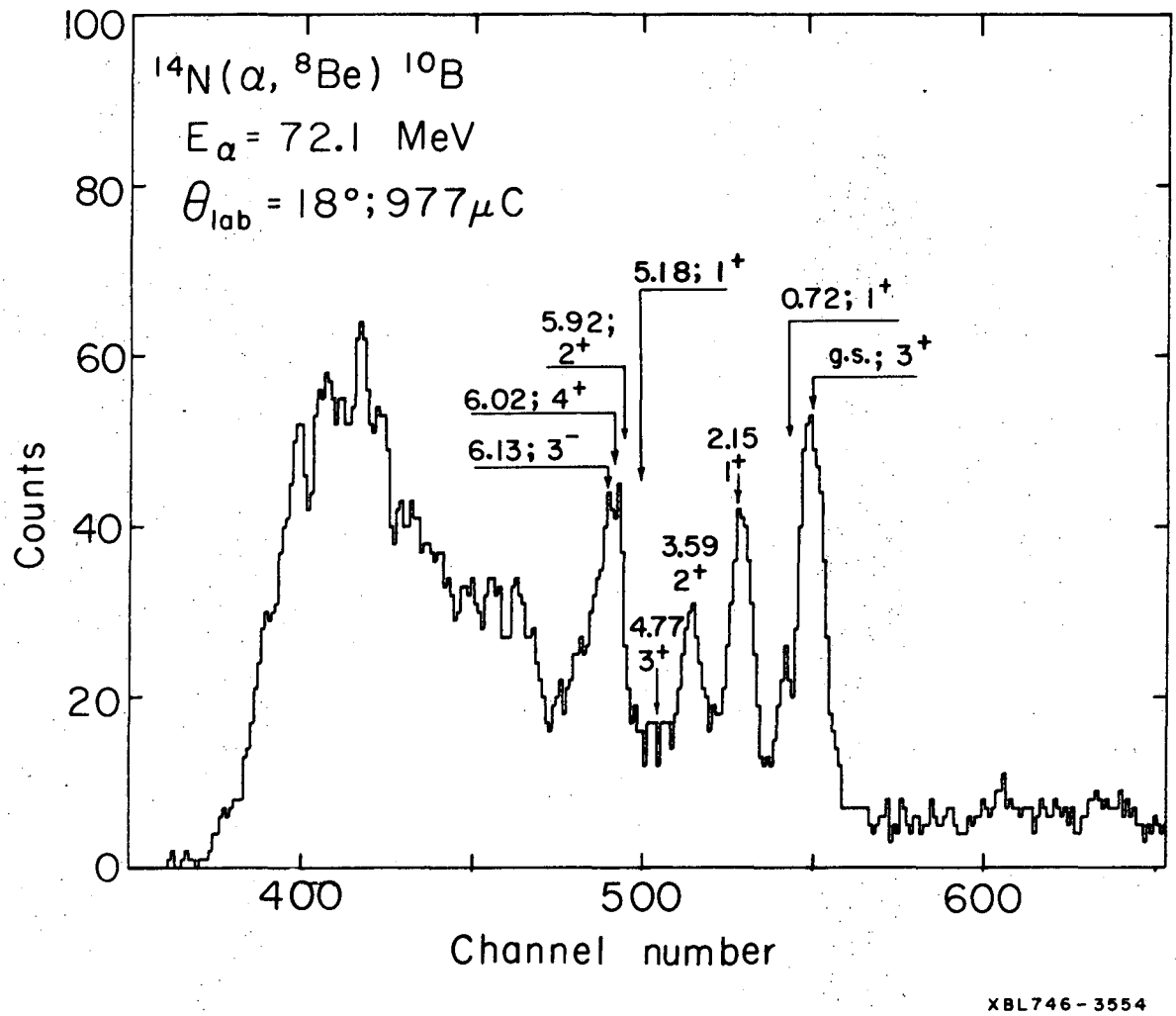

Fig. 5-12. A ^{8}Be energy spectrum from the $^{14}N(\alpha, {}^{8}Be)^{10}B$ reaction at θ_{lab} = 18°. The locations of possible transitions to natural parity states below ~6 MeV are shown (see text).

states and to a state at 6.07 ± .06 MeV which are in qualitative agreement with calculated α-structure factors (see Table V-6). The observed state at 6.07 MeV probably corresponds to the known 4^+ level at 6.02 MeV which has a large theoretical α-structure factor. Weak transitions were observed to the 1^+ 0.72 MeV and 3^+ 4.77 MeV states and no evidence was observed for the excitation of the 1^+ 5.18 MeV state, which is consistent with their small theoretical α-structure factors. No evidence for the population of discrete states above ~6 MeV excitation energy was observed, however, the large level density and poor resolution hindered this search.

The large background level above the ground state is caused by intra-beam-burst pileup events. This is a product of the counting rate of 15 kHz in each of the ΔE detectors and the high radiation field caused by the beam striking the gas isolation foils.

2. Angular distributions

The data points shown in Fig. 5-13 span a very limited angular range, and over which the magnitudes of the angular distributions for the four strongly populated states are similar.

G. The $^{15}N(\alpha, {}^{8}Be)^{11}B$ Reaction

1. Observed energy levels

The $^{15}N(\alpha, {}^{8}Be)^{11}B$ reaction was studied at an incident energy of 72.1 MeV with the same equipment described in Section V-F. $^{15}N_2$ gas isotopically enriched to 99% was used as a target. In Fig. 5-14 is shown a typical spectrum of this reaction. The experimental energy

Table V-6. Comparison of ^{10}B levels observed in the $^{14}N(\alpha, {}^{8}Be)^{10}B$ reaction with those reported previously and with theoretical calculations.

Known levels[a]			Observed levels		Calculated[b] levels		Average[c] relative strengths	Relative α-spectroscopic factors[b]			
MeV	J^{π}	T	MeV	±keV	MeV	J		N_0^2	N_2^2	N_4^2	ΣN_L^2
0.0	3^+	0	0.03	50	0.0	3	1.00 (7.0)[d]		.034	1.901	1.00
.72	1^+	0			.90	1	.13	.011	.348		.19
1.74	0^+	1	---		---		---	---	---	---	---
2.15	1^+	0	2.11	50	2.38	1	.69	.228	.261	---	.25
3.59	2^+	0	3.58	60	3.34	2	.74		.963		.50
4.77	3^+	0	4.76	70	4.72	3	.11		.122	.010	.07
5.11	2^-	0	---		---		---	---	---	---	---
5.17	2^+	1	---		---		---	---	---	---	---
5.18	1^+	0	---		6.19	1	---	.163	.042		.11
5.92	2^+	0	---		5.53	2	---		.001		.001
6.02	4^+	---	6.07		5.72	4	.85			1.121	.58
6.13	3^-	---	---		---		---				---

a) These excitation energies were taken from Se 74.
b) Ku 73.
c) These relative strengths were determined at E_α = 72.1 MeV.
d) The quantity in parenthesis is the absolute differential cross section in the center of mass for this transition.

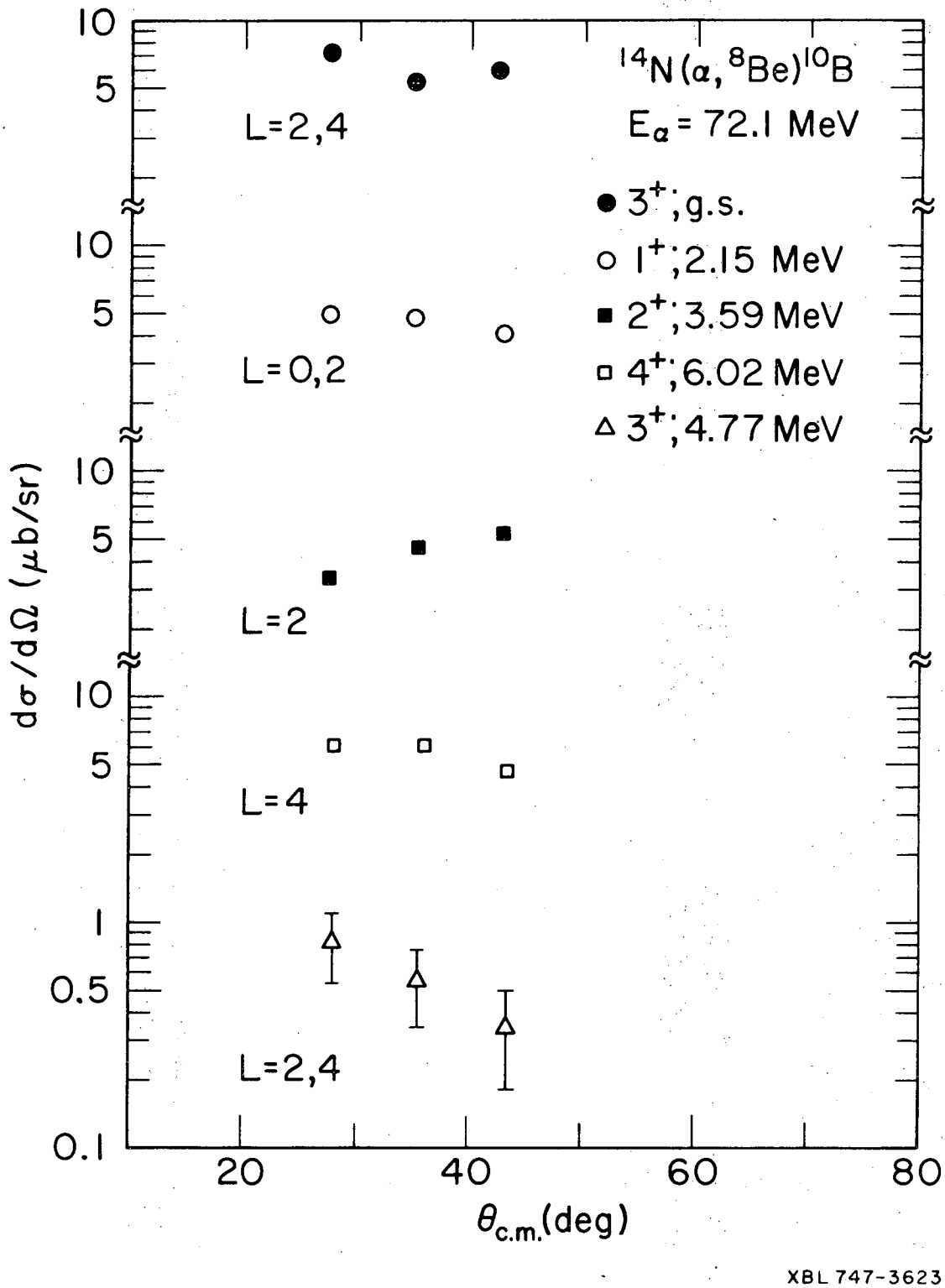

Fig. 5-13. Cross section data for five (α, ^{8}Be) transitions to states in ^{10}B. See discussion in text.

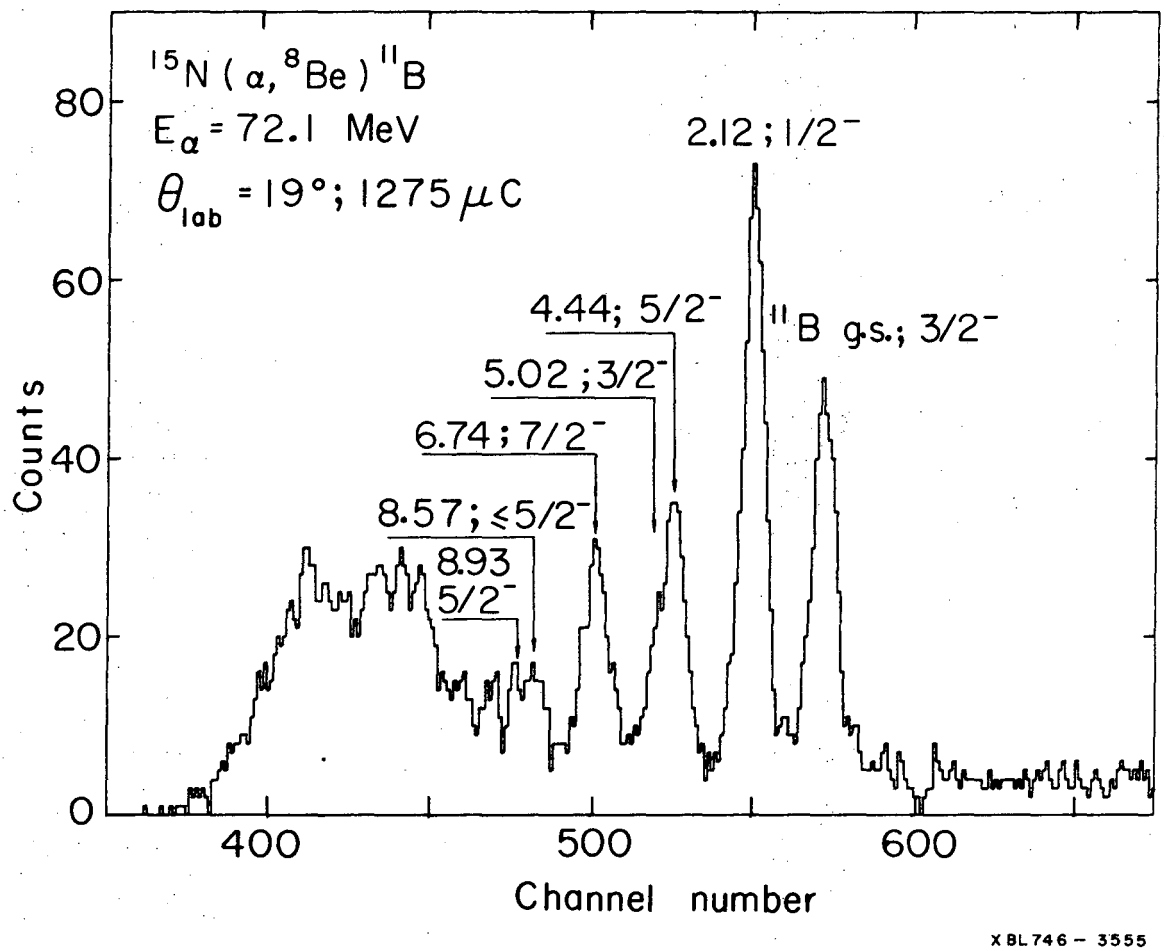

Fig. 5-14. A ^{8}Be energy spectrum from the $^{15}N(\alpha, ^{8}Be)^{11}B$ reaction at $\theta_{lab} = 19°$. The locations of possible transitions to natural parity states below ~9 MeV are shown (see text).

resolution is ~ 800 keV and strong transitions are clearly seen to the $3/2^-$ ground and $1/2^-$ 2.12 MeV states of ^{11}B, which are consistent with their calculated α-structure factors (see Table V-7). The $5/2^-$ 4.44 MeV and $3/2^-$ 5.02 MeV levels are not resolved in this spectrum and were only resolved at $\theta_{lab} = 15°$. However, from the measured excitation energy of 4.50 ± .07 MeV (see Table V-7) for the third peak in the spectra, it seems that at all angles the $5/2^-$ state was populated stronger than the $3/2^-$ one, which is consistent with their theoretical α-structure factors.

No evidence was observed for transitions to the two positive parity states at 7.30 and 8.00 MeV. Thus a third positive parity level at 6.79 MeV was assumed not to be populated even though it could not be seen due to the strong transition to the $7/2^-$ level at 6.74 MeV. This $7/2^-$ state is made very strongly at $\theta_{lab} = 15°$. There is also evidence that two states at 8.57 and 8.92 MeV are being made although their weak strength and the large background hindered their observation. Theoretical α-structure factors (see Table V-7) would indicate that they should be made with a strength similar to what was observed. A $9/2^-$ state predicted by Kurath to lie at 12.7 MeV and to have a large α-structure factor, unfortunately could not be observed over most of the studied angular range due to electronic cutoffs. A strong state of broad width was observed at $\theta_{lab} = 23°$ and ~ 12 MeV excitation which might correspond to this level. However, its nearness to the electronic cutoff and the fact that it was seen clearly at only this angle makes it uncertain that it is the above $9/2^-$ state.

Table V-7. Comparison of ^{11}B levels observed in the $^{15}N(\alpha, {}^{8}Be)^{11}B$ reaction with those reported previously and with theoretical calculations.

Known levels[a]		Observed[b] levels		Calculated[b] levels		Relative strengths	Relative α-spectroscopic factors
MeV	J^{π}	MeV	±keV	MeV	J		Theory[b]
0.0	$3/2^-$	0.02	40	0	3/2	1.00(6.3)[d]	1.00
2.12	$1/2^-$	2.10	40	1.71	1/2	.90	.50
4.44	$5/2^-$	4.50	70	4.35	5/2	.88	.72
5.02	$3/2^-$	---		5.39	3/2	---	.26
6.74	$7/2^-$	6.75	40	5.85	7/2	.59	2.68
6.79	$(1/2, 3/2)^+$	---		---		---	---
7.30	$(3/2, 5/2)^+$	---		---		---	---
8.00	$3/2^+$	---		---		---	---
8.57	$\leq 5/2^-$	8.63	140	8.11	5/2	.36	.15
8.93	$5/2^-$			10.69	5/2		.20
.							
.							
.							
12.0	---	---		12.7	9/2	---	1.25

a) These excitation energies were taken from Se 68.

b) Ku 73.

c) These relative strengths were determined at E_{α} = 72.1 MeV.

d) The quantity in parenthesis is the absolute differential cross section in the center of mass for this transition.

2. Angular distributions

In Fig. 5-15 are shown angular distributions of the first four peaks shown in Fig. 5-14. As the ^{15}N ground state has a spin of 1/2 the transfers to all final states correspond to unique L values. The L = 0 transfer to the $1/2^-$ 2.12 MeV state shows the most structure although it has much less structure than the L = 0 transfers to the ^{8}Be or ^{12}C ground states.

Both the L = 2 transfers are flatter than the L = 0 and show more strength at back angles. Transitions to both the unresolved $5/2^-$ 4.44 MeV and $3/2^-$ 5.02 MeV levels involve L = 2 transfers. Since the 5.02 MeV level was populated at <25% of the 4.44 MeV state's strength at $\theta_{lab} = 15°$ and they were not experimentally resolved at other angles it was assumed that all the experimentally observed strength belonged to the 4.44 MeV level. It is interesting that this L = 2 transfer shows a decrease at forward angles whereas the one to the ground state has a constant amplitude. Both of these L = 2 transfers show a greater strength at back angles over the L = 0 transfer which is a common experimental characteristic they share with the L = 2 transfers to the ^{8}Be and ^{12}C first excited states. The L = 4 transfer to the $7/2^-$ 6.74 MeV is forward peaked and shows no oscillatory nature over this limited angular range.

H. Relative Ground State Spectroscopic Factors

Although good fits to the shapes of the experimental angular distributions were only obtained for the L = 0 transfers on ^{12}C and ^{16}O targets with the diffraction model, it is interesting to see whether this model would reproduce the relative magnitudes of the ground state to ground state transitions for the targets studied. In this spirit,

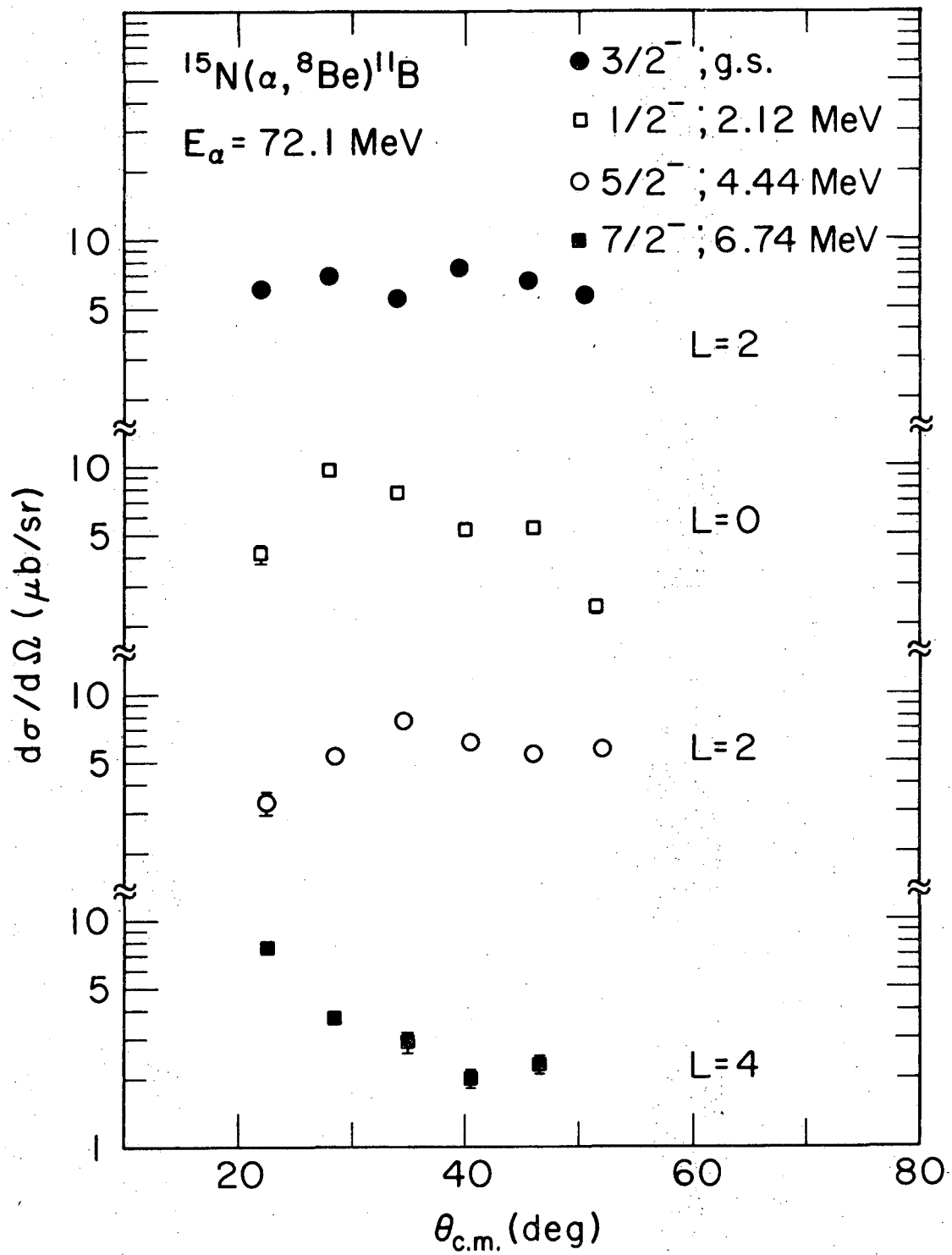

XBL 747-3620

Fig. 5-15. Cross section data for four (α, ^{8}Be) transitions to states in ^{11}B. See discussion in text.

diffraction model calculations were carried out for the ground state to ground state transitions on $^{10,11}B$, ^{12}C, $^{14,15}N$, and ^{16}O. As there was an undetermined normalization factor in the diffraction model cross section expression, this factor was determined by normalizing the calculated cross sections to the experimental data for the ^{16}O target. The parameters R and R_o used in these calculations for A = 15, 16 and A = 10, 11, 12, 14 where identical to those used to fit the L = 0 transfer data from ^{16}O (see Section V-C2) and ^{12}C (see Section V-B3), respectively. The ratios of the experimental to calculated cross sections at the experimental first maximum are given in Table V-8. When the experimental angular distributions had no pronounced maximum, an average value was used. If the observed transition could be populated by more than one L transfer, the theoretical α-structure amplitudes were used to calculate the contributions of the different L-transfers. In this manner a summed differential cross section was obtained which could be compared with the experimental one.

In spite of the above approximations, this prescription gave relative α-spectroscopic factors of similar magnitudes to the theoretical ones as is shown in Table V-8. Only for the (α, ^{8}Be) transition to the $^{6}Li_{g.s.}$ do the experimental numbers disagree with the theoretical ones by more than a factor of three. (The anamolous population of this state by the (α, ^{8}Be), (d, ^{6}Li) and (^{3}He, ^{7}Be) reactions is discussed in Section V-D.) The best agreement with the theory was obtained for the ^{12}C and ^{14}N targets which were determined to have α-spectroscopic factors relative to ^{16}O of 1.6 and 2.4, respectively, compared to Kurath's predictions of 1.5 and 2.4, respectively. The good agreement

Table V-8. Comparison of the theoretical and experimental ground state cross sections for the (α, ^{8}Be) reaction.

Target	Levels in final nucleus	L	$\sigma'_{exp} = \frac{\sigma_{exp}}{\sigma_{exp}(^{16}O)}$	$\frac{\sigma'_{exp}}{\sigma_{calc}}$	$\frac{S_\alpha}{S_\alpha(^{16}O)}$
^{16}O	$^{12}C_{g.s}$	0	1.00	1.00	1.00
^{12}C	$^{8}Be_{g.s}$	0	1.76	1.6	1.48
^{15}N	$^{11}B_{g.s}$	2	.44	0.7	1.92
^{14}N	$^{10}B_{g.s}$	2, 4	.49	2.4	2.44
^{11}B	$^{7}Li_{g.s}$	0, 2	.85	0.5	1.44
^{10}B	$^{6}Li_{g.s}$	0, 2, 4	.40	220.	.01

for the ^{12}C relative spectroscopic factor is very heartening because both the shape and relative magnitude of the oscillations of its L = 0 transition were fit quite well by the diffraction model. However, because the diffraction model poorly accounts for transitions which have multiple L-transfers and because only three targets were studied which gave unique L transfers, further studies on additional targets are necessary before the reliability of using the diffraction model to extract semi-quantitative relative ground state α-spectroscopic factors from (α, ^{8}Be) data can be established.

I. Comparison of Diffraction Model to Full Finite-Range DWBA with Recoil

In the development of the diffraction model described in Section IV, it was postulated that the (α, ^{8}Be) reaction occurred at large distances from the target nucleus and thus it was assumed that nuclear distortion effects were small. In addition, because of the high incident energy ($E_\alpha \sim 65$ MeV), it was assumed that Coulomb distortion effects were also small. To check the validity of these assumptions, full finite-range DWBA calculations which exactly treated recoil effects were carried out with the computer code LOLA (De 73). For the ^{12}C and ^{16}O targets fits were calculated for the L = 0 (α, ^{8}Be) transitions populating the ^{8}Be and ^{12}C ground states, respectively. These fits (solid curves) are shown in Fig. 5-16 and it should be noted that the agreement with the experimental data is good and that the above fits are very similar to those obtained with the diffraction model.

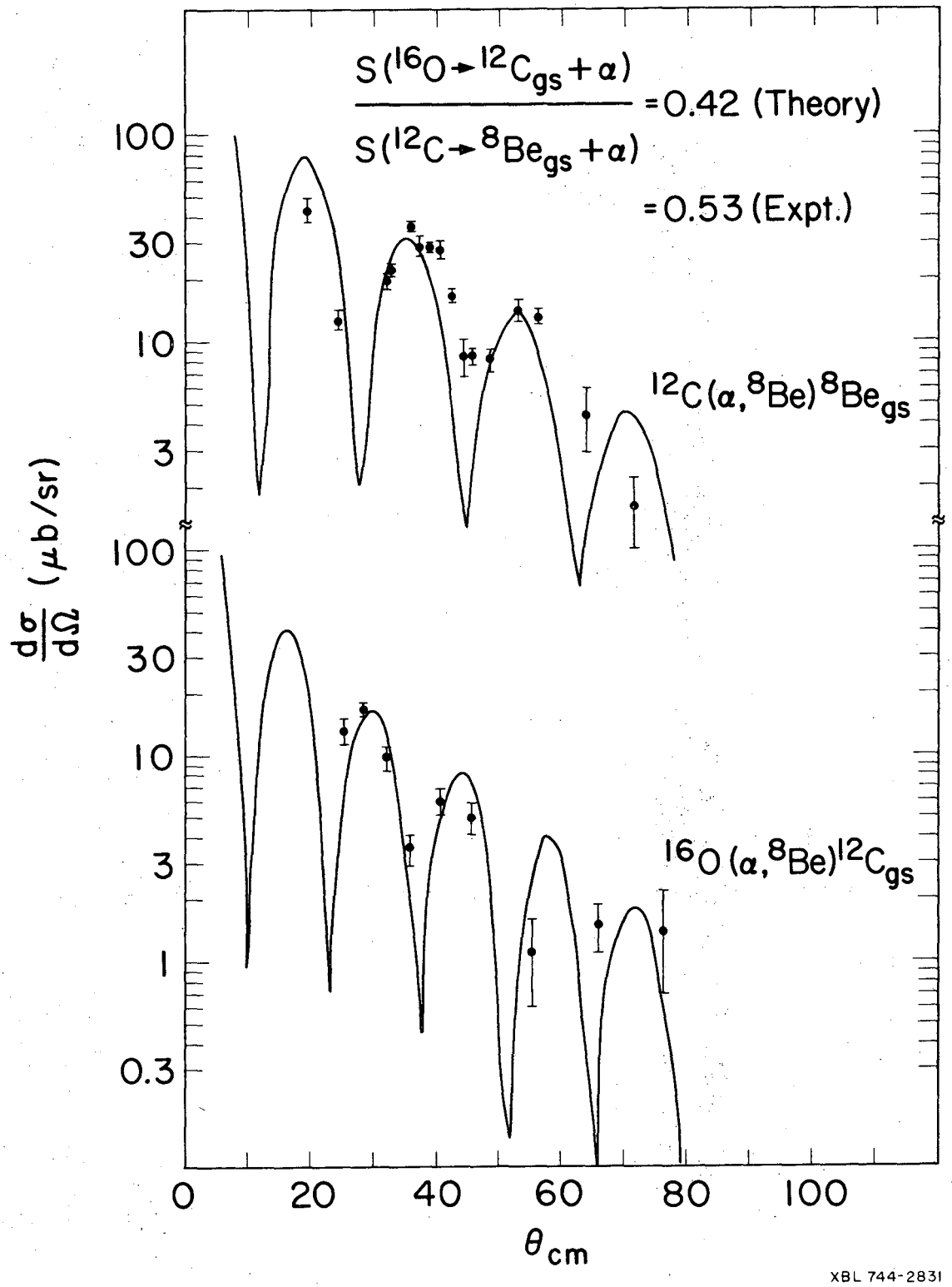

Fig. 5-16. Cross section data for L = 0 transitions to the ground states of ^{8}Be and ^{12}C with distorted wave LOLA fits (solid curves). See discussion in text.

To calculate the above fits, consistent parameters were used to describe the reaction on both targets. Since the results were found to be insensitive to the magnitude of a small binding energy for ^{8}Be, it was assumed to be bound by 100 keV. To describe the α-elastic scattering in the entrance channel, a $^{12}C + \alpha$ optical potential was taken from the literature (see Table V-9). For the exit channel ^{8}Be optical potentials were approximated by a potential of twice the strength of the one used to describe the entrance channel but with modified radius parameters. It was thought that since ^{8}Be is well described by two α-particles that such a potential would adequately describe the exit channel. This prescription gave good agreement with the L = 0 transitions as was seen above. It was found that the LOLA fits were sensitive to the strength of the imaginary potentials and the radius parameter r_o. The optical parameters which were used to obtain the above fits are tabulated in Table V-9.

In an attempt to fit the corresponding L = 2 angular distributions, the same optical parameters were used and the resulting fits are shown in Fig. 5-17. Upon comparing the fits in Fig. 5-17 with those in Figs. 5-5 and 5-8, it is clear that the L = 2 data are not any better reproduced by these DWBA calculations than by diffraction model ones. Extensive variations of these parameters did not improve the L = 2 fits and therefore relative ground to first excited state α-structure factors (S_α(1X/gs) were not extracted. However, because of the good L = 0 fits a relative spectroscopic factor ($S_\alpha(^{12}C/^{16}O)_{gs}$) of 0.53 was extracted from the ground state transitions which is in good agreement with Kurath's theoretical ratio of

Table V-9. Optical-model parameters for the α and ^{8}Be distorted waves.

Entrance channel	(Exit)	V MeV	r_{OR} fm	A_R fm	W MeV	r_{OI} fm	A_I fm	r_{OC} fm
α	^{16}O	116	1.50	.55	24	1.50	.40	1.25
α	^{12}C	116	1.50	.55	24	1.50	.40	1.25
^{8}Be	^{12}C	232	1.0	.55	48	1.0	.60	1.25
^{8}Be	^{8}Be	232	1.20	.55	48	1.40	.60	1.25

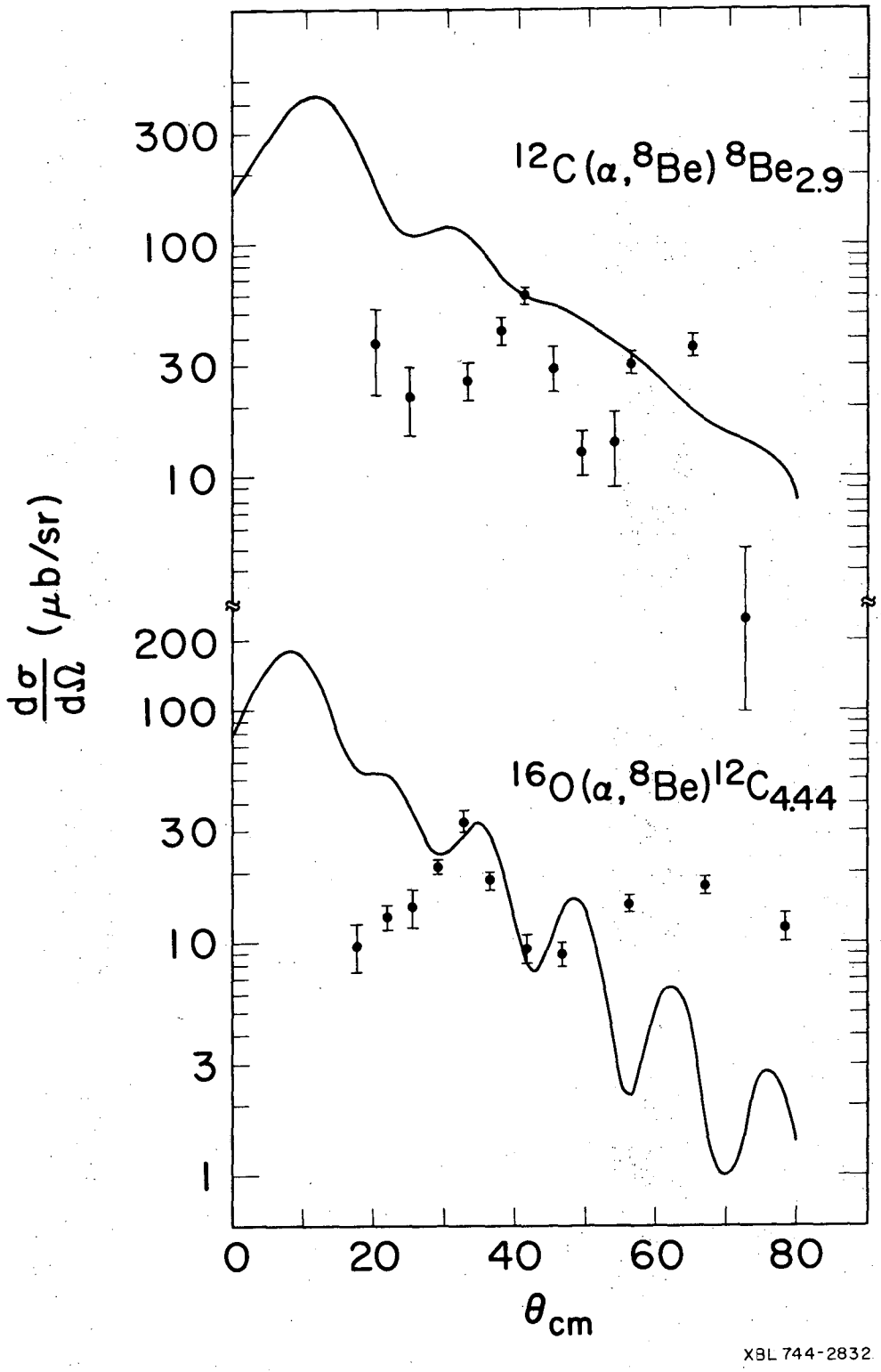

Fig. 5-17. Cross section data for L = 2 transitions to the first excited states of ^{8}Be and ^{12}C with distorted wave LOLA fits (solid curves). See discussion in text.

0.42 and the value of 0.43 which was extracted with the simple diffraction model calculations.

The above agreement between the LOLA calculations and the diffraction model for the ground state transitions validates to some extent the initial assumption that distortion effects are small and supports the choice of the diffraction model to describe the (α, ^{8}Be) reaction mechanism, particularly since prodigious amounts of computer time are required for full finite-range DWBA calculations with recoil. (LOLA calculations were only done for the L = 0 and 2 transfers on ^{12}C and ^{16}O targets.)

J. Comparison of (α, ^{8}Be) with (α, 2α) Results

Since the (α, ^{8}Be) and the (α, 2α) reactions share the same entrance channel and have very similar exit channels, it is interesting to compare the results of these two reactions on ^{12}C and ^{16}O targets. A very prominent systematic feature observed in a study of the (α, 2α) reaction on even-even p-shell and s-d shell targets at E_{α} = 90 MeV was the predominance of the ground state transition at the symmetric quasi-elastic angle. The (α, 2α) reaction on ^{12}C and ^{16}O targets populated the ^{8}Be and ^{12}C ground states a factor of two and four, respectively, larger than their first excited states.

On the other hand the (d, ^{6}Li), (^{3}He, ^{7}Be) and (α, ^{8}Be) reactions all preferentially populate the ^{8}Be 2.9 MeV state larger than its corresponding ground state and in particular populate the ^{12}C 4.44 MeV state a factor of 3 to 4 times stronger than the $^{12}C_{g.s.}$. Kurath's and Rotter's theoretical α-spectroscopic factors (Ku 73, Ro 68) predict

ratios of 1.3 and 5.7, respectively, for the following processes

$$S_\alpha(1\ X/g.s.)_{^8Be}$$

and

$$S_\alpha(1\ X/g.s.)_{^{12}C}.$$

The relative theoretical spectroscopic factors are consistent with ones extracted from the two α-pickup reactions but are in disagreement with the (α, 2α) results. It should be noted in support of the (α, 2α) data at E_α = 90 MeV that at an incident energy of E_α = 70 MeV this reaction gave similar results on an ^{16}O target (Ke 73).

The (p, pα) reaction on ^{12}C and ^{16}O targets at E_p = 160 MeV (Go 70, Ka 68) gave results consistent with the (α, 2α) results. Thus it seems that both α-particle knockout reactions give consistent relative population of states which is inconsistent with the α-particle pickup results. Since the exit channel in both the (α, ^8Be) and (α, 2α) reactions would be identical if the α-particles were in a relative S state, it is intriguing to attempt to understand the different results from these two reactions in the framework of the diffraction model. If the diffraction model discussed in Section IV adequately describes the (α, 2α) process, then the relative strengths of the L = 0 and L = 2 transitions depend on the momentum distribution of their respective α-cluster wave functions in the target. The probability amplitude for a particular recoil momentum (k_R) can be quite sensitive to the angular momentum that the bound α-cluster has relative to the core as was shown in Fig. 4-3.

Referring back to Fig. 4-3, it is seen that for $k_R = 0$ the 3S wave function has a large probability amplitude whereas the 2D and 1G wave functions have probability amplitudes of zero. Since by definition the (α, 2α) reaction at the symmetric quasi-elastic angle leaves the core in a state of zero recoil momentum ($k_R = 0$), it is probing the 3S and 2D wave function at their respective maximum and minimum in momentum space. Thus for the (α, 2α) reaction at or near the symmetric quasi-elastic angle the diffraction model would predict a large L = 0 transition and weak L = 2 or (4) transitions. This prediction is in good account with the observed results.

In addition the diffraction model predicts that at pairs of angles (away from the quasi-elastic one) where the recoil momentum is larger, that the L = 2 transition should increase in strength relative to the L = 0 one. This behavior was observed by Sherman (Sh 73) at forward angle pairs where the magnitude of the L = 2 transfer was comparable to that of L = 0.

In summary the diffraction model shows that the difference between the (α, 2α) and the (α, ^{8}Be) reactions is that they are probing different regions of the bound α-cluster's momentum distribution. Near the quasi-elastic angle the (α, 2α) reaction is sensitive to small recoil momenta whereas the (α, ^{8}Be) reaction at forward angles is sensitive to much larger recoil momenta.

VI. Summary and Conclusion

A broad survey of the (α, ^{8}Be) reaction on p-shell nuclei at high bombarding energies has been presented in Section V. This investigation was undertaken to determine if the (α, ^{8}Be) reaction could be understood in terms of a simple α-cluster pickup process which has been previously used to successfully describe the major features of the (d, ^{6}Li) and (^{3}He, ^{7}Be) reactions. Because the original (α, ^{8}Be) experiments by Brown et al. showed evidence of large non-direct processes at $E_\alpha \sim 40$ MeV, an excitation function was obtained at incident energies near 65 MeV which conclusively demonstrated the direct nature of the (α, ^{8}Be) reaction at these higher bombarding energies.

A systematic feature which emerged from this investigation was the strong population of only those states which are predicted to have significant α-structure factors. This selectivity is evidence that the (α, ^{8}Be) reaction proceeds via a simple α-cluster pickup process. The relative population of states by the (α, ^{8}Be) reaction on p-shell nuclei was generally in good agreement with the previously reported (d, ^{6}Li) and (^{3}He, ^{7}Be) results. However, a notable exception to this arose in that no evidence for the population of the mixed isospin states at ~16 MeV in ^{8}Be by the (α, ^{8}Be) reaction was observed whereas both the (d, ^{6}Li) and (^{3}He, ^{7}Be) reactions populated these levels strongly. Since these states have a dominant single particle nature, the (α, ^{8}Be) was more selective in this case at least in its relative population of final states in ^{8}Be than the other two α-pickup reactions.

The occurrence of a cluster pickup mechanism greatly simplifies the theoretical description. In order to extract α-spectroscopic factors, the data were analyzed with diffraction model calculations. Although this model neglects distortion, Nagarajan has shown that these effects should be small when there is an unbound particle in exit channel. This neglect of distortion was justified by the agreement obtained between diffraction model calculations performed with plane waves and several full finite-range DWBA calculations which exactly treated recoil effects.

Experimental angular distributions for pure $L = 0$ and $L = 2$ transfers were observed to be quite different with the latter showing a much larger strength at back angles. For single L-transfers, the diffraction model adequately reproduced the experimental data. However, it failed to describe the shape of the cross sections for transitions involving more than one L-transfer, indicating the need for further theoretical development.

Using the diffraction model, relative ground-state α-spectroscopic factors were extracted which are in qualitative agreement with theoretical ones (Ku 73). In addition the ratio of experimental spectroscopic factors for transitions to the ground and first excited states of both ^{8}Be and ^{12}C were within 50% of Kurath's predictions (Ku 73).

In order to perform this spectroscopic study which involved low cross sections and the detection of a particle-unstable nucleus in the presence of a high chance α-α background, a unique ^{8}Be detection system was developed. Important design characteristics are discussed

in Section II and with this technique high detection efficiencies (~ 30%), excellent chance background rejection and good energy resolution were obtained. This technique should greatly simplify the study of single and multi-particle transfer reactions involving ^{8}Be, such as (^{9}Be, ^{8}Be), (^{6}Li, ^{8}Be), and (^{11}B, ^{8}Be). An investigation of the (^{9}Be, ^{8}Be) reaction would be of particular interest, because the transferred neutron is bound to the ^{8}Be-core in ^{9}Be by only 1.7 MeV. Thus this reaction should have a very large cross section and might populate with appreciable strength states seen only weakly in other heavy-ion single-nucleon transfer reactions. Since the deuteron is also weakly bound, a comparison with (d, p) results would be valuable.

Many possibilities exist (Ro 73) for the extension of this detection technique to the study of reactions involving the emission of nuclei in resonant states. An immediate application might be to the study of reactions emitting "pseudo diprotons" that were seen in studies of 70 MeV ^{3}He on polyethylene with the Bol system (Da 71). There are a large number of possible reactions of spectroscopic interest involving "pseudo diprotons" in the exit channel, such as (p, 2p), (d, 2p), (t, 2p), (^{3}He, 2p), and (α, 2p). In addition, nuclei far from stability might be investigated (Ce 74) with such reactions as ^{14}C(^{7}Li, 2p)^{19}N or ^{18}O, 2p)^{34}Si.

Acknowledgments

For their contributions to the process of turning an ignorant graduate student into a super researcher I would like to acknowledge the following people:

My mentor, Prof. Joseph Cerny for his advice, his willingness to lend the horsepower needed to overcome obstacles encountered during the course of this project, his patience with my long tenure as a graduate student and most important for recognizing a ^{8}Be when he saw one even through it went by another name.

The senior staff of Bldg. 88, Dr. Bernard Harvey, Dr. David Hendrie, Dr. H. E. Conzett, and Dr. David Clark for their expertise and for teaching me the difference between Physics and Chemistry.

My initial collaborator in ^{8}Be experiments, Dr. Hans Harvey, and his wife, Heidi, who infused me with enough German to pass my language exam.

Dr. Nick Jelley, my inspiring co-collaborator in this work, for the excitement he brought to research, for being a jolly good chap, and for many a fine dinner over which we discussed physics and other things.

Roy Burton for teaching me the rudiments of mechanical design and drafting and for introducing me to the pleasure of sunbathing at the Strawberry Canyon swimming pool.

Jack Walton for managing to build every weird kind of detector I could think of. Don Landis for designing the fast electronics and

for stimulating discussions on electronics. Ed Lampo for his assistance in debugging and making our electronics work.

Dr. M. Nagaragan for explaining reaction theory in terms that a experimentalist could understand.

The former and present postdocs, Dr. R. Mendelson, Dr. J. M. Loiseaux, Dr. A. Bacher, Dr. D. Kovar, Dr. F. Becchetti, Dr. D. Scott, and Dr. C. Maguire for their guidance and wisdom.

The present and former graduate students who worked owl shifts on my experiments: Dr. John Esterl, Dr. George Goth, Dr. John Macdonald, Dr. Rich Sextro, Ken Wilcox, Bob Weisenmiller, Lenard Ho, David Vierra, and Dieter Stahel. In addition, I would like to acknowledge Dr. Mike Zisman's sterling example which helped me to pass both my orals and German and Dr. J. Sherman who introduced me to α-clustering phenomena.

Dr. Creve Maples for the use of several computer codes, and for keeping posted on silver futures and tax loopholes.

Bob Weisenmiller, my officemate, who addicted me to H. P. Lovecraft wherein I found my sanity.

Evelyn, my woman and my wife, for being warm and physical, for typing many drafts of this thesis, for sharing my love of the wilderness and for loving me.

John Bowen, the cyclotron crew, the shops, and other support people for making Bldg. 88 a pleasant place to work.

This work was performed under the auspices of the U. S. Atomic Energy Commission.

FOOTNOTES

[1]Havar is an alloy consisting primarily of Co(42.5%), Ni(13.0%), Cr(20.0%), and Fe(17.9%), with a density of 8.3 gm/cm^3. Hamilton Watch Co., Metals Division, Lancaster, Penn.

[2]Our positive-sensitive detectors were obtained from Edax International, Incorporated.

REFERENCES

Ar 71 A. Arima and V. Gillet, Ann. Phys. 66, 117 (1971).

Ar 71a A. Arima and I. Hamamoto, Ann. Rev. Nucl. Sci. 21, 55 (1971).

Aro 71 V. J. Arora, C. Détraz, C. E. Moss, C. D. Zafiratos, and C. S. Zaidins, Univ. of Colo. Progress Report 1971 (unpublished).

Au 70 N. Austern, Direct Nuclear Reaction Theories, Interscience, New York, 1970.

Ba 69 J. Bang and J. Zimanyi, Nucl. Phys. A139, 534 (1969).

Be 68 T. Berggren, Nucl. Phys. A109, 265 (1968).

Be 70 K. Bethge, Annual Review of Nuclear Science Vol. 20, (1970).

Be 72 M. Bedjidian, M. Chevallier, J. Y. Grossiord, A. Guichard, M. Gusakow, J. R. Pizzi, and C. Ruhla, Nucl. Phys. A189, 403 (1972).

Bo 64 A. N. Boyarkina, Bull. Acad. of Sci. USSR, Phys. Ser. 28, 255 (1964).

Br 65 R. E. Brown, J. S. Blair, D. Bodansky, N. Cue, and C. D. Kavaloski, Phys. Rev. 138, B 1394 (1965).

Br 66 D. M. Brink, Proc. Int. School of Physics "Enrico Fermi" course 36 (Academic Press, New York, 1966).

Br 69 H. Brunnader, UCRL-18716 (Ph.D. Thesis - unpublished) January 1969.

Br 72 G. Bruge, A. Chameaux, R. De Vries, and P. LeLeux, Annual Report 71-72, Department De Physique Nucleaire, Saclay, France.

Br 73 F. Brochard, P. Chavallier, D. Disdier, G. Rudolf, and F. Scheibling in Proceedings of the Inter. Conf. on Nucl. Phys. ed. by J. de Boer and H. J. Mang (North-Holland 1973) Vol. 1, p. 204.

Bro 66 G. E. Brown and A. M. Green, Nucl. Phys. 75, 401 (1966).

Bu 66 P. J. A. Buttle and L. J. B. Goldfarb, Nucl. Phys. 78, 409 (1966).

Bu 70 G. W. Butler, A. M. Poskanzer, and D. A. Landis, Nucl. Instr. and Meth. 89, 189 (1970).

Ce 71 A. E. Ceballos, H. J. Erramuspe, A. M. J. Ferrero, M. J. Sametband, and J. E. Testoni, Phys. Rev. C4, 1959 (1971).

Ce 74 Joseph Cerny in Proc. Inter. Conf. Reactions Between Complex Nuclei, Nashville, Tennessee (1974).

Ch 67 P. Chevallier, F. Scheibling, G. Goldring, I. Plesser, and M. W. Sachs, Phys. Rev. 160, 827 (1967).

Co 70 B. J. Cole, R. Huby, and J. R. Mines, Phys. Lett. 33B, 320 (1970).

Co 72 J. R. Comfort, W. J. Braithwaite, J. R. Duray, H. T. Fortune, W. J. Courtney, and H. G. Bingham, Phys. Lett. 40B, 456 (1972).

Co 73 B. J. Cole and R. Huby, Phys. Letters 46B, 55 (1973).

Cr 71 G. M. Crawley, P. S. Miller, and W. F. Steele, Annual Report 1970-71, Cyclotron Laboratory, Dept. of Physics, Michigan State University.

Cr 73 J. G. Cramer, K. A. Eberhard, N. R. Fletcher, E. Mathiak, H. H. Rossner, and A. Weidinger, Nucl. Instr. and Meth. 111, 425 (1973).

Da 71 R. Van Dantzig et al., Nucl. Instr. and Meth. 92, 205 (1971).

De 66 L. J. Denes, W. W. Daehnick, and R. M. Drisko, Phys. Rev. 148, 1097 (1966).

De 70 C. Détraz, H. H. Duhm and H. Hafner, Nucl. Phys. A147, 488 (1970).

De 71 C. Détraz, C. D. Zafiratos, C. E. Moss, and C. S. Zaidins, Nucl. Phys. A177, 258 (1971).

De 72 C. Détraz, C. D. Zafiratos, H. Rudolph, and C. S. Zaidins, Phys. Rev. Lett. 28, 117 (1972).

De 73 R. M. De Vries, LOLA (internal report), Nuclear Physics Laboratory, University of Washington, October 1973.

Do 65 L. R. Dodd and K. R. Greider, Phys. Rev. Lett. 14, 959 (1965).

Do 69 L. R. Dodd and K. R. Greider, Phys. Rev. 180, 1187 (1969).

Ei 69 J. Eichler in Proc. Fifth Conf. on Nucl. Reactions Induced by Heavy Ions, Heidelberg, Germany, 1969 ed. by R. Bock and W. R. Hering. (Amsterdam: North-Holland 1970) 347.

Ei 70 W. Eichelberger, R. D. Plieninger, and E. Velton, Nucl. Phys. A149, 441 (1970).

Fo 70 H. T. Fortune and B. Zeidman in Proc. Fifth Conf. Nuclear Reactions Induced by Heavy Ions, ed. R. Bock, W. R. Hering, Amsterdam: North-Holland 307 (1970).

Fr 63 P. Franzini and L. A. Radicati, Phys. Lett. 6, 322 (1963).

Ga 72 J. D. Garrett in the Proceedings of the Symposium on Two-Nucleon Transfer and Pairing Excitations, Argonne Physics Division Informal Report PHY-1972 H, 232 (1972).

Ge 67 W. J. Gerace and A. M. Green, Nucl. Phys. A93, 110 (1967).

Go 70 B. Gottschalk and S. L. Kannenberg, Phys. Rev. C2, 24 (1970).

Gr 66 K. R. Greider and L. R. Dodd, Phys. Rev. 146, 671 (1966).

Gr 69 K. R. Greider in Proc. Fifth Conf. Nuclear Reactions Induced by Heavy Ions, ed. R. Bock, W. R. Hering. (Amsterdam: North-Holland) (1970) 217.

Gu 71 H. H. Gutbrod, H. Yoshida, and R. Bock, Nucl. Phys. A165, 240 (1971).

Ha 72 H. L. Harney and G. J. Wozniak, Lawrence Berkeley Laboratory Report LBL-1214 September 72.

Ho 69 H. D. Holgren, 1969. Int. Conf. Clustering Phenomena Nuclei, 17, Vienna: IAEA.

Ho 72 H. Ho, D. Dehnhard, W. Dunnweber, K. Mudersbach, and J. P. Wurm, Jahresbericht, Max-Planck-Institut fur

Kernphysik (Heidelberg, Germany, 1972).

Hu 65 R. Huby and J. R. Mines, Rev. Mod. Phys. 37, 406 (1965).

Hu 69 R. Huby, Nucl. Phys. A138, 442 (1969).

Hu 70 R. Huby, Phys. Lett. 33B, 323 (1970).

Ja 68 K. S. Jayaraman and H. D. Holmgren, Phys. Rev. 172, 1015 (1968).

Ja 73 D. R. James, J. L. Artz, M. B. Greenfield, and N. R. Fletcher in Proceedings of the Inter. Conf. on Nucl. Phys. ed. by J. de Boer and H. J. Mang (North Holland 1973) Vol. 1, p. 164.

Je 74 N. A. Jelly, LBL internal report, to be published.

Ka 68 S. L. Kannenberg, Ph.D. Thesis, 1968 (unpublished).

Ke 73 R. Kenefick, private communication.

Ku 73 D. Kurath, Phys. Rev. C7, 1390 (1973).

Lo 66 J. Lowe, A. R. Polletti, and D. H. Wilkinson, Phys. Rev. 148, 1045 (1966).

Ma 71 C. C. Maples, LBL-253 (Ph.D. Thesis), September 1971 (unpublished).

Ma 72 Ph. Martin and T. R. Ophel, Nucl. Phys. A194, 491 (1972).

Ma 73 P. Martin, J. B. Viano, J. M. Loiseaux, and Y. Le Chalony, Nucl. Phys. A212, 304 (1973).

Mc 71 R. L. McGrath, D. L. Hendrie, E. A. McClatchie, B. G. Harvey, and J. Cerny, Phys. Lett. 34B, 289 (1971).

Mc 74 A. Menchaca-Rocha, Nucl. Instr. and Meth. 114, 425 (1974).

Na 74 M. A. Nagarajan, Lawrence Berkeley Laboratory Report LBL-2918, May 1974 (to be published).

Ph 60 G. C. Phillips and T. A. Tombrello, Nucl. Phys. 19, 555 (1960), and references therein.

Ri 68 G. Ripka, Advances in Nuclear Physics, Vol. 1 (Plenum Press, New York, 1968).

Ro 68 I. Rotter, Fortschr. Phys. 16, 195 (1968).

Ro 73 D. Robson, Nucl. Phys. A204, 523 (1973).

Se 68 F. Ajzenberg-Selove and T. Lauritsen, Nucl. Phys. A114, 1 (1968).

Se 74 F. Ajzenberg-Selove and T. Lauritsen, Nucl. Phys. A227, 1 (1974).

Sh 73 J. D. Sherman, LBL-1690 (Ph.D. Thesis, 1973 (unpublished).

Ta 63 A. de-Shalit and I. Talmi, Nuclear Shell Theory (Academic, New York, 1963).

Vi 68 C. M. Vincent, Phys. Rev. 175, 1309 (1968).

Wi 37 E. P. Wigner, Phys. Rev. 51, 106 (1937).

Wi 58 K. Wildermuth and T. Kananoplous, Nucl. Phys. 7, 150 (1958); 9, 449 (1958).

Wi 61 D. H. Wilkinson in Proc. Rutherford Jubilee Int. Conf., Manchester, ed. J. Birks, 339 (1961).

Wi 66 K. Wildermuth and W. McClure, in Springer Tracts in Modern Physics, Vol. 41 (Springer-Verlog, Berlin, Heidelberg, New York, 1966).

Wo 72 G. J. Wozniak, H. L. Harney, K. H. Wilcox, and J. Cerny, Phys. Rev. Lett. 28, 1278 (1972).

Wo 73 G. J. Wozniak, N. A. Jelley, and Joseph Cerny, Phys. Rev. Lett. 31, 607 (1973).

Wo 74 G. J. Wozniak, N. A. Jelley, and Joseph Cerny, Nucl. Instr. and Meth., (to be published).

Wo 74a G. J. Wozniak, unpublished data.

Za 71 C. D. Zafiratos, C. Détraz, C. E. Moss, and C. S. Zaidins, Phys. Rev. Lett., 27, 437 (1971).

Ze 70 B. Zeidman, H. T. Fortune, and A. Richter, Phys. Rev. C2, 1612 (1970).

LEGAL NOTICE

This report was prepared as an account of work sponsored by the United States Government. Neither the United States nor the United States Atomic Energy Commission, nor any of their employees, nor any of their contractors, subcontractors, or their employees, makes any warranty, express or implied, or assumes any legal liability or responsibility for the accuracy, completeness or usefulness of any information, apparatus, product or process disclosed, or represents that its use would not infringe privately owned rights.

TECHNICAL INFORMATION DIVISION
LAWRENCE BERKELEY LABORATORY
UNIVERSITY OF CALIFORNIA
BERKELEY, CALIFORNIA 94720